Università degli Studi Roma Tre

Department of Mathematics and Physics
Ph.D. program in Physics
XXXV Cycle

Virtual Photon Emission in Leptonic Decays of Pseudoscalar Mesons

A dissertation submitted in partial fulfillment
of the requirements for the degree of
Doctor of Philosophy in Physics

Supervisor
Prof. Vittorio Lubicz

Author
Filippo Mazzetti

PhD Program Coordinator
Prof. Giuseppe Degrassi

October 2022

To JackObs

Abstract

We study the radiative leptonic decays $P \to \ell\nu_\ell\, \ell'^+\ell'^-$, where P is a pseudoscalar meson and ℓ and ℓ' are charged leptons. In such decays the emitted photon is off-shell and, in addition to the "point-like" contribution in which the virtual photon is emitted either from the lepton or the meson treated as a point-like particle, four structure-dependent (SD) form factors contribute to the amplitude. We present a strategy for the extraction of the SD form factors and implement it in an exploratory lattice computation of the decay rates for the four channels of kaon decays $(\ell, \ell' = e, \mu)$. It is the SD form factors which describe the interaction between the virtual photon and the internal hadronic structure of the decaying meson, and in our procedure we separate the SD and point-like contributions to the amplitudes. We demonstrate that the form factors can be extracted with good precision and, in spite of the unphysical quark masses used in our simulation ($m_\pi \simeq 320\,\mathrm{MeV}$ and $m_K \simeq 530\,\mathrm{MeV}$), the results for the decay rates are in reasonable semiquantitative agreement with experimental data.

Contents

Introduction

The Standard Model (SM) is the most complete physical theory, which describes the fundamental constituents of our universe and three of the four fundamental forces, which are the electromagnetic, the weak and the strong interactions. Nevertheless, one of the main goal of the high energy physics is the search of new physics, beyond the Standard Model, since there are several arguments suggesting the necessity of some kind of extension. Phenomenological observations like the dark matter and the smallness of neutrino masses can not be explained in the actual theory, so as the strong asymmetry between baryons and antibaryons. Moreover, the Standard Model does not include gravity, which has not been successfully quantized in a renormalizable theory, and it does not provide any justification for the very precise equivalence between the electron and proton electric charges. Another mysterious fact is the observed value of 125 GeV for the Higgs mass. To justify that value within the Standard Model one has to invoke an incredible ad hoc *fine-tuning* of the parameters. All these problems suggest considering the SM as an effective theory, valid at low energies, of a more complete one. We could hope to reach the energy scale of the new physics in the experiments, so to view direct evidences (e.g. discovering a new particle), but we don't know where exactly that scale of energy is, and reaching it could require an indeterminate amount of time. In the meantime, another way of searching for new physics is to look for indirect evidence of it, that is, finding some kind of inconsistencies between prediction of SM and experimental data.

To do so, an excellent ground is precision flavor physics, which studies processes where different species of quark mix among each other. The reason for the interest in studying flavor physics in the quark sector is the observed strong hierarchy in the quark mass spectrum and the fact that the mixing phenomenon is severely restricted in the Standard Model, as we now explain. In the SM, mixing among quarks is carried by the charged weak current, and it is parametrized by the Cabibbo-Kobayashi-Maskawa (CKM) matrix, that is a 3×3 matrix where each element represents the complex coupling relating the mixing between an *up*-type and a *down*-type of quark. It reads

$$V = \begin{pmatrix} V_{ud} & V_{us} & V_{ub} \\ V_{cd} & V_{cs} & V_{cb} \\ V_{td} & V_{ts} & V_{tb} \end{pmatrix} . \tag{1}$$

So the first prediction of the SM is the absence of flavor changing neutral current at tree level, transition between different species of quarks with the same electric charge can occur only through loop corrections in the weak interaction. Moreover, the GIM mechanism provides a partial cancellation of the loop contributions coming from the different quarks. The resulting extreme suppression in the SM makes these processes very useful to test small hypothetical effects of new physics. Besides forbidding flavor changing neutral currents at tree level, SM also provides several constraints on the nine complex entries of the CKM matrix. Indeed, the SM requires the matrix V to be unitary, that is it must obey the relation

$$V\,V^\dagger = V^\dagger\,V = 1 \tag{2}$$

Eq. (2), together with the arbitrariness of the quark field phases, reduces the number of independent real parameters appearing in V from eighteen to only four. In other words, the CKM matrix provides several tests for the validity of the Standard Model. This is the reason why there is a great effort to measure CKM matrix elements with extreme precision.

However, the extraction of the CKM elements from experimental data requires an accurate knowledge of a number of hadronic quantities, that constitute the main source of theoretical uncertainty. Indeed, the non-perturbative nature of strong interaction at low energy makes any computations extremely hard, or even impossible, to be performed analytically. In this context, Lattice Quantum Chromodynamics (LQCD) has proved to be the most successful tool for evaluating non-perturbative hadronic effects. By formulating the theory on a finite four-dimensional hypercube, and in Euclidean space-time, LQCD allows a numerical evaluation of the path integrals, without introducing any other assumptions besides the validity of the theory itself. This is achieved due to the finite number, although very large, of degrees of freedom of the discretized theory and to the fact that in Euclidean space-time the generating functional assumes the form of a partition function. These two facts allow a numerical evaluation of the path integrals which non-perturbatively define correlation functions, by employing Monte Carlo methods through the importance sampling technique, that is by weighting the contributions of field configurations to the integral using the Boltzmann factor. Also, the finite lattice provides a natural regularization of both infrared and ultraviolet divergences. Finally, all the systematic effects due to the discretization, the finite volume, and in some cases also due to unphysical quark masses that are simulated can be precisely evaluated and taken into account. Many other details on LQCD and its fundamental techniques are collected in the thesis in Appendix B.

For all its features, LQCD is today the most powerful technique for the evaluation of non-perturbative hadronic effects from first principles only, and it constitutes the main tool that has been used in this thesis. Our work focused on the decay

$$P^+ \to \ell^+\,\nu_\ell\,\ell'^+\,\ell'^- \,, \tag{3}$$

where P^+ is a charged pseudoscalar meson, that decays in three charged leptons ℓ^+, ℓ'^+, ℓ'^- and a neutrino ν_ℓ. ℓ and ℓ' are two lepton flavors, that can be equal or different, that is $\ell,\, \ell' = e\,,\ \mu\,,\ \tau$. The results obtained in this study have been in published in [1]. These are very rare processes, since at leading order the decay, besides being induced by the weak interactions, is also mediated by a virtual photon, so that the matrix element is proportional to the electromagnetic coupling constant $\alpha_{em} = \frac{1}{137}$ and the squared amplitude entering the branching ratios is suppressed by a factor α_{em}^2 with respect to the other, more common, decays. For each decay $P^+ \to \ell^+\,\nu_\ell\,\ell'^+\,\ell'^-$, the computation of the decay rate requires the knowledge of four Structure Dependent (SD) hadronic form factors, that depend on the invariant masses of the two leptonic pairs $\ell\,\nu_\ell$ and $\ell'^+\ell'^-$ as well as of the leptonic decay constant f_P. The "point-like" (or inner-bremsstrahlung) contribution to the decay rate, in which the virtual photon is emitted either from the lepton ℓ^+ or from the meson P^+ treated as a point-like particle, is readily calculable in perturbation theory, requiring only the known value of f_P as the non-perturbative input. The SD form factors describe instead the interaction between the virtual photon and the internal hadronic structure of the decaying meson, and their computation in Lattice QCD is the main subject of this thesis. The procedure developed in this work is a natural extension of the detailed studies and computations of isospin breaking corrections to leptonic decays [2, 3, 4, 5] and to the calculation of leptonic radiative decays of the type $P \to \ell\nu_\ell\gamma$ where γ is a real photon [6, 7].

Given the strong suppression of these processes, only a few experimental measurements exist. For the pion, the only measured decay rate is for the process $\pi^+ \to e^+\,\nu_e\,e^+\,e^-$, for which the Particle Data Group (PDG) reports a branching ratio of $(3.2 \pm 0.5) \times 10^{-9}$ [8]. For kaon decays, the measurement of the (partial) branching ratios has been performed by the E865 experiment at the Brookhaven National Laboratory AGS for the decays $K^+ \to e^+\,\nu_e\,e^+\,e^-$, $K^+ \to \mu^+\,\nu_\mu\,e^+\,e^-$ and $K^+ \to e^+\,\nu_e\,\mu^+\,\mu^-$ [9, 10]. The branching ratios are found to be of $O(10^{-8})$. For decays with a e^+e^- pair in the final state, a lower limit of about 150 MeV is imposed on the invariant mass of the lepton pair. Without such a cut, the branching ratio would be dominated by the point-like contribution in the low e^+e^- invariant mass region which is of $O(10^{-5})$, so that the relevant SD contribution would not be detectable. For D mesons no experimental data are available yet, while for B mesons there is an upper bound on $\mathrm{BR}(B^+ \to \mu^+\,\nu_\mu\,\mu^+\,\mu^-)$ of 1.6×10^{-8} [11].

Despite the theoretical and experimental difficulties, achieving numerical predictions and experimental measurements for the processes $P^+ \to \ell^+\,\nu_\ell\,\ell'^+\,\ell'^-$ would result in a precious source of information. Indeed, in order to place constraints on new physics, a theoretical prediction for the emission of an off-shell photon provides several possibilities. One example are the recent experimental results suggesting the violation of Lepton Flavor Universality, which is an important feature of the SM (see e.g. Refs.[12, 13] and references therein). A simple extension of the SM has been considered by adding a new $U_{\mu_R}(1)$ gauge interaction, in order to explain the discrepancy between some different measurements of the proton charge radius [14]. In [15] the non-observation of missing mass events in the leptonic kaon decays has been used to place strong constraints on a parity-violating gauge interaction of μ_R. But it is also pointed out in [15] that if we allow the new gauge boson to decay in a leptonic pair $\ell^+\,\ell^-$, like in [14], then in order to place a constraint it is necessary to have a SM prediction for the $P^+ \to \ell^+\,\nu_\ell\,\ell'^+\,\ell'^-$ process, in which the virtual photon emission enters. Also, a non-perturbative evaluation of the form factors relevant for the emission of a virtual photon in the B decays can be used to investigate new particles with flavor-violating couplings to b-quark. This is the case of the axion [16, 17], which would provide an explanation for the absence of CP-violating effects in strong interactions [18] and at the same time it is also a candidate for dark matter [19]. In [20] it is compared the decay rate for $B \to \mu^+\,\mu^-\,a$ to the SM background $B \to \mu^+\,\mu^-\,\gamma$, for which a non-perturbative estimate of the $B \to \gamma^{(*)}$ form factors with on- or off-shell photon is necessary. In [21] is explained how to extract the $B \to \mu^+\,\mu^-\,\gamma$ spectrum as a contamination in the tail of the LHC collected data for the process $B \to \mu^+\,\mu^-$. In [20] the off shell radiative form factors are computed with QCD sum rules. It is precisely the strong suppression of processes like the one in Eq. (3) that makes them excellent places where to look for these hypothetical new physics effects. The reason is that effects of new physics, if present, are supposed to be very small, otherwise we would have already detected them somewhere. Thus, if the leading Standard Model contribution to some process is also small, due to any mechanism, we can expect hypothetical new physics contributions to be comparable in size, and so detectable without the need of extraordinary precision.

For all the motivations shown before, we believe that a non-perturbative, model-independent lattice computation of the radiative structure dependent form factors describing virtual photon emission is today extremely useful to make progress in the theoretical predictions of SM hadronic quantities (like the Cabibbo-Kobayashi-Maskawa matrix elements) and also for the search of new physics.

In this thesis, we present for the first time a general strategy for the computation of the SD form factors and implement the procedure in an exploratory lattice simulation for kaon decays, i.e. for $P = K$. The computation is performed using a single gauge ensemble of $N_f = 2+1+1$ flavors of twisted mass fermions generated by the European Twisted Mass Collaboration (ETMC) on a $32^3 \times 64$ lattice with lattice spacing $a = 0.0885\,\text{fm}$ and with unphysical light-quark masses such that the pion and kaon masses are $m_\pi \simeq 320\,\text{MeV}$ and $m_K \simeq 530\,\text{MeV}$ [2]. Our method enables us to determine each of the four SD form factors contributing to the amplitude with good precision, and to study their dependence on the kinematic variables. Using these form factors one can reconstruct separately all the contributions to the branching ratios; the point-like contribution, the SD one and that coming from the interference between the two. There has been one previous lattice study of these decays, in which a method was presented and implemented to compute the branching ratio for the decays $K^+ \to \ell^+\,\nu_\ell\,\ell'^+\,\ell'^-$ without separating the point-like contribution and determining the SD form factors themselves [22]. In addition to the lattice results for the kaon form factors from the computation reported here, theoretical information about kaon and pion form factors comes from Chiral Perturbation Theory (ChPT), which has been used at next-to-leading order (NLO) to estimate their value and their contribution to the branching ratios [23]. It is worth noting that at NLO order in ChPT the form factors are constants, i.e. independent from the kinematical variables. In spite of the unphysical quark masses used in our simulation, it has been interesting and instructive to compare our results with those from experiments (where available) and from NLO ChPT, as well as with those from Ref. [22]. Perhaps surprisingly, due to the still approximate estimates of systematic effects, as can be seen from Tabs. 3.1 - 3.4 below, the results are generally in reasonable semi-quantitative agreement but with some differences. In particular, we speculate that the form factor H_1, defined in Eq. (1.21) may have to increase by $O(20\%)$ in order to get precise agreement with the experimental data (although there are also discrepancies in the experimental determination of H_1 from different decay channels). It will be important therefore, after this successful exploratory computation, to focus our future work on controlling and reducing the systematic uncertainties in order to obtain robust results at physical quark masses and in the continuum and infinite-volume limits. It will then be interesting to see whether the form factor H_1 will indeed change or whether there will be a different explanation for the differences between the experimentally observed rates and our current results. For heavy mesons, ChPT does not apply, instead theoretical predictions for B decays into two lepton pairs have been performed by using QCD factorization [24, 25, 26, 27, 28] or Vector Meson Dominance [29, 30]. The prediction presented in [30] for the $B^+ \to \mu^+\,\nu_\mu\,\mu^+\,\mu^-$ branching ratio, however, is almost four times larger than the experimental upper limit obtained in Ref. [11], while the value from [25] is only marginally compatible with the upper limit. It is therefore clear that a non-perturbative, model independent lattice evaluation of the SD form factors is required.

The main numerical results of this work are the following[1]

- We computed on the lattice the coefficients for a polynomial and a pole-like parametrization of the structure dependent form factors entering $K^+ \to \ell^+ \nu_\ell \ell'^+ \ell'^-$ decays. They read

$$F_{\text{poly}}(x_k, x_q) = a_0 + a_k x_k^2 + a_q x_q^2 \,, \tag{4}$$

and

$$F_{\text{pole}}(x_k, x_q) = \frac{A}{(1 - R_k x_k^2)\left(1 - R_q x_q^2\right)} \tag{5}$$

where x_k and x_q are the normalized invariant masses of the two leptonic pairs $\ell^+,\ \nu_\ell$ and $\ell'^+,\ \ell'^-$. The numerical lattice results for all the parameters appearing in Eqs. (4) - (5) are collected in the following table.

	a_0	a_k	a_q	A	R_k	R_q
H_1	0.1755(88)	0.113(30)	0.086(24)	0.1792(78)	0.453(88)	0.40(10)
H_2	0.199(21)	0.341(84)	-0.03(3)	0.217(17)	0.87(12)	-0.2(2)
F_A	0.0300(43)	0.04(4)	0.00(1)	0.0320(30)	0.74(50)	0.0(3)
F_V	0.0912(39)	0.044(18)	0.0246(59)	0.0921(38)	0.38(13)	0.233(49)

Table 1: *Values of the fit parameters for all the form factors, as obtained from the polynomial and pole-like fits of Eqs. (2.4) and (2.5).*

We considered two different parametrizations in order to check that the result of the interpolation would not depend significantly on the choice of the functional form, and indeed the two fits give almost the same results in the whole phase space of the processes, as it is shown in Figs. 2.5 and 2.6 in Chapter 2.

- By employing our numerical predictions for the form factors, the branching ratios for all the different channels of $K^+ \to \ell^+ \nu_\ell \ell'^+ \ell'^-$ have been evaluated. The lattice predictions we obtained are

$$\begin{aligned}
\text{BR}\left[K^+ \to e^+ \nu_e \mu^+ \mu^-\right] &= 0.762(49) \times 10^{-8} \,, &(6)\\
\text{BR}\left[K^+ \to \mu^+ \nu_\mu e^+ e^-\right] &= 8.26(13) \times 10^{-8} \quad \text{with } m_{ee} > 140 \text{ MeV} &(7)\\
\text{BR}\left[K^+ \to \mu^+ \nu_\mu \mu^+ \mu^-\right] &= 1.178(35) \times 10^{-8} \,, &(8)\\
\text{BR}\left[K^+ \to e^+ \nu_e e^+ e^-\right] &= 1.95(11) \times 10^{-8} \quad \text{with } m_{ee} > 140 \text{ MeV} \,. &(9)
\end{aligned}$$

[1]We remark that the lattice analysis is affected by systematic uncertainties due to the missing chiral, continuum and infinite-volume extrapolations that will be studied in future works. As a consequence, all the present numerical results should be taken as qualitative ones and as an indication of the feasibility of the method, and not as definitive physical results.

Much more details can be found in Chapter 3, Tabs. 3.1 - 3.4, where the values are compared to other predictions, experimental data, and the trivial point-like contribution to each channel is separated.

This thesis is structured as follows,

- In Chapter 1 we show in detail the method we developed for the lattice evaluation of the SD form factors. We start defining the different contributions to the amplitude of the process. The SD form factors are then defined from the Lorentz decomposition of the hadronic tensor, which encodes the strong dynamics involved in the interaction between the decaying meson and the virtual photon. Then we proceed by defining the Euclidean three-point lattice correlator employed in the simulation, and we study its relation to the physical hadronic tensor. In the final section of this chapter, we build the lattice estimators from which the value for SD form factors can be extract. Two delicate issues that are discussed in detail in the chapter are the Wick rotation to Euclidean time and the subtraction of the point-like term from the hadronic tensor computed on the lattice. Wick rotation is a necessary step of any lattice computation, and dependably on the analytic structure of the correlator at hand it can give rise to unphysically contributions exponentially enhanced by the size of the lattice. This issue is intimately related to the presence of internal states propagating in the correlator with less energy of the external ones [31]. To keep under control these potentially dangerous effects we studied in detail the kinematical limitation of the lattice computation finding that contributions of the form $K \to \pi\pi\, \ell\nu_\ell \to \ell\nu_\ell\gamma$, with an on-shell $\pi\pi\, \ell\nu_\ell$ intermediate state, arise in the region of phase space in which $k^2 > 4m_\pi^2$, where k is the four-momentum of the virtual photon. Besides the exponentially enhanced contributions, this also leads to finite-volume effects, which decrease only as inverse powers of the volume and not exponentially [32, 33, 34]. In our computation and also that in Ref. [22], the kaon mass is smaller than twice the pion mass, $m_K < 2m_\pi$, and so the problem does not occur. This issue, together with a complete study of all the systematic effects (due to discretization, finite volume and unphysical quark masses) will be the object of our future studies. The second issue, instead, arises if a naive subtraction of the point-like term from the hadronic tensor is performed on the lattice. As shown in [6], residual discretization errors in the subtraction appear in the form factor estimators enhanced by inverse powers of the photon momentum, and are divergent in the infrared limit. We generalize the method proposed in [6] in order to reduce this dangerous discretization effect in our lattice computation.

- In Chapter 2 we apply the formalism developed in the previous chapter in the first lattice determination of the structure dependent form factors entering $K^+ \to \ell^+\, \nu_\ell\, \ell'^+\, \ell'^-$ decays. We first perform the lattice simulation at fifteen different kinematics (generic spatial momenta can be assigned in our simulation, since we employ twisted boundary conditions to the valence quark fields [35]). These fifteen points have been chosen equally spaced in the relevant phase space region, and they are interpolated in order to fit a continuum function of the kinematical variables for each of the form factors. The results of the fits are then compared with the Chiral Perturbation Theory predictions at next-to-leading order and with the values extracted from the experiments assuming the Vector Meson Dominance model to describe the kinematical dependence of the form factors. At the end of the chapter, we check the consistency of our lattice determination with the one obtained in [6] concerning the real photon emission.

- Finally, in Chapter 3 we use the numerical lattice predictions obtained in Chapter 2 for the SD form factors in order to compute the differential decay rates and the branching ratios for the $K^+ \to \ell^+ \nu_\ell \ell'^+ \ell'^-$ processes. The decay rate formulae and the integration over the phase space are sensibly different, dependably in the final state there are identical leptons $\ell = \ell'$ or not. If not, the differential decay rate can be integrated analytically in the phase space variables, except for the two from which the form factors depend. Instead, when $\ell = \ell'$, the contribution coming from the exchange of the two identical leptons must be added to the amplitude. As a consequence, in the full amplitude the form factors appear evaluated at different values of their variables, and the full four-body phase space must be integrated numerically via Monte Carlo methods. For each of the four possible channels, our lattice prediction for the $K^+ \to \ell^+ \nu_\ell \ell'^+ \ell'^-$ decays is compared with experimental data, ChPT predictions and the only other lattice computation [22].

- In order to help the reader and simplify the text, we transferred the supplementary material which is not central to explain the original results of this thesis and most of the technical details in the three appendices. In Appendix A we present the basic notation and the conventions used in this thesis concerning the $SU(3)$ generators, the Dirac matrices and the Grassmann algebra. Appendix B is devoted to an introduction to Lattice QCD. We start from the path-integral formulation of quantum field theory, then we show a possible way to discretize the continuum QCD action, namely the Wilson twisted mass action. Discretization is the regularization of the theory, and to obtain physical predictions it is necessary to perform a renormalization procedure. We present a nonperturbative renormalization scheme known as RI-MOM scheme, to be implemented when performing the continuum limit and to compute the renormalization constants relating bare lattice operators to the physical continuum ones. We also present some statistical methods to be used in actual simulations and we show how two- and three-point Green functions computed on the lattice can be used to extract the hadronic quantities. Finally, The explicit, partially integrated, decay rate formulae for the processes with different leptons in the final state are given in Appendix C.

Chapter 1

Lattice evaluation of the structure dependent form factors

In this chapter we present our method for computing on the lattice the structure-dependent form factors contributing to the processes $P^+ \to \ell^+ \, \nu_\ell \, \ell'^+ \, \ell'^-$, where P^+ is a generic charged pseudoscalar meson, ℓ^+ and ν_l are respectively a generic charged lepton and its corresponding neutrino, while ℓ'^+ and ℓ'^- constitute an additional charged leptonic pair, that can be either the same flavor of ℓ or different. Most of the content presented in this Chapter have been published in our article:

- G. Gagliardi, F. Sanfilippo, S. Simula, V. Lubicz, F. Mazzetti, G. Martinelli, C. T. Sachrajda, and N. Tantalo *Virtual photon emission in leptonic decays of charged pseudoscalar mesons* Phys. Rev. D, 105 (2022) 114507 [arXiv:2202.03833 [hep-lat]] [1]

1.1 The matrix element, the hadronic tensor, and the structure dependent form factors

At lowest order in the electroweak interaction, $P^+ \to \ell^+ \, \nu_\ell \, \ell'^+ \, \ell'^-$ decays are obtained from the diagrams depicted in Fig. 1.1, where u and $\overline{d}$ represent an up-type of quark and a down-type of anti-quark respectively, that are the valence quark content which constitutes a generic charged pseudoscalar meson P^+. The virtual photon γ can be emitted from the final charged lepton (Fig. 1.1a), or from one of the two valence quarks (Figs. 1.1b and 1.1c), or finally it can be emitted from one sea-quark (Figs. 1.1d), whose generic flavour is indicated with f. If $\ell = \ell'$, we also need to consider the diagrams obtained by interchanging the two identical charged leptons, which are depicted in Fig. 1.2. Indeed, when $\ell = \ell'$, the final state in the diagrams of Fig. 1.1 is indistinguishable from the one of the diagrams in Fig. 1.2.

The two close dots represent the action of the weak interaction, that at low energy can be described by a contact interaction of four fields, that is the effective Fermi Hamiltonian, given by

$$\mathcal{H}_{\mathcal{F}} = \frac{4G_F}{\sqrt{2}} J^\mu_{weak} \, J^\dagger_{weak,\,\mu} \,, \tag{1.1}$$

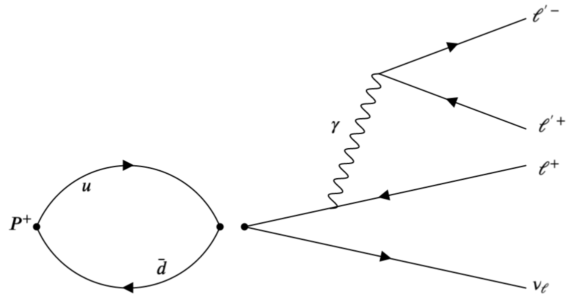

(a) *Photon emission from charged lepton.*

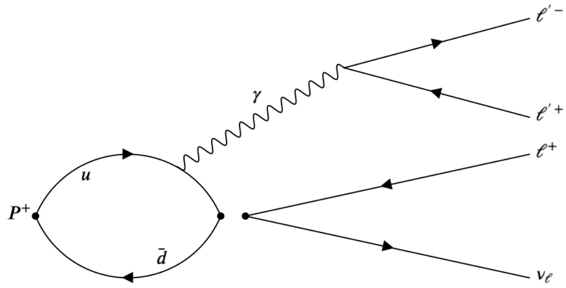

(b) *Photon emission from up-type valence quark.*

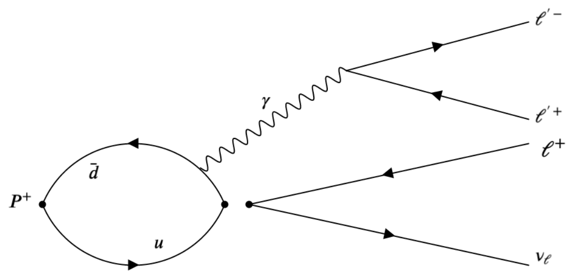

(c) *Photon emission from down-type valence anti-quark.*

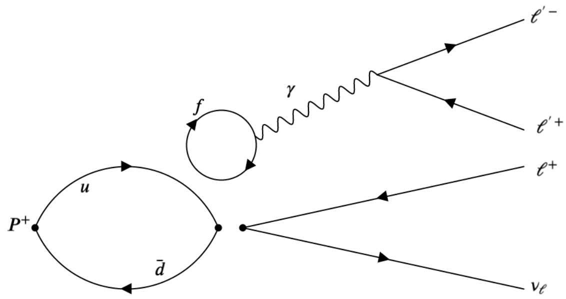

(d) *Photon emission from sea quark with generic flavour f.*

Figure 1.1: *Diagrams contributing to the process $P^+ \to \ell^+ \, \nu_\ell \, \ell'^+ \, \ell'^-$.*

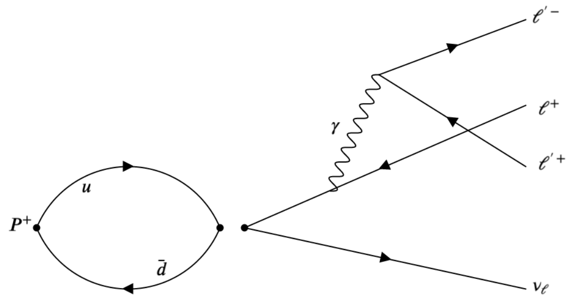

(a) *Photon emission from charged lepton*

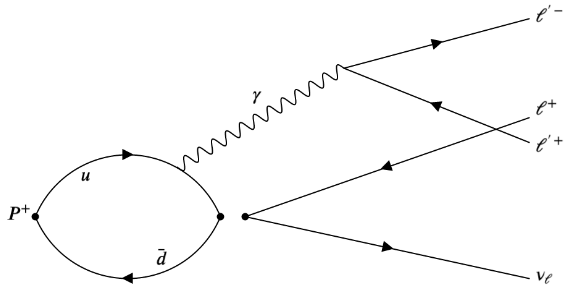

(b) *Photon emission from up-type valence quark.*

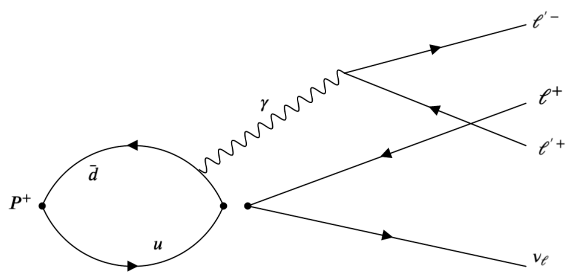

(c) *Photon emission from down-type valence anti-quark.*

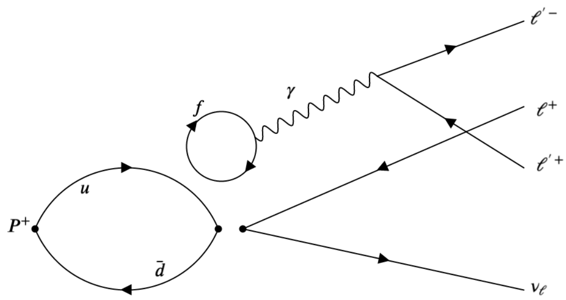

(d) *Photon emission from sea quark with generic flavour f.*

Figure 1.2: *Exchange diagrams, contributing to the $P^+ \to \ell^+ \, \nu_\ell \, \ell'^+ \, \ell'^-$ process, when $\ell = \ell'$.*

where J^μ_{weak} represents the charged weak current of the Standard Model. In terms of the quark and lepton fields, it reads

$$J^\mu_{weak} = \sum_{i=1}^{3} V_{u_i d_i}\, \overline{\psi}_{u_i}\gamma^\mu(1-\gamma_5)\psi_{d_i} + \overline{\psi}_{\nu_i}\gamma^\mu(1-\gamma_5)\psi_{\ell_i}\,, \tag{1.2}$$

where the index i refers to the flavour generation of both the quark and lepton isospin doublet and $V_{u_i d_i}$ is the CKM matrix element relating the up-type and the down-type quarks.

G_F is the Fermi coupling constant whose value is conventionally defined from the measured value of the muon life-time using the expression [36]

$$\frac{1}{\tau_\mu} = \frac{G_F^2 m_\mu^5}{192\pi^3}\left[1-\frac{8m_e^2}{m_\mu^2}\right]\left[1+\frac{\alpha}{2\pi}\left(\frac{25}{4}-\pi^2\right)\right]. \tag{1.3}$$

The Review of Particle Physics from the Particle Data Group [8] reports the value

$$G_F = 1.1663787(6)\times 10^{-5}\ \mathrm{GeV}^{-2}\,. \tag{1.4}$$

The error made by using the Fermi Hamiltonian instead of the SM is of order $O(q^2/M_W^2)$, where q is the transferred momentum of the process (i.e. the momentum of the exchanged W boson). For the decays that we consider in this thesis, we have $q^2 < m_P^2 << M_W^2$.

1.1.1 Diagram amplitudes

We now consider the case $\ell \neq \ell'$, and we write down the amplitudes corresponding to the *direct* diagrams (Fig. 1.1). The contributions from the corresponding *exchange* diagrams (Fig. 1.2) can be obtained from the original one by simply interchanging the external momenta assigned to the two identical leptons in the amplitudes.

The diagram in which the photon is emitted from the final lepton, Fig. 1.1a, can readily be computed in perturbation theory, with the meson decay constant as the only required non-perturbative input. By using the standard Feynman rules for QED, the amplitude associated to Fig. 1.1a reads

$$\begin{aligned} i\mathcal{M}_a \quad &= \quad \frac{G_F\,V_{ud}^*}{\sqrt{2}}\,\frac{e^2}{k^2}\,\langle 0|\overline{\psi}_u\,\gamma^\alpha\,(1-\gamma_5)\,\psi_d|P(p)\rangle \\ &\times\ \left[\overline{u}_{\nu_\ell}(p_{\nu_\ell})\,\gamma_\alpha(1-\gamma_5)\,\frac{-(p_{\ell^+}+k)+m_\ell}{m_\ell^2-(p_{\ell^+}+k)^2}\,\gamma_\mu\, v_\ell(p_{\ell^+})\right]\overline{u}_{\ell'}(p_{\ell'^-})\,\gamma^\mu\, v_{\ell'}(p_{\ell'^+})\,, \end{aligned} \tag{1.5}$$

where $k=(E_\gamma,\boldsymbol{k})$ is the four-momentum of the virtual photon and $p=(E,\boldsymbol{p})$ is that of the incoming pseudoscalar meson P. The meson and photon energies satisfy $E=\sqrt{m_P^2+\boldsymbol{p}^2}$ and $E_\gamma=\sqrt{k^2+\boldsymbol{k}^2}$. ψ_u and ψ_d indicate the fields of an up-type or a down-type quark. u_{ν_ℓ}, $u_{\ell'}$, v_ℓ and $v_{\ell'}$ are the Dirac spinors for the various leptons and anti-leptons, denoted by the subscript, while e is the value of the positron electric charge. p_ℓ, p_{ν_ℓ}, $p_{\ell'^+}$ and $p_{\ell'^-}$ are the external four-momenta of the four final leptons and m_ℓ is the mass of the charged lepton ℓ.

Now we can substitute

$$\langle 0|\bar{\psi}_d\, \gamma^\alpha (1-\gamma_5)\, \psi_u|P\,(p)\rangle = -i\, f_P\, p^\alpha, \tag{1.6}$$

and after some algebraic manipulation we arrive to the expression

$$\begin{aligned} i\mathcal{M}_a \;&=\; -i\frac{G_F\, V_{ud}^*}{\sqrt{2}}\frac{e^2}{k^2} f_P \Big[\overline{u}_{\nu_\ell}(p_{\nu_\ell})\, \gamma^\mu\, (1-\gamma_5)\, v_\ell(p_{\ell^+}) \\ &\quad + m_\ell\, \overline{u}_{\nu_\ell}(p_{\nu_\ell})\, (1+\gamma_5)\, \frac{2\, p^\mu_{\ell^+} + \not{k}\, \gamma^\mu}{m_\ell^2 - (p_{\ell^+}+k)^2}\, v_\ell(p_{\ell^+})\Big] \overline{u}_{\ell'}(p_{\ell'^-})\gamma_\mu\, v_{\ell'}(p_{\ell'^+})\,. \end{aligned} \tag{1.7}$$

We notice that in Eq. (1.7) there are no hadronic parameters except for the meson decay constant f_P, whose value is precisely known from Lattice QCD. Thus, as we said before, this contribution to the matrix element is straightforward to evaluate and to take into account.

Instead, the theoretical challenge consists in evaluating the contribution to the total matrix element coming from the other diagrams, Figs. 1.1b - 1.1d, where the photon is emitted from the meson and interacts nonperturbatively with its internal hadronic structure.

The diagrams in Figs. 1.1b - 1.1d correspond to the following contribution to the matrix element:

$$\begin{aligned} i\mathcal{M}_{b-d} \;&=\; i\,\frac{G_F\, V_{ud}^*}{\sqrt{2}}\frac{e^2}{k^2}\, \overline{u}_{\ell'}(p_{\ell'^-})\, \gamma_\mu\, v_{\ell'}(p_{\ell'^+}) \int d^4x\, e^{ik\cdot x}\, \langle 0|T\,[J^\mu_{\rm em}(x) J^\nu_W(0)]|P(p)\rangle \\ &\quad \times\, \overline{u}_{\nu_\ell}(p_{\nu_\ell})\, \gamma_\nu\, (1-\gamma_5)\, v_\ell(p_\ell)\,, \end{aligned} \tag{1.8}$$

The operators

$$J^\mu_{\rm em}(x) = \sum_f q_f \bar{\psi}_f(x)\gamma^\mu\psi_f(x) \qquad J^\nu_W(x) = J^\nu_V(x) - J^\nu_A(x) = \bar{\psi}_d(x)\, (\gamma^\nu - \gamma^\nu\gamma_5)\, \psi_u(x)\,, \tag{1.9}$$

are respectively the electromagnetic hadronic current and the hadronic weak current expressed in terms of the quark fields ψ_f having electric charge q_f in units of the charge of the positron.

We notice that, in Eq. (1.8), the matrix element is factorized in an hadronic tensor which is contracted with the leptonic currents. That is, the non-perturbative contribution to the matrix element is entirely encoded in the following hadronic tensor:

$$H^{\mu\nu}(k,p) = \int d^4x\, e^{ik\cdot x}\, \langle 0|T[J^\mu_{\rm em}(x) J^\nu_W(0)]|P(p)\rangle\ . \tag{1.10}$$

When working with such matrix elements, it is useful to separate the kinematics from the dynamics, performing the decomposition into form factors. Form factors are scalar, Lorentz-invariant functions of the kinematical invariants of the process, encoding all the non-perturbative strong dynamics. In this way we will be able to write down the whole matrix element, as an expression of the unknown form factors. Evaluating on the lattice the form factors will then allow us to compute the squared amplitude, so to reconstruct the differential decay rates and the branching ratios for the different channels.

1.1.2 Form factor decomposition of the hadronic tensor

We now perform in detail the form factor decomposition of the hadronic tensor of Eq. (1.32), following Bijnens et al. [23].

In order to isolate the structure dependent contribution, as a first step we separate in the hadronic tensor the contribution given by one-particle internal states from the one coming from multi-particle internal states, that is

$$H^{\mu\nu} = H^{\mu\nu}_{1\text{P}} + H^{\mu\nu}_{\text{MP}} \,. \tag{1.11}$$

The first term in Eq. (1.11) is obtained by considering the electromagnetic scattering of the initial meson P, which propagates as a virtual state before being annihilated into the vacuum due to the action of the weak current. This contribution reads

$$\begin{aligned} H^{\mu\nu}_{1\text{P}} &\equiv \langle 0|J^\nu_W|P(p-k)\rangle \, \frac{i}{(p-k)^2 - m_P^2} \left\langle P^+(p-k)\middle|J^\mu_{\text{em}}(k)\middle|P(p)\right\rangle \\ &= -f_P \, F^P_{\text{em}}(k^2) \, \frac{(2p-k)^\mu (p-k)^\nu}{(p-k)^2 - m_P^2} \\ &= -f_P \, \left(1 + \overline{F}(k^2)\right) \, \frac{(2p-k)^\mu (p-k)^\nu}{(p-k)^2 - m_P^2} \,. \end{aligned} \tag{1.12}$$

$F^P_{\text{em}}(k^2) = 1 + \overline{F}(k^2)$ is the electromagnetic form factor of the decaying meson, where we separated the term which depends on its internal hadronic structure, $\overline{F}(k^2)$, from the contribution coming from the point-like approximation of the meson, which is equal to one.

The contribution coming from multi-particle internal states, can be decomposed in the most general structure as

$$\begin{aligned} H^{\mu\nu}_{\text{MP}} = & -i \, \frac{F_V}{m_P} \, \epsilon^{\mu\nu\alpha\beta} \, k_\alpha \, p_\beta + \frac{F_A}{m_P} (p-k)^\mu \, k^\nu + \frac{H_1}{m_P} k^\mu \, k^\nu + A_1 \, k^2 \, (p-k)^\mu \, (p-k)^\nu \\ & + A_2 \, g^{\mu\nu} + A_3 \, k^\mu (p-k)^\nu \,, \end{aligned} \tag{1.13}$$

where all the form factors are functions of k^2 e $(p-k)^2$, and $\epsilon^{\mu\nu\alpha\beta}$ is the totally antisymmetric tensor with $\epsilon^{01234} = 1$.

However, not all these form factors are independent, because the tensor $H^{\mu\nu}$ must satisfy the Ward identities, derived in [23],

$$k_\mu \, H^{\mu\nu} = f_P \, p^\nu \tag{1.14}$$

which imply

$$\begin{aligned} [k \cdot (p-k)] \, \frac{F_A}{m_P} + k^2 \frac{H_1}{m_P} + A_2 &= f_P \,, \\ k^2 \, [k \cdot (p-k)] \, A_1 + k^2 \, A_3 &= f_P \, \overline{F}(k^2) \,, \end{aligned} \tag{1.15}$$

and so we have

$$\begin{aligned} A_2 &= f_P - k^2 \frac{H_1}{m_P} - [k \cdot (p-k)] \frac{F_A}{m_P} \,, \\ A_3 &= f_P \, \frac{\overline{F}(k^2)}{k^2} - [k \cdot (p-k)] \, A_1 \,. \end{aligned} \tag{1.16}$$

Now we can replace these expressions in the general decomposition of $H^{\mu\nu}$ and we obtain

$$\begin{aligned} H^{\mu\nu} &= f_P \Big\{ g^{\mu\nu} - \frac{(2p-k)^\mu (p-k)^\nu}{(p-k)^2 - m_P^2} \Big\} + \frac{F_A}{m_P} \{ (k \cdot p - k^2) g^{\mu\nu} - (p-k)^\mu k^\nu) \} \\ &+ \frac{H_1}{m_P} \{ k^2 g^{\mu\nu} - k^\mu k^\nu \} - i \frac{F_V}{m_P} \epsilon^{\mu\nu\alpha\beta} k_\alpha p_\beta \\ &+ \Big\{ 2 f_P \frac{\overline{F}(k^2)}{[m_P^2 - (p-k)^2] k^2} - A_1 \Big\} [(k \cdot p - k^2) k^\mu - k^2 (p-k)^\mu] (p-k)^\nu \,. \end{aligned} \tag{1.17}$$

Now we can rename

$$\frac{H_2}{m_P \left[(p-k)^2 - m_P^2 \right]} \equiv \Big\{ 2 f_P \frac{\overline{F}(k^2)}{[m_P^2 - (p-k)^2] k^2} - A_1 \Big\} \tag{1.18}$$

and so we have obtained our final expression:

$$H^{\mu\nu} = H^{\mu\nu}_{\mathrm{pt}} + H^{\mu\nu}_{\mathrm{SD}} \,, \tag{1.19}$$

$$H^{\mu\nu}_{\mathrm{pt}} = f_P \left[g^{\mu\nu} - \frac{(2p-k)^\mu (p-k)^\nu}{(p-k)^2 - m_P^2} \right] \,, \tag{1.20}$$

$$\begin{aligned} H^{\mu\nu}_{\mathrm{SD}} &= \frac{H_1}{m_P} \left(k^2 g^{\mu\nu} - k^\mu k^\nu \right) + \frac{H_2}{m_P} \frac{[(k \cdot p - k^2) k^\mu - k^2 \, (p-k)^\mu]}{(p-k)^2 - m_P^2} \, (p-k)^\nu \\ &+ \frac{F_A}{m_P} \left[(k \cdot p - k^2) g^{\mu\nu} - (p-k)^\mu k^\nu \right] - i \frac{F_V}{m_P} \epsilon^{\mu\nu\alpha\beta} k_\alpha p_\beta \,. \end{aligned} \tag{1.21}$$

With this decomposition we have separated the point-like contribution to the hadronic tensor, that is $H^{\mu\nu}_{\mathrm{pt}}$, from the structure-dependent (SD) one, which is $H^{\mu\nu}_{\mathrm{SD}}$. The former depends only on the meson decay constant f_P and it can be obtained directly by assuming a point-like meson, that is by employing the Feynman rules of scalar QED, as it has been done in [37]. The point-like approximation is valid in the infrared region of photon momenta, where the soft photon cannot resolve the internal structure of the hadron, and so it interacts with it as if the decaying meson were an elementary particle.

Instead, the structure-dependent contribution $H^{\mu\nu}_{\mathrm{SD}}$ describes the interaction between the virtual photon and the hadronic structure of the pseudoscalar meson, and it vanishes in the infrared limit of vanishing photon momentum. The SD form factors, H_1, H_2, F_A and F_V, are scalar functions of k^2 and $(p-k)^2$. Note that, compared to similar decompositions, see for example Eq. (B4) of Ref. [37], we have modified the definitions of $H_{1,2}$ by a factor of m_P and introduced the denominator

$(p-k)^2 - m_P^2$ in the factor multiplying H_2. With the definitions in Eq. (1.21) all four form factors are now dimensionless, and it can be shown that they are finite in the infrared limit.

The main goal of this thesis is to compute the SD form factors, using lattice QCD simulation, and with them to reconstruct the full matrix element and subsequently the branching ratio for the decay. We will explicitly separate the point-like contribution from the one which depends on the hadronic structure. This separation is instructive, because the point-like contribution is trivial to compute and well known. The structure dependent term of the decay rate encodes instead the genuine non-perturbative interaction of the virtual photon with the internal structure of the meson, and represents therefore an interesting quantity to predict and to compare with the experiments.

Now that we have decomposed the hadronic tensor $H^{\mu\nu}$ into form factors, we can write down our final expression for the total amplitude of the process.

1.1.3 Matrix element for $P^+ \to \ell^+ \nu_\ell \ell'^+ \ell'^-$ decays

The first contribution we consider is the one coming from the point-like term of the hadronic tensor, that is

$$
\begin{aligned}
i\mathcal{M}_{H_{\rm pt}} &= i\,\frac{G_F\,V_{ud}^*}{\sqrt{2}}\,\frac{e^2}{k^2}\,H_{\rm pt}^{\mu\nu}\left[\overline{u}_{\nu_\ell}(p_{\nu_\ell})\,\gamma_\nu\,(1-\gamma_5)\,v_\ell(p_\ell)\right]\left[\overline{u}_{\ell'}(p_{\ell'^-})\,\gamma_\mu\,v_{\ell'}(p_{\ell'^+})\right] \\
&= i\,\frac{G_F\,V_{ud}^*}{\sqrt{2}}\,\frac{e^2}{k^2}\,f_P\left[g^{\mu\nu} - \frac{(2p-k)^\mu(p-k)^\nu}{(p-k)^2-m_P^2}\right] \\
&\quad\times\left[\overline{u}_{\nu_\ell}(p_{\nu_\ell})\,\gamma_\nu\,(1-\gamma_5)\,v_\ell(p_\ell)\right]\left[\overline{u}_{\ell'}(p_{\ell'^-})\,\gamma_\mu\,v_{\ell'}(p_{\ell'^+})\right]. \qquad (1.22)
\end{aligned}
$$

After contracting the Lorentz indices and doing some algebraic manipulation, we arrive to the expression

$$
\begin{aligned}
i\mathcal{M}_{H_{\rm pt}} &= -i\,\frac{G_F\,V_{ud}^*}{\sqrt{2}}\,\frac{e^2}{k^2}\,f_P\Big[-\overline{u}_{\nu_\ell}(p_{\nu_\ell})\,\gamma^\mu\,(1-\gamma_5)\,v_\ell(p_{\ell^+}) \\
&\quad + m_\ell\frac{(2p-k)^\mu}{2p\cdot k-k^2}\overline{u}_{\nu_\ell}(p_{\nu_\ell})\,(1+\gamma_5)\,v_\ell(p_\ell)\Big]\left[\overline{u}_{\ell'}(p_{\ell'^-})\,\gamma_\mu\,v_{\ell'}(p_{\ell'^+})\right]. \qquad (1.23)
\end{aligned}
$$

This contribution, coming from the point-like term in the hadronic tensor $H_{\rm pt}$, must be combined with the contribution corresponding to the diagram of Fig. 1.1a, in which the photon is emitted from the final lepton, in order to get the total point-like contribution to the amplitude. This is the contribution to the process that is simply proportional to f_P and that we would have for the decay of a point-like, elementary meson.

By putting together $i\mathcal{M}_{H_{\rm pt}}$ from Eq. (1.23) with $i\mathcal{M}_a$ from Eq. (1.7), we get the total point-like contribution to the matrix element

$$
i\mathcal{M}_{\rm pt} \equiv i\mathcal{M}_a + i\mathcal{M}_{H_{\rm pt}} = -i\frac{G_F}{\sqrt{2}}\,V_{ud}^*\,\frac{e^2}{k^2}\,\bar{u}(p_{\ell'^-})\gamma_\mu v(p_{\ell'^+})\;f_P\,L^\mu(p_{\ell'^+},p_{\ell'^-},p_{\ell^+},p_{\nu_\ell})\,, \qquad (1.24)
$$

with

$$L^\mu(p_{\ell'^+}, p_{\ell'^-}, p_{\ell^+}, p_{\nu_\ell}) \;=\; m_\ell\, \bar{u}(p_{\nu_\ell})(1+\gamma_5)\left\{\frac{2p^\mu - k^\mu}{2p\cdot k - k^2} - \frac{2p^\mu_{\ell^+} + \not{k}\gamma^\mu}{2p_{\ell^+}\cdot k + k^2}\right\} v(p_{\ell^+})\,. \tag{1.25}$$

What remains to consider in the amplitude is the contribution coming from the structure dependent form factors, i.e. the contribution that actually contains information about the internal structure of the meson and its interaction with the virtual photon. This is given by

$$i\mathcal{M}_{\rm SD} = i\frac{G_F}{\sqrt{2}}\, V^*_{ud}\, \frac{e^2}{k^2}\, \bar{u}(p_{\ell'^-})\gamma_\mu v(p_{\ell'^+})\, H^{\mu\nu}_{\rm SD}(\,p,\,k)\, l_\nu(p_{\ell^+}, p_{\nu_\ell})\,, \tag{1.26}$$

with

$$l^\mu(p_{\ell^+}, p_{\nu_\ell}) \;=\; \bar{u}\,(p_{\nu_\ell})\,\gamma^\mu\,(1-\gamma_5)\,v(p_{\ell^+})\,. \tag{1.27}$$

We now have all the ingredients to write down the final expression for the total matrix element contributing to the $P^+ \to \ell^+\,\nu_\ell\,\ell'^+\,\ell'^-$ decays. It reads

$$i\mathcal{M} = -i\frac{G_F}{\sqrt{2}}\, V^*_{ud}\, \frac{e^2}{k^2}\; \bar{u}(p_{\ell'})\gamma_\mu v(p_{\ell'^+})\;\Big[f_P L^\mu(p_{\ell'^+}, p_{\ell'^-}, p_{\ell^+}, p_{\nu_\ell}) - H^{\mu\nu}_{\rm SD}(p,k)\, l_\nu(p_{\ell^+}, p_{\nu_\ell})\Big]\,. \tag{1.28}$$

In Eq. (1.28), we remark once again that the first term in the square parentheses gives the decay rate in the approximation in which the decaying meson is treated as a point-like particle and includes the radiation from both the meson and charged lepton [1]. Except for the meson decay constant f_P, the non-perturbative contribution to the rate is entirely contained in the second term of Eq. (1.28), which contains the structure dependent form factors that describe the interaction between the virtual photon and the internal hadronic structure of the decaying meson.

When $\ell = \ell'$, since the final-state positively-charged leptons are indistinguishable, the exchange contribution, in which the momenta $p_{\ell'^+}$ and p_{ℓ^+} are interchanged, must be added to the amplitude $\mathcal{M}$, resulting in the replacement

$$\mathcal{M}(p_{\ell'^+}, p_{\ell'^-}, p_{\ell^+}, p_{\nu_\ell}) \to \mathcal{M}(p_{\ell'^+}, p_{\ell'^-}, p_{\ell^+}, p_{\nu_\ell}) - \mathcal{M}(p_{\ell^+}, p_{\ell'^-}, p_{\ell'^+}, p_{\nu_\ell})\,. \tag{1.29}$$

Eqs. (1.28) and (3.4), together with Eqs. (1.21), (1.25) and (1.27), are the final formulae for the matrix element of the process, that we will use in Chap. 3 to compute the squared amplitude, the differential decay rate and the branching ratio.

1.1.4 The real photon emission $P^+ \to \ell^+\,\nu_\ell\,\gamma$

The hadronic tensor $H^{\mu\nu}$ of Eqs. (1.19) - (1.21), also enters the computation of the real radiative correction to leptonic decays, that is of the process $P^+ \to \ell^+\,\nu_\ell\,\gamma$. In that case, however, not all the form factors contribute to the decay rate. Indeed, for real photon we have $k^2 = 0$ and for physical gauges the polarization vector satisfies $\epsilon(k)\cdot k = 0$. In the decay rate for the process $P^+ \to \ell^+\,\nu_\ell\,\gamma$,

[1] This term is frequently referred to as the *inner-brehmstrahlung* contribution.

it then appears the quantity

$$H^\nu \quad = \quad \epsilon^*_\mu \, H^{\mu\nu} \, , \tag{1.30}$$

for which we have

$$H^\nu_{\rm SD} = -\epsilon^*_\mu \left\{ i \frac{F_V}{m_P} \epsilon^{\mu\nu\alpha\beta} k_\alpha p_\beta - \frac{F_A}{m_P} \left(\, k \cdot p \, g^{\mu\nu} - p^\mu k^\nu \, \right) \right\} \tag{1.31}$$

showing that the structure dependent contribution can be parametrized in terms of only two form factors F_V and F_A, also they depend just on the only independent Lorentz invariant kinematical variables of the process $(p-k)^2$. The lattice computation of F_A and F_V in real photon emission and of the corresponding contributions to the decay rates has been performed for the first time in [6]. The work of this thesis is a generalization of the method presented there, in order to compute for the first time all the form factors that contribute to the virtual photon emission and to obtain an *ab initio* theoretical prediction for the branching ratios, with non-perturbative accuracy in the strong interactions. There are several difficulties in this generalization, some of them are the following

- The correlators computed on the lattice is a linear combination of four structure dependent form factors, instead than just two of them.
- All the form factors depend on two independent kinematical variables, instead than just one.
- The virtuality of the photon may give rise to internal hadronic states with less energy than the external ones, an issue that prevents from performing a naive Wick rotation and relating the Euclidean lattice correlators to the Minkowskian physical one.
- The method presented in [6] for performing the subtraction of the point-like term to the lattice correlators including lattice artifacts to all orders in the lattice spacing is not usable for some of the lattice correlators needed for the study of virtual photon emission.
- The squared amplitude of the process, in particular when there are two identical charged leptons in the final state, consists in thousands of terms, which need to be integrated in the phase space of four final particles, making the computation of the decay rates very lengthy and complex.

The first four issues will be addressed in the rest of this chapter, devoted to the lattice computation of the structure dependent form factors. Instead, the determination of the branching ratios and the comparison with the experiments will be the object of Chapter 3.

1.2 The hadronic tensor in Euclidean space

In order to show how the hadronic tensor can be extracted from Euclidean correlation functions, it is useful to express $H^{\mu\nu}(k,p)$ in terms of the contributions coming from the two different time–orderings. This is done starting from the definition of the hadronic tensor

$$H^{\mu\nu}(k,p) = \int d^4x \, e^{ik\cdot x} \, \langle 0 | T[J^\mu_{\rm em}(x) J^\nu_W(0)] | P(p) \rangle \ , \tag{1.32}$$

separating the two time-orderings $t_x < 0$ and $t_x > 0$, where $x = (t_x, \boldsymbol{x})$, and inserting a complete set of intermediate states. Defining

$$J^\mu_{\rm em}(\boldsymbol{k}) = \int d^3x \, e^{-i\boldsymbol{k}\cdot\boldsymbol{x}} J^\mu_{\rm em}(0,\boldsymbol{x}) \,, \tag{1.33}$$

we have

$$H^{\mu\nu}(k,p) = H_1^{\mu\nu}(k,p) + H_2^{\mu\nu}(k,p) \,, \tag{1.34}$$

$$\begin{aligned}
H_1^{\mu\nu}(k,p) &= \int_{-\infty}^0 dt_x \, e^{it_x E_\gamma} \, \langle 0|J^\nu_W(0) \, e^{it_x H} J^\mu_{\rm em}(\boldsymbol{k}) \, e^{-it_x H}|P(p)\rangle \\
&= \sum_{n_f:\boldsymbol{p}_{n_f}=\boldsymbol{p}-\boldsymbol{k}} \frac{\langle 0|J^\nu_W(0)|n_f\rangle \, \langle n_f|J^\mu_{\rm em}(0)|P(p)\rangle}{2E_{n_f}} \int_{-\infty}^0 dt_x \, e^{it_x(E_\gamma+E_{n_f}-E)} \\
&= -i \sum_{n_f:\boldsymbol{p}_{n_f}=\boldsymbol{p}-\boldsymbol{k}} \frac{\langle 0|J^\nu_W(0)|n_f\rangle \, \langle n_f|J^\mu_{\rm em}(0)|P(p)\rangle}{2E_{n_f}(E_\gamma + E_{n_f} - E + i\epsilon)} \,,
\end{aligned} \tag{1.35}$$

$$\begin{aligned}
H_2^{\mu\nu}(k,p) &= \int_0^{+\infty} dt_x \, e^{it_x E_\gamma} \, \langle 0|e^{it_x H} J^\mu_{\rm em}(\boldsymbol{k}) \, e^{-it_x H} J^\nu_W(0)|P(p)\rangle \\
&= \sum_{n:\boldsymbol{p}_n=\boldsymbol{k}} \frac{\langle 0|J^\mu_{\rm em}(0)|n\rangle \, \langle n|J^\nu_W(0)|P(p)\rangle}{2E_n} \int_0^{+\infty} dt_x \, e^{-it_x(E_n - E_\gamma)} \\
&= -i \sum_{n:\boldsymbol{p}_n=\boldsymbol{k}} \frac{\langle 0|J^\mu_{\rm em}(0)|n\rangle \, \langle n|J^\nu_W(0)|P(p)\rangle}{2E_n(E_n - E_\gamma + i\epsilon)} \,.
\end{aligned} \tag{1.36}$$

We have used the relation

$$\mathcal{O}(t) = e^{itH}\mathcal{O}(0)e^{-itH} \,, \tag{1.37}$$

where $\mathcal{O}(t)$ is a generic operator in Heisenberg representation at time t and H is the Hamiltonian operator. We have also used the completeness relation

$$\mathbb{I} = \sum_n \frac{|n\rangle\langle n|}{(2\pi)^3 2E_n} \,, \tag{1.38}$$

where $|n\rangle$ is a complete basis of four-momentum eigenstates with covariant normalization.

In Eqs. (1.35) - (1.36) the spatial Fourier transform has fixed the spatial momentum $\boldsymbol{p}_n$ as indicated. The states $|n_f\rangle$ have the same flavour quantum numbers as the initial meson P, while the states $|n\rangle$ have zero additive flavour quantum numbers. For example, if we consider the decay of a K^+ and $J^\nu_W = \bar{s}\gamma^\nu(1-\gamma^5)u$, then the $|n_f\rangle$ states have strangeness $S = -1$ and the $|n\rangle$ states have $S = 0$.

On the lattice, correlators can be computed only in Euclidean space-time, and we have to translate our Minkowskian Green function to an equivalent Euclidean Green function. We then perform the Wick rotation (see Section B.2.1 of Appendix D) through the transformation

$$x^0_M \quad \to \quad -ix^4_E\,, \tag{1.39}$$

and we obtain from Eq. (1.32) the Euclidean expression

$$H_E^{\mu\nu}(k,p) = -i\int d^4x\, e^{tE_\gamma - i\boldsymbol{k}\cdot\boldsymbol{x}}\, \langle 0|T[\, J^\mu_{\mathrm{em}}(x) J^\nu_W(0)\,]|P(p)\rangle\ . \tag{1.40}$$

As done before, we use the completeness relation to insert a complete basis of four-momentum eigenstates with covariant normalization and obtain

$$H_E^{\mu\nu}(k,p) \quad = \quad H_{E,1}^{\mu\nu}(k,p) + H_{E,2}^{\mu\nu}(k,p)\,, \tag{1.41}$$

$$\begin{aligned} H_{E,1}^{\mu\nu}(k,p) \quad &= \quad -i\int_{-\infty}^{0} dt_x\, e^{t_x E_\gamma}\, \langle 0|J^\nu_W(0)\, e^{t_x H} J^\mu_{\mathrm{em}}(\boldsymbol{k})\, e^{-t_x H}|P(p)\rangle \\ &= \quad -i\sum_{n_f:\boldsymbol{p}_{n_f}=\boldsymbol{p}-\boldsymbol{k}} \frac{\langle 0|J^\nu_W(0)|n_f\rangle\ \langle n_f|J^\mu_{\mathrm{em}}(0)|P(p)\rangle}{2E_{n_f}} \int_{-\infty}^{0} dt_x\, e^{t_x(E_\gamma + E_{n_f} - E)}\,, \end{aligned} \tag{1.42}$$

$$\begin{aligned} H_{E,2}^{\mu\nu}(k,p) \quad &= \quad -i\int_{0}^{+\infty} dt_x\, e^{t_x E_\gamma}\, \langle 0|\, e^{t_x H} J^\mu_{\mathrm{em}}(\boldsymbol{k})\, e^{-t_x H} J^\nu_W(0)|P(p)\rangle \\ &= \quad -i\sum_{n:\boldsymbol{p}_n=\boldsymbol{k}} \frac{\langle 0|J^\mu_{\mathrm{em}}(0)|n\rangle\ \langle n|J^\nu_W(0)|P(p)\rangle}{2E_n} \int_{0}^{+\infty} dt_x\, e^{-t_x(E_n - E_\gamma)}\,. \end{aligned} \tag{1.43}$$

If the conditions (to be further discussed later)

$$E_\gamma + E_{n_f} - E > 0\,, \tag{1.44}$$

$$E_n - E_\gamma > 0\,, \tag{1.45}$$

are satisfied, then the time integrals converge, and we have

$$H_{E,1}^{\mu\nu}(k,p) \quad = \quad -i\sum_{n_f:\boldsymbol{p}_{n_f}=\boldsymbol{p}-\boldsymbol{k}} \frac{\langle 0|J^\nu_W|n_f\rangle\ \langle n_f|J^\mu_{\mathrm{em}}|P(p)\rangle}{2E_{n_f}(E_\gamma + E_{n_f} - E)}\,, \tag{1.46}$$

$$H_{E,2}^{\mu\nu}(k,p) \quad = \quad -i\sum_{n:\boldsymbol{p}_n=\boldsymbol{k}} \frac{\langle 0|J^\mu_{\mathrm{em}}|n\rangle\ \langle n|J^\nu_W|P(p)\rangle}{2E_n(E_n - E_\gamma)}\,. \tag{1.47}$$

Therefore, provided that the conditions (1.44) - (1.45) are satisfied, the Wick rotation leaves the hadronic tensor $H^{\mu\nu}$ unchanged, and the lattice calculation with Euclidean time can be done without particular difficulties. In such situations, the $i\epsilon$ in the second line of Eqs. (1.35) and (1.36) is also unnecessary.

If the conditions (1.44) - (1.45) are not verified, however, the time integrals in the Euclidean space-time are divergent and the Euclidean correlator (1.40) is not defined. This is a crucial feature, and often a limitation, of lattice simulations. In the next section we explain in detail the physical meaning of the conditions (1.44) - (1.45) and we check their validity.

1.2.1 Internal lighter states

The conditions (1.44) - (1.45) are a consequence of the analytic structure of the correlation function, which determines whether it is possible to perform the Wick rotation. The presence of a singularity (poles or cuts) in the Minkowsky case can prevent the possibility of making the naive Wick rotation (B.24). The pathology manifests as divergent time integrals of growing exponentials [31].

The presence of these poles is directly related to the presence of intermediate states with less energy than the external ones. Indeed, we now show that the conditions (1.44) - (1.45) correspond to require that the internal states $|n\rangle$ contributing to the correlation function must have more energy than the external states. We also study the conditions (1.44) - (1.45) in order to find the kinematical regions under which they are satisfied.

For that purpose, we employ the reference system in which the decaying meson is at rest. Clearly, the time-component of a four-vector is not a Lorentz invariant quantity, so that the value of the difference of the energies of two four-momenta depends on the choice of the reference frame. Nevertheless, what really matters in the conditions (1.44) - (1.45) is only in the sign of that difference, and the sign of the time component of a time-like four-vector (which is the case for the difference of the four-momenta of two physical states) is a Lorentz invariant quantity. Therefore, in the following analysis, we are allowed to check the conditions in any reference frame.

In the P meson rest frame, we have

$$E = m_P\,, \qquad k_0 = E_\gamma = \sqrt{k^2 + \boldsymbol{k}^2}\,, \qquad q_0 = \sqrt{q^2 + \boldsymbol{q}^2}\,, \tag{1.48}$$

where m_P is the mass of the decaying meson, q^2 is the invariant mass of the off-shell W and k^2 is the invariant mass of the off-shell photon. In other words, q^2 is the invariant mass of the lepton-neutrino pair $\ell^+\,\nu_\ell$ generated by the W decay and k^2 is the invariant mass of the lepton pair $\ell'^+\,\ell'^-$ generated by the photon decay. Since four-momentum is conserved,

$$\begin{aligned} m_P &= E_\gamma + q_0, \\ |\,\boldsymbol{q}\,| &= |\,\boldsymbol{k}\,| = |\,\boldsymbol{p}_n\,|, \end{aligned} \tag{1.49}$$

and so, for now on, we indicate $\boldsymbol{k}^2$ equivalently for $\boldsymbol{q}^2$, $\boldsymbol{k}^2$ and $\boldsymbol{p}_n^2$.

Since the internal states contributing to the correlator are different depending on the time-ordering of the two currents, we now examine separately the two cases. Obviously, the internal state energy can be compared indistinctly to the initial or the final state, since the external states must have the same energy.

Time-ordering $t_x < 0$

In this time-ordering, the electromagnetic current acts before than the weak current and the process is represented by the diagram of Fig. 1.3a. As we can see from the figure, the internal energy is the sum of the photon energy E_γ and the energy E_{n_f} of the hadronic state resulting from the application of the electromagnetic current on the initial state $|P(p)\rangle$. The initial state has the

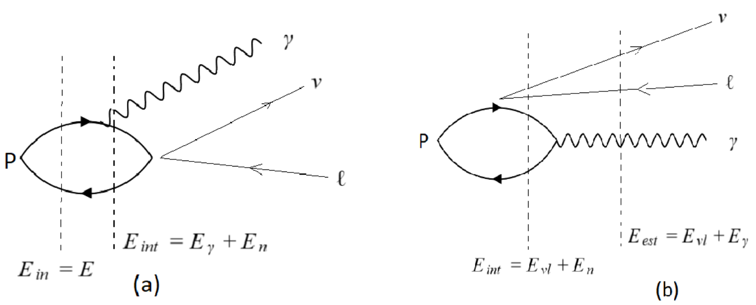

Figure 1.3: *Diagrams, which represent the correlator in the two time-orderings (a) $t_{\rm em} < t$ and (b) $t_{\rm em} > t$.*

energy m_P of the pseudoscalar meson and so the condition is

$$E_\gamma + E_{n_f} > m_P \quad \Rightarrow \quad E_\gamma + E_{n_f} - m_P > 0\,. \tag{1.50}$$

With Eq. (1.50), we explicitly derived the condition (1.44) by requiring that the internal states must have more energy than the initial one.

The electromagnetic current conserve the flavour and the electric charge. Thus, the lightest state $|n_f\rangle$, resulting from the application of $J^\mu_{\rm em}(\boldsymbol{k})$ to the initial state, is still the pseudoscalar meson P, but now with a spatial momentum $\boldsymbol{k}$ (see Eq. (1.49)) and energy $E_{n_f} = \sqrt{m_P^2 + \boldsymbol{k}^2}$. Of course, there are many other states $|n_f\rangle$ that contribute to the correlation function, but this is the one with the lowest energy.

Because the initial state meson P is at rest, we have necessarily $E_{n_f} > m_P$. Thus, being $E_\gamma > 0$, we can be sure that $E_\gamma + E_{n_f} - m_P > 0$, and so the condition of (1.50) is always verified.

Time-ordering $t_x > 0$

In this time-ordering, the process is represented by the diagram of Fig. 1.3b. In this case, it is convenient to compare the energy of the internal state with the energy of the final one. The energy of the internal state is the sum of the energy $E_{\ell\nu}$ of the leptonic pair and the energy E_n of the hadronic state resulting from the application of the weak current on the initial state $|P(p)\rangle$. The final state has a total energy of $E_{\ell\nu}$ and E_γ, so the condition is

$$E_{\ell\nu} + E_n > E_{\ell\nu} + E_\gamma \quad \Rightarrow \quad E_n - E_\gamma > 0\,. \tag{1.51}$$

With Eq. (1.51), we explicitly derived the condition (1.45) by requiring that the internal states must have more energy than the initial one.

In this time-ordering, the internal hadronic state $|n\rangle$ is obtained applying the weak current J^ν_W to the charged pseudoscalar meson P, and it must be capable of decaying into a photon through the application of the electromagnetic current $J^\mu_{\rm em}$. The lightest state $|n\rangle$ is thus a state of two pions with total spatial momentum $\boldsymbol{k}$. Indeed, a one-particle state, in order to decay into a photon, should be a vector meson like the ρ.

The kinematic configuration which minimizes E_n is the one in which the pions are collinear and with the same momentum $\frac{\boldsymbol{k}}{2}$, and so $E_n = 2\sqrt{m_\pi^2 + \left(\frac{\boldsymbol{k}}{2}\right)^2}$.

If we compare the internal state with the final one, we obtain the condition

$$E_n > E_\gamma \quad \Rightarrow \quad 2\sqrt{m_\pi^2 + \left(\frac{\boldsymbol{k}}{2}\right)^2} > \sqrt{k^2 + \boldsymbol{k}^2} \quad \Rightarrow \quad 4m_\pi^2 > k^2. \tag{1.52}$$

In this time-ordering, the condition is not always satisfied, but it imposes an upper limit of $2m_\pi$ on the invariant mass of the lepton pair created by the photon.

In conclusion, we have shown that the Wick rotation of the Hadronic tensor to Euclidean space-time can be performed straightforwardly only if $k^2 < 4m_\pi^2$. This condition is quite limiting, especially for the decay of heavy mesons like the D and B. It should be also noted, however, that on the actual simulation we work with a finite lattice extent. When considering the lattice correlators, we will see that, at finite time extent T, the divergent integrals become only exponentially enhanced. Moreover, on a finite lattice we do not have a continuum of states, but they are discretized due to the quantization of the spatial momentum. In practice, if the number of such states is small, the terms with the exponentially growing exponentials can be explicitly subtracted, thus extending the validity of the method beyond the region $k^2 < 4m_\pi^2$. The remaining issue is the correction for the non-exponential finite-volume effects (analogous to those corrected by the Lellouch-Lüscher factor in $K \to \pi\pi$ decays [32]). We postpone such a discussion to a future study and for now we restrict our numerical analysis to kaon decays in a lattice gauge ensemble with an unphysical pion mass, such that the condition $m_K < 2m_\pi$ is always fulfilled. Thus, two-pion internal states have always larger energy than the external ones and the conditions (1.44) - (1.45) are both satisfied.

Now that we have discussed the analytic continuation to Euclidean space-time, we proceed to the presentation of our strategy for extracting the SD form factors from suitable three-point lattice correlation functions.

1.3 The three-point lattice correlator

The principal ingredient in evaluating the decay amplitude on a Euclidean lattice, with finite space-time volume $V = L^3 \times T$, is the correlation function

$$M_W^{\mu\nu}(t_x, t; \boldsymbol{k}, \boldsymbol{p}) = T\langle J_W^\nu(t)\, \hat{J}_{\rm em}^\mu(t_x, \boldsymbol{k})\, \hat{P}(0, \boldsymbol{p})\rangle_{LT}\,, \tag{1.53}$$

where $\langle \ldots \rangle_{LT}$ denotes the average over the gauge field configurations at finite L and T. Note that in Eq. (1.53) we have placed the interpolating operator $\hat{P}(0, \boldsymbol{p})$ at time 0 and the weak current $J_W(t)$ at time t. The three operators in Eq. (1.53) are as follows:

- $\hat{P}(0, \boldsymbol{p})$ is the spatial Fourier transform of the interpolating operator for the decaying pseudoscalar meson at time $t = 0$:

$$\hat{P}(0, \boldsymbol{p}) = \sum_{\boldsymbol{z}} e^{i\boldsymbol{p}\cdot\boldsymbol{z}} P(0, \boldsymbol{z})\,, \tag{1.54}$$

where $P(0, z) = i\overline{\psi}_U(0, \boldsymbol{z})\gamma_5\psi_D(0, \boldsymbol{z})$ for a positively charged meson or $P(0, z) = i\overline{\psi}_D(0, \boldsymbol{z})\gamma_5\psi_U(0, \boldsymbol{z})$ for a negatively charged one and $\psi_{U,D}$ indicate the fields of up-type and down-type quarks respectively.

• The renormalized hadronic weak current, $J_W^\nu(t) = J_V^\nu(t) - J_A^\nu(t)$ is placed at a generic time t and at the origin in space. The vector and axial currents, $J_V^\nu(t)$ and $J_A^\nu(t)$ respectively, satisfy the continuum Ward identities (up to discretization effects). In the Twisted-Mass discretization of the fermionic action [38], the vector and axial vector currents we use are given by

$$J_V^\nu(t) = Z_A\,\bar{\psi}_D(t)\gamma^\nu\psi_U(t)\;,\quad J_A^\nu(t) = Z_V\,\bar{\psi}_D(t)\gamma^\nu\gamma_5\psi_U(x), \tag{1.55}$$

for a positively charged meson or their Hermitian conjugates for a negatively charged one, where $Z_{A,V}$ are the renormalization factors ensuring that the Ward identities are satisfied [2].

• The electromagnetic current, $J_{\rm em}^\mu(t_x,\boldsymbol{x})$, is defined by

$$J_{\rm em}^\mu(t_x,\boldsymbol{x}) = \sum_f q_f\,J_f^\mu(t_x,\boldsymbol{x})\,, \tag{1.56}$$

where f is the flavour index and the charge q_f is equal to $2/3$ for up-type quarks and to $-1/3$ for down-type quarks. A possible choice for the lattice electromagnetic current is the local operator $J_f^\mu(t_x,\boldsymbol{x}) = Z_V^{\rm loc}\bar{q}_f(t_x,\boldsymbol{x})\gamma^\mu q_f(t_x,\boldsymbol{x})$, where $Z_V^{\rm loc}$ is the finite renormalization constant of the vector current ($Z_V^{\rm loc} = Z_A$ with Twisted-Mass at maximal twist). We choose instead to use the exactly conserved lattice vector current which with Twisted-Mass Fermions at maximal twist is given by [3]

$$J_f^\mu(x) = -\left\{\bar{\psi}_f(x)\frac{i\,r_f\gamma_5 - \gamma^\mu}{2}\,U_\mu(x)\psi_f(x+\hat{\mu}) - \bar{\psi}_f(x+\hat{\mu})\frac{i\,r_f\gamma_5 + \gamma^\mu}{2}U_\mu(x)^\dagger\psi_f(x)\right\}\,. \tag{1.57}$$

In Eq. (1.57), $U_\mu(x)$ are the QCD link variables and $r_f = \pm 1$ is the Wilson parameter of the flavour f [40]. The spatial momentum $\boldsymbol{k}$ of the current is assigned by defining

$$\hat{J}_{\rm em}^\mu(t_x,\boldsymbol{k}) = \sum_{\boldsymbol{x}} e^{-i\boldsymbol{k}\cdot(\boldsymbol{x}+\hat{\boldsymbol{\imath}}/2)}\,J_{\rm em}^\mu(t_x,\boldsymbol{x})\,. \tag{1.58}$$

In order to obtain the decay amplitude, we need to integrate $M_W^{\mu\nu}(t_x,t;\boldsymbol{k},\boldsymbol{p})$ over t_x, as seen for example in Eq. (1.32). To this end we construct the function:

$$\begin{aligned}
&C^{\mu\nu}(t,E_\gamma,\boldsymbol{k},\boldsymbol{p}) = \\
&-i\theta\,(T/2-t)\sum_{t_x=0}^{T}\left(\theta\,(T/2-t_x)\,e^{E_\gamma\,t_x} + \theta\,(t_x-T/2)\,e^{-E_\gamma(T-t_x)}\right)M_W^{\mu\nu}(t_x,t;\boldsymbol{k},\boldsymbol{p}) \\
&-i\theta\,(t-T/2)\sum_{t_x=0}^{T}\left(\theta\,(T/2-t_x)\,e^{-E_\gamma\,t_x} + \theta\,(t_x-T/2)\,e^{-E_\gamma(t_x-T)}\right)M_W^{\mu\nu}(t_x,t;\boldsymbol{k},\boldsymbol{p})\,.
\end{aligned} \tag{1.59}$$

On a lattice with a large but finite temporal extent T, the required matrix element can be obtained from the first term on the top line of Eq. (1.59). This is illustrated in the left-hand diagram of

[2] Note that the renormalization factors to be used in Twisted-Mass at maximal twist are chirally-rotated with respect to the ones of standard Wilson fermions [39]. This is a consequence of the fact that the up-type and down-type quark fields in the action are discretised with opposite values of the Wilson parameter.

[3] With twisted boundary conditions we use the corresponding conserved current given by Eq. (B10) of Ref. [6]

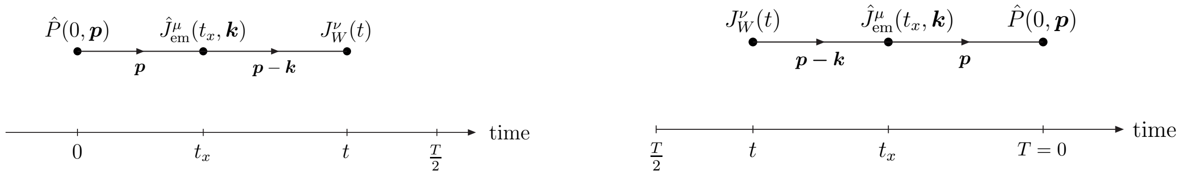

Figure 1.4: *Schematic diagrams representing the correlation function $C^{\mu\nu}(t, E_\gamma, \boldsymbol{k}, \boldsymbol{p})$ used to extract the form factors, see Eqs. (1.53) and (1.59). The interpolating operators for the meson $\hat{P}$ and the weak current J_W are placed at fixed times 0 and t, while the electromagnetic current $\hat{J}_{\rm em}$ is inserted at t_x which is integrated over $0 \le t_x \le T$, where T is the temporal extent of the lattice. The left and right panels correspond to the leading contributions to the correlation functions for $t < \frac{T}{2}$ and $t > \frac{T}{2}$ respectively, with mesons propagating with momenta $\boldsymbol{p}$ or $\boldsymbol{p} - \boldsymbol{k}$.*

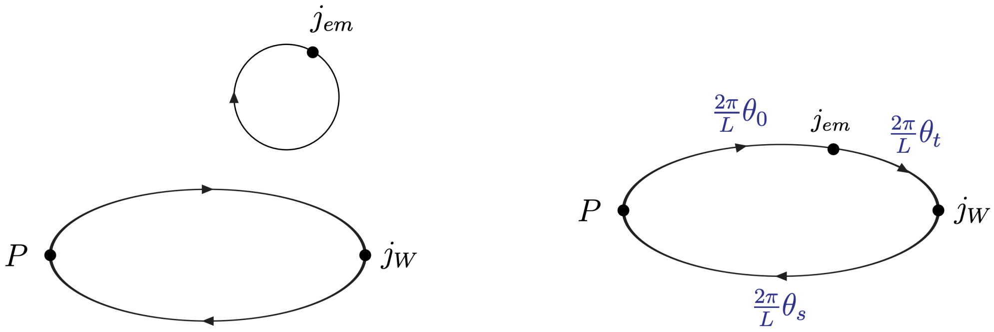

Figure 1.5: *The diagram on the left represents the contributions to the correlation functions arising from the emission of the photon by the sea quarks. In our numerical simulations, we work in the electroquenched approximation and neglect such diagrams. The diagram on the right explains our choice of the spatial boundary conditions, which allow us to set arbitrary values for the meson and photon spatial momenta. The spatial momenta of the valence quarks, modulo $2\pi/L$, in terms of the twisting angles are as indicated. Each diagram implicitly includes all orders in QCD.*

Fig. 1.4, and it should be remembered that t_x can also be larger than t. The second term on the second line of Eq. (1.59) represents the time-reversed process (we discuss the properties of the matrix element under time reversal in the next section) and is illustrated in the right-hand diagram of Fig. 1.4, and again it should be remembered that t_x can also be smaller than t. The second term on the top line of Eq. (1.59) represents, on a periodic lattice of finite temporal extent, the ordering where the electromagnetic current acts at an earlier time than the meson source that, in the reduction formula to create an initial meson state, should be asymptotically far in the past. Indeed, the contribution of this term disappears in the limit $T \to \infty$. On the lattice with finite temporal extension, however, we have found that its inclusion corrects sizeable finite T effects and improves the quality of the numerical fits of $C^{\mu\nu}(t, E_\gamma, \boldsymbol{k}, \boldsymbol{p})$. Similarly, the first term on the second line of Eq. (1.59) represents, for the time-reversed process, the electromagnetic currents acting at a time larger than the meson source. Its contribution also disappears in the infinite T limit, but its inclusion improves the quality of the fit of $C^{\mu\nu}(t, E_\gamma, \boldsymbol{k}, \boldsymbol{p})$.

Fig. 1.5 contains two diagrams presented to illustrate two important points concerning our numerical calculation of the correlation functions and of the form factors. The diagram in the left panel shows a *quark-disconnected* contribution to the correlation function originating from the possibility that the virtual photon is emitted from sea quarks. In this paper we use the so-called electroquenched approximation in which the sea-quarks are electrically neutral. In practice, this means that we have neglected the contributions represented by the diagram in the left panel of Fig. 1.5. We note that the contribution of these diagrams vanishes in the limit of exact $SU(3)$ flavour symmetry.

The quark-connected diagram in the right panel of Fig. 1.5 is shown in order to explain the strategy we have used to set the values of the spatial momenta. We have exploited the fact that by working within the electroquenched approximation, it is possible to choose arbitrary values of the spatial momenta by using different spatial boundary conditions for the quark fields [35]. More precisely, we set the spatial boundary conditions for the "spectator" quark such that

$$\psi(x + \boldsymbol{n}L) = \exp(2\pi i \boldsymbol{n} \cdot \boldsymbol{\theta_s})\psi(x) \,, \tag{1.60}$$

where $\boldsymbol{n}$ is a three-vector of integers and $\boldsymbol{\theta_s}$ is a three-vector of angles. For the temporal direction, we employ anti-periodic boundary conditions. For each quark flavor f, we impose different boundary conditions on q_f and $\bar{q}_f$, the two component fields of J^μ_f. This is possible at the price of accepting violations of unitarity that are exponentially suppressed with the volume [41, 42]. By setting the boundary conditions as illustrated in the figure we have thus been able to choose arbitrary (non-quantized) values for the meson and photon spatial momenta

$$\boldsymbol{p} = \frac{2\pi}{L}\left(\boldsymbol{\theta}_0 - \boldsymbol{\theta}_s\right) \,, \qquad \boldsymbol{k} = \frac{2\pi}{L}\left(\boldsymbol{\theta}_0 - \boldsymbol{\theta}_t\right) \,, \tag{1.61}$$

by tuning the real three-vectors $\boldsymbol{\theta}_{0,t,s}$. We find that the most precise results are obtained with small values of $|\boldsymbol{p}|$ and in particular with $\boldsymbol{p} = \boldsymbol{0}$.

1.3.1 Spectral decomposition

In order to show that it is possible to extract the hadronic tensor $H^{\mu\nu}$ from the function in Eq. (1.59) we now perform a spectral decomposition of $C^{\mu\nu}(t, E_\gamma, \boldsymbol{k}, \boldsymbol{p})$, defined in Eqs. (1.59) and (1.53). In the following, we shall use continuum notation for the time integrals, but we will consider the finite time-extent of the lattice T. We analyze each different time–ordering separately. In order to keep the notation clean, in the following, when inserting a complete set of internal states, we will always use $|n\rangle$ without distinguishing the difference in the flavor of the intermediate hadronic states contributing to the different time-orderings.

Time-ordering $t_x < t < \dfrac{T}{2}$

The contribution to $C^{\mu\nu}(t, E_\gamma, \boldsymbol{k}, \boldsymbol{p})$ coming from this time ordering is:

$$C_1^{\mu\nu} \;\; = \;\; -i \int_0^t e^{E_\gamma t_x} \, \langle 0 | J^\nu_W(t) \, \hat{J}^\mu_{\rm em}(t_x, \boldsymbol{k}) \, \hat{P}(0, \boldsymbol{p}) | 0 \rangle \; dt_x \,. \tag{1.62}$$

The lightest state interpolated by the operator $\hat{P}(0, \boldsymbol{p})$ is by construction the charged pseudoscalar meson P with energy $E = \sqrt{m_P^2 + \boldsymbol{p}^2}$, and so we have

$$C_1^{\mu\nu} \;\; = \;\; -i \int_0^t e^{E_\gamma t_x} \, \langle 0 | J^\nu_W(t) \, \hat{J}^\mu_{\rm em}(t_x, \boldsymbol{k}) | P(p) \rangle \, \frac{\langle P(p) | P | 0 \rangle}{2E} \, dt_x + \ldots \,, \tag{1.63}$$

Where the dots represent terms exponentially suppressed by the energy gap between the fundamental state $|P\rangle$ and the excited ones.

We now insert a complete set of intermediate states between the two currents operator, and we obtain

$$\begin{aligned}
C_1^{\mu\nu} &= -i\frac{\langle P(p)|P|0\rangle}{2E}\int_0^t e^{E_\gamma t_x}\sum_n \frac{\langle 0|J_W^\nu(t)|n\rangle\ \langle n|\hat{J}^\mu_{\rm em}(t_x,\boldsymbol{k})|P(p)\rangle}{2E_n}\,dt_x+\dots\\
&= -i\frac{\langle P(p)|P|0\rangle}{2E}\sum_{n:\boldsymbol{p}_n=\boldsymbol{p}-\boldsymbol{k}}\frac{\langle 0|J_W^\nu|n\rangle\ \langle n|J^\mu_{\rm em}|P(p)\rangle}{2E_n}\,e^{-tE_n}\int_0^t e^{(E_\gamma+E_n-E)t_x}\,dt_x+\dots\\
&= -i\frac{\langle P(p)|P|0\rangle}{2E}\sum_{n:\boldsymbol{p}_n=\boldsymbol{p}-\boldsymbol{k}}\frac{\langle 0|J_W^\nu|n\rangle\ \langle n|J^\mu_{\rm em}|P(p)\rangle}{2E_n}\,e^{-tE_n}\,\frac{e^{t(E_\gamma+E_n-E)}-1}{(E_\gamma+E_n-E)}+\dots\\
&= -i\frac{\langle P(p)|P|0\rangle}{2E}\,e^{-t(E-E_\gamma)}\sum_{n:\boldsymbol{p}_n=\boldsymbol{p}-\boldsymbol{k}}\frac{\langle 0|J_W^\nu|n\rangle\ \langle n|J^\mu_{\rm em}|P(p)\rangle}{2E_n(E_n+E_\gamma-E)}\left(1-e^{-t(E_\gamma+E_n-E)}\right)+\dots
\end{aligned}\tag{1.64}$$

As we have shown in Sec. 1.2.1, we have $E_\gamma+E_n-E>0$. Thus, the last exponential in the last formula gives, for large t, a subleading contribution and can be neglected.

Time-ordering $t<t_x<\dfrac{T}{2}$

The contribution to $C^{\mu\nu}(t,E_\gamma,\boldsymbol{k},\boldsymbol{p})$ coming from this time ordering is:

$$\begin{aligned}
C_2^{\mu\nu} &= -i\int_t^{\frac{T}{2}} e^{E_\gamma t_x}\,\langle 0|\hat{J}^\mu_{\rm em}(t_x,\boldsymbol{k})\,J_W^\nu(t)\,\hat{P}(0,\boldsymbol{p})|0\rangle\,dt_x\\
&= -i\int_t^{\frac{T}{2}} e^{E_\gamma t_x}\,\langle 0|\hat{J}^\mu_{\rm em}(t_x,\boldsymbol{k})\,J_W^\nu(t)|P(p)\rangle\,\frac{\langle P(p)|P|0\rangle}{2E}\,dt_x+\dots\\
&= -i\frac{\langle P(p)|P|0\rangle}{2E}\int_t^{\frac{T}{2}} e^{E_\gamma t_x}\sum_n\frac{\langle 0|\hat{J}^\mu_{\rm em}(t_x,\boldsymbol{k})|n\rangle\ \langle n|J_W^\nu(t)|P(p)\rangle}{2E_n}\,dt_x+\dots\\
&= -i\frac{\langle P(p)|P|0\rangle}{2E}\sum_{n:\boldsymbol{p}_n=\boldsymbol{k}}\frac{\langle 0|J^\mu_{\rm em}|n\rangle\ \langle n|J_W^\nu|P(p)\rangle}{2E_n}\,e^{t(E_n-E)}\int_t^{\frac{T}{2}} e^{(E_\gamma-E_n)t_x}\,dt_x+\dots\\
&= -i\frac{\langle P(p)|P|0\rangle}{2E}\sum_{n:\boldsymbol{p}_n=\boldsymbol{k}}\frac{\langle 0|J^\mu_{\rm em}|n\rangle\ \langle n|J_W^\nu|P(p)\rangle}{2E_n}\,e^{t(E_n-E)}\,\frac{e^{\frac{T}{2}(E_\gamma-E_n)}-e^{t(E_\gamma-E_n)}}{(E_\gamma-E_n)}+\dots\\
&= -i\frac{\langle P(p)|P|0\rangle}{2E}\,e^{-t(E-E_\gamma)}\sum_{n:\boldsymbol{p}_n=\boldsymbol{k}}\frac{\langle 0|J^\mu_{\rm em}|n\rangle\ \langle n|J_W^\nu|P(p)\rangle}{2E_n(E_n-E_\gamma)}\left(1-e^{-\left(\frac{T}{2}-t\right)(E_n-E_\gamma)}\right)+\dots
\end{aligned}\tag{1.65}$$

Since we are working under the assumption $k^2<4m_\pi^2$, the last exponential in the last formula gives a subleading contribution in the region $0\ll t\ll T/2$, being satisfied the condition on the internal state $E_n-E_\gamma>0$.

Time-ordering $t < \dfrac{T}{2} < t_x$

The contribution to $C^{\mu\nu}(t, E_\gamma, \boldsymbol{k}, \boldsymbol{p})$ coming from this time ordering is:

$$\begin{aligned}
C_3^{\mu\nu} &= -i \int_{\frac{T}{2}}^{T} e^{-E_\gamma(T-t_x)} \, \langle 0|\hat{J}^\mu_{\text{em}}(t_x, \boldsymbol{k}) \, J^\nu_W(t) \, \hat{P}(0, \boldsymbol{p})|0\rangle \; dt_x \\
&= -i \int_{\frac{T}{2}}^{T} e^{-E_\gamma(T-t_x)} \, \langle 0|\hat{J}^\mu_{\text{em}}(t_x, \boldsymbol{k}) \, J^\nu_W(t)|P(p)\rangle \, \frac{\langle P(p)|P|0\rangle}{2E} \, dt_x + \dots \\
&= -i \frac{\langle P(p)|P|0\rangle}{2E} \int_{\frac{T}{2}}^{T} e^{-E_\gamma(T-t_x)} \sum_n \frac{\langle 0|\hat{J}^\mu_{\text{em}}(t_x, \boldsymbol{k})|n\rangle \, \langle n|J^\nu_W(t)|P(p)\rangle}{2E_n} \, dt_x + \dots \\
&= -i \frac{\langle P(p)|P|0\rangle}{2E} \sum_{n:\boldsymbol{p}_n=\boldsymbol{k}} \frac{\langle 0|J^\mu_{\text{em}}|n\rangle \, \langle n|J^\nu_W|P(p)\rangle}{2E_n} \, e^{t(E_n-E)} \, e^{-TE_\gamma} \int_{\frac{T}{2}}^{T} e^{(E_\gamma-E_n)t_x} \, dt_x + \dots \\
&= -i \frac{\langle P(p)|P|0\rangle}{2E} \sum_{n:\boldsymbol{p}_n=\boldsymbol{k}} \frac{\langle 0|J^\mu_{\text{em}}|n\rangle \, \langle n|J^\nu_W|P(p)\rangle}{2E_n} \, e^{t(E_n-E)} \\
&\quad \times \, e^{-TE_\gamma} \, \frac{-e^{T(E_\gamma-E_n)} + e^{\frac{T}{2}(E_\gamma-E_n)}}{(E_n - E_\gamma)} + \dots \\
&= -i \frac{\langle P(p)|P|0\rangle}{2E} \, e^{-t(E-E_\gamma)} \sum_{n:\boldsymbol{p}_n=\boldsymbol{k}} \frac{\langle 0|J^\mu_{\text{em}}|n\rangle \, \langle n|J^\nu_W|P(p)\rangle}{2E_n(E_n - E_\gamma)} \\
&\quad \times \, \left(e^{-\left(\frac{T}{2}-t\right)(E_\gamma+E_n)} - e^{-tE_\gamma} \, e^{-(T-t)E_n} \right) + \dots
\end{aligned} \tag{1.66}$$

We observe that, for $0 \ll t \ll \frac{T}{2}$, this contribution is always exponentially suppressed with respect to $C_1^{\mu\nu}$ and $C_2^{\mu\nu}$, for any values of E_γ and E_n. The contribution $C_3^{\mu\nu}$ comes from the second term in the first line of Eq. (1.59), and so we have explicitly shown the sub-leading nature of this term, as anticipated.

Time-ordering $t_x < \dfrac{T}{2} < t$

In this time-ordering, and in the next ones, we have $t > \frac{T}{2}$. Thus, thanks to the periodic boundary conditions on the time extent of the lattice, the interpolating pseudoscalar operator P gives the leading contribution when annihilating the pseudoscalar meson P^- at the time T , instead of creating P^+ at time 0. Later on, we will see that this is consistent with the interpretation about the correlator representing the charge and parity (CP) conjugate process when $t > \frac{T}{2}$. Due to the CPT symmetry, this is equivalent to saying that, for t in the second half of the lattice, the correlator represents the time-reversed process. Thus, in the next formulae, we will indicate as $|\overline{P}(p)\rangle$ and $|\overline{n}\rangle$ the charge conjugate states of $|P(p)\rangle$ and $|n\rangle$

The contribution to $C^{\mu\nu}(t, E_\gamma, \boldsymbol{k}, \boldsymbol{p})$ coming from this time ordering is:

$$C_4^{\mu\nu} = -i \int_0^{\frac{T}{2}} e^{-E_\gamma t_x} \, \langle 0|\hat{P}(T, \boldsymbol{p}) \, J^\nu_W(t) \, \hat{J}^\mu_{\text{em}}(t_x, \boldsymbol{k})|0\rangle \; dt_x$$

$$
\begin{aligned}
&= -i\int_0^{\frac{T}{2}} e^{-E_\gamma t_x} \left\langle \overline{P}(p)\left| J_W^\nu(t)\, \hat{J}^\mu_{\rm em}(t_x,\boldsymbol{k})\right|0\right\rangle \frac{\left\langle 0\middle|P\middle|\overline{P}(p)\right\rangle\, e^{-TE}}{2E}\, dt_x + \ldots \\
&= -i\frac{\left\langle 0\middle|P\middle|\overline{P}(p)\right\rangle}{2E}\, e^{-TE} \int_0^{\frac{T}{2}} e^{-E_\gamma t_x} \sum_n \frac{\left\langle \overline{P}(p)\left|J_W^\nu(t)\right|\overline{n}\right\rangle \langle \overline{n}\,|\hat{J}^\mu_{\rm em}(t_x,\boldsymbol{k})|0\rangle}{2E_n}\, dt_x + \ldots \\
&= -i\frac{\left\langle 0\middle|P\middle|\overline{P}(p)\right\rangle}{2E} \sum_{n:\boldsymbol{p}_n=\boldsymbol{k}} \frac{\left\langle \overline{P}(p)\left|J_W^\nu\right|\overline{n}\right\rangle \langle \overline{n}\,|J^\mu_{\rm em}|0\rangle}{2E_n}\, e^{-TE} e^{-t(E_n-E)} \int_0^{\frac{T}{2}} e^{(E_n-E_\gamma)t_x}\, dt_x + \ldots \\
&= -i\frac{\left\langle 0\middle|P\middle|\overline{P}(p)\right\rangle}{2E} \sum_{n:\boldsymbol{p}_n=\boldsymbol{k}} \frac{\left\langle \overline{P}(p)\left|J_W^\nu\right|\overline{n}\right\rangle \langle \overline{n}\,|J^\mu_{\rm em}|0\rangle}{2E_n}\, e^{-TE} e^{-t(E_n-E)}\, \frac{e^{\frac{T}{2}(E_n-E_\gamma)}-1}{(E_n-E_\gamma)} + \ldots \\
&= -i\frac{\left\langle 0\middle|P\middle|\overline{P}(p)\right\rangle}{2E}\, e^{-(T-t)(E-E_\gamma)} \sum_{n:\boldsymbol{p}_n=\boldsymbol{k}} \frac{\left\langle \overline{P}(p)\left|J_W^\nu\right|\overline{n}\right\rangle \langle \overline{n}\,|J^\mu_{\rm em}|0\rangle}{2E_n(E_n-E_\gamma)} \\
&\quad \times \left(e^{-TE_\gamma} - e^{-(t-\frac{T}{2})E_n}\, e^{-(\frac{3}{2}T-t)E_\gamma}\right) + \ldots
\end{aligned}
\tag{1.67}
$$

As for $C_3^{\mu\nu}$, this contribution is exponentially suppressed, when $\frac{T}{2} \ll t \ll T$, for any values of E_n and E_γ. This contribution is the one coming from the first term in the second line of Eq. (1.59).

Time-ordering $\dfrac{T}{2} < t_x < t$

The contribution to $C^{\mu\nu}(t, E_\gamma, \boldsymbol{k}, \boldsymbol{p})$ coming from this time ordering is:

$$
\begin{aligned}
C_5^{\mu\nu} &= -i\int_{\frac{T}{2}}^{t} e^{-E_\gamma(t_x-T)}\, \langle 0|\hat{P}(T,\boldsymbol{p})\, J_W^\nu(t)\, \hat{J}^\mu_{\rm em}(t_x,\boldsymbol{k})|0\rangle\, dt_x \\
&= -i\int_{\frac{T}{2}}^{t} e^{-E_\gamma(t_x-T)} \left\langle \overline{P}(p)\left| J_W^\nu(t)\, \hat{J}^\mu_{\rm em}(t_x,\boldsymbol{k})\right|0\right\rangle \frac{\left\langle 0\middle|P\middle|\overline{P}(p)\right\rangle\, e^{-TE}}{2E}\, dt_x + \ldots \\
&= -i\frac{\left\langle 0\middle|P\middle|\overline{P}(p)\right\rangle}{2E}\, e^{-TE}\, e^{TE_\gamma} \int_{\frac{T}{2}}^{t} e^{-E_\gamma t_x} \sum_n \frac{\left\langle \overline{P}(p)\left|J_W^\nu(t)\right|\overline{n}\right\rangle \langle \overline{n}\,|\hat{J}^\mu_{\rm em}(t_x,\boldsymbol{k})|0\rangle}{2E_n}\, dt_x + \ldots \\
&= -i\frac{\left\langle 0\middle|P\middle|\overline{P}(p)\right\rangle}{2E} \sum_{n:\boldsymbol{p}_n=\boldsymbol{k}} \frac{\left\langle \overline{P}(p)\left|J_W^\nu\right|\overline{n}\right\rangle \langle \overline{n}\,|J^\mu_{\rm em}|0\rangle}{2E_n} \\
&\quad \times\, e^{-T(E-E_\gamma)} e^{-t(E_n-E)} \int_{\frac{T}{2}}^{t} e^{(E_n-E_\gamma)t_x}\, dt_x + \ldots \\
&= -i\frac{\left\langle 0\middle|P\middle|\overline{P}(p)\right\rangle}{2E} \sum_{n:\boldsymbol{p}_n=\boldsymbol{k}} \frac{\left\langle \overline{P}(p)\left|J_W^\nu\right|\overline{n}\right\rangle \langle \overline{n}\,|J^\mu_{\rm em}|0\rangle}{2E_n} \\
&\quad \times\, e^{-T(E-E_\gamma)} e^{-t(E_n-E)}\, \frac{e^{t(E_n-E_\gamma)} - e^{\frac{T}{2}(E_n-E_\gamma)}}{(E_n-E_\gamma)} + \ldots
\end{aligned}
$$

$$= -i\frac{\left\langle 0\middle|P\middle|\overline{P}(p)\right\rangle}{2E}\, e^{-(T-t)(E-E_\gamma)} \sum_{n:\boldsymbol{p}_n=\boldsymbol{k}} \frac{\left\langle \overline{P}(p)\middle|J_W^\nu\middle|\overline{n}\right\rangle \langle \overline{n}\,|J_{\rm em}^\mu|0\rangle}{2E_n(E_n-E_\gamma)} \left(1-e^{-(t-\frac{T}{2})(E_n-E_\gamma)}\right)+\dots \tag{1.68}$$

Once again, the last exponential in the last formula gives a subleading contribution in the region $T/2 \ll t \ll T$, being $E_n - E_\gamma > 0$.

Time-ordering $\frac{T}{2} < t < t_x$

The contribution to $C^{\mu\nu}(t, E_\gamma, \boldsymbol{k}, \boldsymbol{p})$ coming from this time ordering is:

$$\begin{aligned}
C_6^{\mu\nu} &= -i\int_t^T e^{-E_\gamma(t_x-T)}\, \langle 0|\hat{P}(T,\boldsymbol{p})\, \hat{J}_{\rm em}^\mu(t_x,\boldsymbol{k})\, J_W^\nu(t)|0\rangle\, dt_x \\
&= -i\int_t^T e^{-E_\gamma(t_x-T)} \left\langle \overline{P}(p)\middle|\hat{J}_{\rm em}^\mu(t_x,\boldsymbol{k})\, J_W^\nu(t)\middle|0\right\rangle \frac{\left\langle 0\middle|P\middle|\overline{P}(p)\right\rangle e^{-TE}}{2E}\, dt_x+\dots \\
&= -i\frac{\left\langle 0\middle|P\middle|\overline{P}(p)\right\rangle}{2E}\, e^{-TE}\, e^{TE_\gamma} \int_t^T e^{-E_\gamma t_x} \sum_n \frac{\left\langle \overline{P}(p)\middle|\hat{J}_{\rm em}^\mu(t_x,\boldsymbol{k})\middle|\overline{n}\right\rangle \langle \overline{n}\,|J_W^\nu(t)|0\rangle}{2E_n}\, dt_x+\dots \\
&= -i\frac{\left\langle 0\middle|P\middle|\overline{P}(p)\right\rangle}{2E} \sum_{n:\boldsymbol{p}_n=\boldsymbol{p}-\boldsymbol{k}} \frac{\left\langle \overline{P}(p)\middle|J_{\rm em}^\mu\middle|\overline{n}\right\rangle \langle \overline{n}\,|J_W^\nu|0\rangle}{2E_n} \\
&\quad\times e^{-T(E-E_\gamma)}\, e^{tE_n} \int_t^T e^{-(E_\gamma+E_n-E)t_x}\, dt_x+\dots \\
&= -i\frac{\left\langle 0\middle|P\middle|\overline{P}(p)\right\rangle}{2E} \sum_{n:\boldsymbol{p}_n=\boldsymbol{p}-\boldsymbol{k}} \frac{\left\langle \overline{P}(p)\middle|J_{\rm em}^\mu\middle|\overline{n}\right\rangle \langle \overline{n}\,|J_W^\nu|0\rangle}{2E_n} \\
&\quad\times e^{-T(E-E_\gamma)}\, e^{tE_n} \frac{e^{-t(E_\gamma+E_n-E)}-e^{-T(E_\gamma+E_n-E)}}{E_\gamma+E_n-E}+\dots \\
&= -i\frac{\left\langle 0\middle|P\middle|\overline{P}(p)\right\rangle}{2E} \sum_{n:\boldsymbol{p}_n=\boldsymbol{p}-\boldsymbol{k}} \frac{\left\langle \overline{P}(p)\middle|J_{\rm em}^\mu\middle|\overline{n}\right\rangle \langle \overline{n}\,|J_W^\nu|0\rangle}{2E_n(E_\gamma+E_n-E)}\, e^{-(T-t)(E-E_\gamma)} \left(1-e^{-(T-t)(E_\gamma+E_n-E)}\right)
\end{aligned} \tag{1.69}$$

As for the previous terms, the last exponential in the last formula gives a subleading contribution in the region $T/2 \ll t \ll T$.

1.4 The hadronic tensor from the lattice correlator

In this section, we use the information we got from the spectral decomposition to establish the relation between the lattice three-point function of Eq. (1.59) and the hadronic matrix element $H^{\mu\nu}$. In the following, we will also assume the validity of the internal state conditions (1.44) and (1.45).

In the first half of the lattice, that is, for $t < \frac{T}{2}$ we have

$$\theta(T/2-t)C^{\mu\nu}(t,k,p) = C_1^{\mu\nu} + C_2^{\mu\nu} + C_3^{\mu\nu} = -i\frac{e^{-t(E-E_\gamma)}\,\langle P(p)|P|0\rangle}{2E}$$
$$\times\left[\sum_n \frac{\langle 0|J_W^\nu(0)|n\rangle\,\langle n|J_{\rm em}^\mu(0,\boldsymbol{k})|P(p)\rangle}{2E_n\,(E_\gamma+E_n-E)} + \sum_n \frac{\langle 0|J_{\rm em}^\mu(0,\boldsymbol{k})|n\rangle\,\langle n|J_W^\nu(0)|P(p)\rangle}{2E_n\,(E_n-E_\gamma)}\right], \tag{1.70}$$

where we neglected all the terms that are exponentially suppressed in the time region $0 \ll t \ll \frac{T}{2}$.

By comparing Eq. (1.70) with Eqs. (1.35) and (1.36), we recognize the relation

$$\theta(T/2-t)C^{\mu\nu}(t,k,p) = \frac{e^{-t(E-E_\gamma)}\,\langle P(p)|P|0\rangle}{2E}\,[H^{\mu\nu}(k,p)]\,. \tag{1.71}$$

Now let's consider the second half of the lattice. From the spectral analysis we obtained:

$$\theta(t-T/2)C^{\mu\nu}(t,k,p) = C_4^{\mu\nu} + C_5^{\mu\nu} + C_6^{\mu\nu} = -i\,\frac{e^{-(T-t)\,(E-E_\gamma)}\langle 0|P|\,\overline{P}(p)\,\rangle}{2E}$$
$$\times\left[\sum_n \frac{\left\langle \overline{P}(p)\left|J_{\rm em}^\mu(0,\boldsymbol{k})\right|\overline{n}\right\rangle\,\langle \overline{n}\,|J_W^\nu(0)|0\rangle}{2E_n\,(E_\gamma+E_n-E)} + \sum_n \frac{\left\langle \overline{P}(p)\left|J_W^\nu(0)\right|\overline{n}\right\rangle\,\langle \overline{n}\,|J_{\rm em}^\mu(0,\boldsymbol{k})|0\rangle}{2E_n\,(E_n-E_\gamma)}\right]. \tag{1.72}$$

Looking at Eq. (1.72) we recognize that we obtained the time reversal process of the original one, or, which is equivalent to say, the CP (parity and charge) conjugate process. It can be demonstrated that, in the second half of the lattice, the correlator is equal to

$$\theta(t-T/2)C^{\mu\nu}(t,E_\gamma,\boldsymbol{k},\boldsymbol{p}) \;=\; \frac{e^{-(T-t)\,(E-E_\gamma)}\langle P(E,-\boldsymbol{p})|P|0\rangle}{2E}\,H^{\mu\nu}(E_\gamma,-\boldsymbol{k},E,-\boldsymbol{p})\,. \tag{1.73}$$

Thus, our final formula, which relates the Euclidean lattice correlator to the physical Minkowskian hadronic tensor in both halves of the lattice, is

$$\begin{aligned} C^{\mu\nu}(t,E_\gamma,\boldsymbol{k},\boldsymbol{p}) \;=\;& \theta(T/2-t)\,\frac{e^{-t(E-E_\gamma)}\,\langle P|P|0\rangle}{2E}H^{\mu\nu}(E_\gamma,\boldsymbol{k},E,\boldsymbol{p}) \\ &+\theta(t-T/2)\,\frac{e^{-(T-t)\,(E-E_\gamma)}\langle P(E,-\boldsymbol{p})|P|0\rangle}{2E}H^{\mu\nu}(E_\gamma,-\boldsymbol{k},E,-\boldsymbol{p})\,. \end{aligned} \tag{1.74}$$

By looking at the form factor decomposition in Eqs. (1.19) - (1.21), we can deduce the properties of the different Lorentz components when inverting the spatial momenta $\boldsymbol{p}$ and $\boldsymbol{k}$. For example, when both indices are either temporal or spatial ones, the axial component of the hadronic tensor is even with respect to the spatial momenta, while the vector component is odd. Vice versa, with one temporal index and a spatial one, the axial component of the hadronic tensor is odd while the vector one is even.

We use these time reversal properties of the lattice correlators, to either symmetrize or anti-symmetrize the correlators between the two halves $[0, \frac{T}{2}]$ and $[\frac{T}{2}, T]$ of the lattice, and then we will work just within the first half of the lattice time-extent, defining

$$H_L^{\mu\nu}(t,k,\boldsymbol{p}) = \frac{2E}{e^{-t(E-E_\gamma)}\,\langle P(p)|P|0\rangle} C^{\mu\nu}(t,E_\gamma,\boldsymbol{k},\boldsymbol{p}) = H^{\mu\nu}(k,\boldsymbol{p}) + ... \tag{1.75}$$

where the subscript L stands for "lattice" and the ellipsis represents the sub-leading exponentials.

As we have shown, the average of the correlator between the two halves of the lattice is equivalent to the average between opposite directions of the spatial momenta. By working with a twisted mass lattice action at maximal twist, this fact ensures the $O(a)$-improvement, with a being the lattice spacing, i.e. the reduction of the discretization errors to ones of $O(a^2)$ [43].

On the lattice, it is useful to compute and study separately the axial and the vector part of the correlators in order to determine the corresponding form factors.

1.4.1 Infrared behavior of the lattice three-point functions

In this section we study the behavior of the lattice Euclidean correlation function $C^{\mu\nu}(t,E_\gamma,\boldsymbol{k},\boldsymbol{p})$ in the limit $k \to 0$ which, as we will see below, is nontrivial. From the spectral analysis, see for example Eq. (1.64), one can see that

$$C^{\mu\nu}(t,E_\gamma,\boldsymbol{k},\boldsymbol{p}) = c_1^{\mu\nu} e^{-tE(\boldsymbol{p})} + c_2^{\mu\nu} e^{-t\{E(\boldsymbol{p}-\boldsymbol{k})+E_\gamma\}} + \dots \ , \tag{1.76}$$

where the dots represent exponentially suppressed contributions with an energy gap which, in the soft photon limit, is of the order of $2m_\pi$. The first exponential corresponds to the on-shell external meson $P(\boldsymbol{p})$ with spatial momentum $\boldsymbol{p}$, and gives the contribution we aim to isolate, while the second exponential corresponds to the $P(\boldsymbol{p}-\boldsymbol{k})+\gamma$ internal state, composed of an on-shell meson $P(\boldsymbol{p}-\boldsymbol{k})$ with spatial momentum $\boldsymbol{p}-\boldsymbol{k}$, and a virtual photon with spatial momentum $\boldsymbol{k}$ and off-shell energy E_γ. In other words, the second exponential represents the unphysical contribution given from the lightest internal state contributing to the correlator in the time-ordering $t_x < t$. Previously, in Sec. 1.2.1, we demonstrated the validity of the condition $E(\boldsymbol{p}-\boldsymbol{k})+E_\gamma > E(\boldsymbol{p})$. However, this is true only for non-vanishing values of the photon four-momentum. Indeed, when either $\boldsymbol{k}$ or E_γ are non-zero, it is possible to isolate the matrix element corresponding to the ground state $P(\boldsymbol{p})$, since the second exponential in Eq. (1.76) is subleading at large time separations t. Instead, in the exact limit $k \to 0$, the energy-gap between the two states vanishes, and the lattice Euclidean correlator $C^{\mu\nu}(t,0,\boldsymbol{0},\boldsymbol{p})$ has a non-trivial behavior which we now discuss, paying special attention to the leading cutoff effects. This has been already done for $P \to \ell\nu_\ell\gamma$ decays, with the emission of a real photon, in Appendix C of Ref. [6], focusing on the spatial components of $C^{\mu\nu}$, which are the only ones relevant in that case. Now, we generalize the analysis of Ref. [6] to the components $C^{0\nu}$ and $C^{\mu 0}$, with $\mu,\nu = 0,1,2,3$.

The starting point is the electromagnetic Ward Identity that, for Wilson-like Fermions adopted in this study, reads [6]

$$\sum_{\mu=0}^{3} \frac{2}{a} \sin\left(ak_\mu/2\right) C_A^{\mu\nu}(t,k,\boldsymbol{p}) = C_A^{\nu}(t,\boldsymbol{p}) - C_A^{\nu}(t,E_\gamma,\boldsymbol{p}-\boldsymbol{k})\,, \tag{1.77}$$

where we have defined

$$C_A^{\mu\nu}(t,k,\boldsymbol{p}) = -i\int d^4y\, d^3\boldsymbol{x}\, e^{-ik\cdot(y+\hat{\mu}/2)-i\boldsymbol{p}\cdot\boldsymbol{x}}\langle 0|T[\, J_A^\nu(0)\, J_{\rm em}^\mu(y)\, P(-t,-\boldsymbol{x})\,]|0\rangle\,, \quad (1.78)$$

$$\begin{aligned} C_A^{\nu}(t,\boldsymbol{p}) &= \int d^3\boldsymbol{x}\, e^{-i\boldsymbol{p}\cdot\boldsymbol{x}}\langle 0|T[\, J_A^\nu(0)\, P(-t,-\boldsymbol{x})\,]|0\rangle \\ &= p^\nu\, \frac{\hat{f}_P(\boldsymbol{p})\,\hat{G}_P(\boldsymbol{p})}{2\hat{E}(\boldsymbol{p})} e^{-t\hat{E}(\boldsymbol{p})} + \dots\,, \end{aligned} \quad (1.79)$$

$$\begin{aligned} C_A^{\nu}(t,\hat{E}_\gamma,\boldsymbol{p}-\boldsymbol{k}) &= e^{-\hat{E}_\gamma t}\int d^3\boldsymbol{x}\, e^{-i(\boldsymbol{p}-\boldsymbol{k})\cdot\boldsymbol{x}}\langle 0|T[\, J_A^\nu(0)\, P(-t,-\boldsymbol{x})\,]|0\rangle \\ &= u^\nu\, \frac{\hat{f}_P(\boldsymbol{p}-\boldsymbol{k})\,\hat{G}_P(\boldsymbol{p}-\boldsymbol{k})}{2\hat{E}(\boldsymbol{p}-\boldsymbol{k})} e^{-t\hat{E}(\boldsymbol{p}-\boldsymbol{k})-t\hat{E}_\gamma} + \dots\,, \end{aligned} \quad (1.80)$$

and where the ellipsis represents sub-leading exponentials with an energy gap that, in the infrared limit, starts at order $2m_\pi$. In Eqs. (1.78) - (1.80) the integrals are to be read as lattice sums, $k = (i\hat{E}_\gamma, \boldsymbol{k})$ is the Euclidean photon's four-momentum, while the on-shell Euclidean four-momenta of the mesons $P(\boldsymbol{p})$ and $P(\boldsymbol{p}-\boldsymbol{k})$ are given respectively by

$$p = \Big(i\hat{E}(\boldsymbol{p}),\, \boldsymbol{p}\Big)\,, \qquad u = \Big(i\hat{E}(\boldsymbol{p}-\boldsymbol{k}),\, \boldsymbol{p}-\boldsymbol{k}\Big)\,. \quad (1.81)$$

In the previous expressions, the hat symbol denotes lattice quantities, which are related to their continuum counterpart by [4]

$$\begin{aligned} &\hat{f}_P(\boldsymbol{p}) = f_P + O(a^2)\,, \quad \hat{G}_P(\boldsymbol{p}) = G_P + O(a^2)\,, \\ &\hat{E}(\boldsymbol{p}) = E + O(a^2)\,, \quad \hat{E}_\gamma = E_\gamma + O(a^2)\,, \end{aligned} \quad (1.82)$$

where f_P, G_P, $E(\boldsymbol{p})$ and E_γ are respectively the continuum decay constant, the continuum matrix element of the pseudoscalar density used as the interpolating operator ($G_P = \langle 0|P|P(\boldsymbol{p})\rangle$), the continuum energy of the meson and of the virtual photon.

We now differentiate Eq. (1.77) with respect to k^μ and then set $k=0$. Since we are considering a generic off-shell photon, the temporal and spatial components of the photon momentum k^μ are treated as independent quantities. When the indices μ and ν are spatial, one obtains the result quoted in Eq. (C17) of Ref. [6],

$$\begin{aligned} C_A^{ij}(t,0,\boldsymbol{p}) = {}& \frac{\hat{f}_P(\boldsymbol{p})\hat{G}_P(\boldsymbol{p})}{2\hat{E}(\boldsymbol{p})} e^{-t\hat{E}(\boldsymbol{p})} \\ &\times \left\{ \delta^{ij} + p^j \left[\frac{1}{\hat{f}_P(\boldsymbol{p})}\frac{\partial \hat{f}_P(\boldsymbol{p})}{\partial p^i} + \frac{1}{\hat{G}_P(\boldsymbol{p})}\frac{\partial \hat{G}_P(\boldsymbol{p})}{\partial p^i} - \left(t + \frac{1}{\hat{E}(\boldsymbol{p})}\right)\frac{\partial \hat{E}(\boldsymbol{p})}{\partial p^i} \right] \right\} + \dots\,. \end{aligned} \quad (1.83)$$

[4] In our Twisted mass formulation, cut-off effects on parity-even observables start at order $\mathrm{O}(a^2)$.

Moreover, the $H(3)$ symmetry of the lattice implies

$$\frac{\partial \hat{f}_P(\boldsymbol{p})}{\partial p^i} = p^i \times O(a^2), \quad \frac{\partial \hat{G}_P(\boldsymbol{p})}{\partial p^i} = p^i \times O(a^2), \quad \frac{\partial \hat{E}(\boldsymbol{p})}{\partial p^i} = \frac{p^i}{E(\boldsymbol{p})} \times \Big(1 + O(a^2)\Big) \tag{1.84}$$

so that

$$C_A^{ij}(t,0,\boldsymbol{p}) = \frac{\hat{f}_P(\boldsymbol{p})\,\hat{G}_P(\boldsymbol{p})}{2\hat{E}(\boldsymbol{p})} e^{-t\hat{E}(\boldsymbol{p})} \left\{ \delta^{ij} - \frac{p^i\,p^j}{\hat{E}^2(\boldsymbol{p})} \Big(1 + t\,\hat{E}(\boldsymbol{p}) + O(a^2)\Big) \right\} + \dots . \tag{1.85}$$

In the rest frame of the meson, $\boldsymbol{p} = \boldsymbol{0}$, which we use in our study, we therefore obtain for the spatial components of the correlation function:

$$C_A^{ij}(t,0,\boldsymbol{0}) = \delta^{ij}\,\frac{\hat{f}_P(\boldsymbol{0})\,\hat{G}_P(\boldsymbol{0})}{2\hat{E}(\boldsymbol{0})} e^{-t\hat{E}(\boldsymbol{0})} + \dots . \tag{1.86}$$

For the component C_A^{00} the same procedure gives

$$C_A^{00}(t,0,\boldsymbol{p}) = -t\,\hat{E}(\boldsymbol{p})\,\frac{\hat{f}_P(\boldsymbol{p})\,\hat{G}_P(\boldsymbol{p})}{2\hat{E}(\boldsymbol{p})} e^{-t\hat{E}(\boldsymbol{p})} + \dots . \tag{1.87}$$

For the components C_A^{i0}, i.e. for the correlation function with J_A^0 and $J_{\rm em}^i$, we obtain

$$\begin{aligned} C_A^{i0}(t,0,\boldsymbol{p}) &= \frac{\hat{f}_P(\boldsymbol{p})\,\hat{G}_P(\boldsymbol{p})}{2\hat{E}(\boldsymbol{p})} e^{-t\hat{E}(\boldsymbol{p})} \times \hat{E}(\boldsymbol{p}) \left[\frac{1}{\hat{f}_P(\boldsymbol{p})} \frac{\partial \hat{f}_P(\boldsymbol{p})}{\partial p^i} + \frac{1}{\hat{G}_P(\boldsymbol{p})} \frac{\partial \hat{G}_P(\boldsymbol{p})}{\partial p^i} - t\,\frac{\partial \hat{E}(\boldsymbol{p})}{\partial p^i} \right] + \dots \\ &= -\frac{\hat{f}_P(\boldsymbol{p})\,\hat{G}_P(\boldsymbol{p})}{2\hat{E}(\boldsymbol{p})} e^{-t\hat{E}(\boldsymbol{p})} \times \hat{E}(\boldsymbol{p})\,p^i \Big(t + O(a^2)\Big) + \dots , \end{aligned} \tag{1.88}$$

that in our reference frame becomes

$$C_A^{i0}(t,0,\boldsymbol{0}) \;=\; 0 + \dots . \tag{1.89}$$

Similarly, for the components C_A^{0i}, differentiating equation Eq. (1.77) results in

$$C_A^{0j}(t,0,\boldsymbol{p}) \;=\; -p^j\,t\,\frac{\hat{f}_P(\boldsymbol{p})\,\hat{G}_P(\boldsymbol{p})}{2\hat{E}(\boldsymbol{p})} e^{-t\hat{E}(\boldsymbol{p})} + \dots , \tag{1.90}$$

which in the rest frame of the meson becomes

$$C_A^{0j}(t,0,\boldsymbol{0}) \;=\; 0 + \dots . \tag{1.91}$$

As we will see in the next section, Eq. (1.86) allows one to subtract the point-like contribution from the diagonal spatial components C_A^{ii} components, non-perturbatively to all orders in the lattice

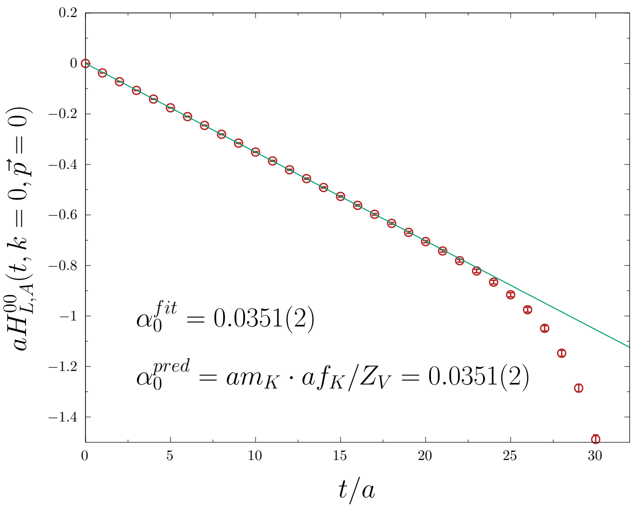

Figure 1.6: *Determination of the* 00 *component of the hadronic tensor, from the lattice three-point correlation function at* $k = 0$*. The green line is the result of a linear fit in time* $aH^{00}_{L,A}(t, 0, \mathbf{0}) = -\alpha_0^{fit} t$*, where* α_0^{fit} *is a fit parameter, and which is compared with the predicted value,* α_0^{pred}*, derived from Eq. (1.87). The fit was performed in the interval* $t = (4, 21)$*, away from the center of the lattice, where backward propagating contributions to the correlation function become significant.*

spacing a. From Eqs. (1.89) and (1.90), we see that, instead, in the limit $k \to 0$ the contribution from the $P(\boldsymbol{p} - \boldsymbol{k}) + \gamma$ state exactly cancels the signal. Hence, for such components, it is not possible to extract, in the exact limit $k = 0$, the physical matrix element from the Euclidean three point function.

Finally, it is worthwhile noting the peculiar behavior in t of the purely temporal component of the lattice three point function, $C^{00}_A(t, 0, \boldsymbol{p})$. From Eq. (1.87) it can be seen that $C^{00}_A(t, 0, \boldsymbol{p})$ exhibits a time-behavior of type $t\, e^{-t\hat{E}_P(\boldsymbol{p})}$, which is a manifestation of the singular behavior of the correlation function at large distances, and which gives rise to a double pole in momentum space. In our simulation, we found numerical evidence for the presence of such a behavior. This is shown in Fig. 1.6, where we compare our numerical data for $H^{00}_{L,A}(t, 0, \mathbf{0})$, defined in Eq. (1.75), with the prediction of Eq. (1.87).

We remark that in our analysis we have not used the purely temporal component C^{00}_A, which would make it difficult to identify the plateaux due to the presence of a large contribution from the excited state $P(\boldsymbol{p} - \boldsymbol{k}) + \gamma$, at small values of k.

1.5 Form factor lattice estimators

In the last section, we explained in detail how the hadronic tensor $H^{\mu\nu}$ can be extracted on the lattice from the Euclidean three-point function $C^{\mu\nu}$. Now we face the problem of employing the lattice quantity $H^{\mu\nu}_L$, defined in Eq. (1.75), to define lattice estimators for the structure dependent form factors. To this end, we first need to choose a specific reference frame.

1.5.1 Reference frame and non-zero components

In our numerical study we choose the meson to be at rest, $\boldsymbol{p} = \boldsymbol{0}$, since we found that the lattice correlation functions are less noisy in this case, and the spatial momentum of the photon to be in the z-direction, $\boldsymbol{k} = (0, 0, k_z)$. The form-factors depend on two independent variables which can be chosen to be the invariants k^2, where k is the four-momentum of the photon, and $q^2 \equiv (p - k)^2$. In Chapter 2 we present our results in terms of the dimensionless variables x_k and x_q defined in Eq. (2.1) in terms of k^2 and q^2. In this section however, in which we discuss the extraction of the form factors from correlation functions computed in the frame defined above, it is more transparent to present the discussion with k^2 and k_z as the independent variables, together with the energy of the photon E_γ given by $E_\gamma^2 = k^2 + k_z^2$.

In the rest frame of the meson and with $\boldsymbol{k} = (0, 0, k_z)$, the only non-zero elements of the vector component of the hadronic tensor, $H_V^{\mu\nu}$, are H_V^{12} and H_V^{21} which are related to the vector form factor F_V by

$$H_V^{12} = -H_V^{21} = iF_V k_z \,. \tag{1.92}$$

The axial component of the hadronic tensor, $H_A^{\mu\nu}$, is parametrized by the SD form factors F_A, H_1 and H_2, and by the meson decay constant f_P. In the reference frame defined above, the non-zero elements of $H_A^{\mu\nu}$ are given by

$$\begin{aligned}
H_A^{00} &= -H_1 \frac{k_z^2}{m_P} - H_2 \frac{k_z^2\,(m_P - E_\gamma)}{2m_P E_\gamma - k^2} - F_A \frac{k_z^2}{m_P} + f_P \frac{2m_P^2 - m_P E_\gamma + k_z^2}{2m_P E_\gamma - k^2}\,, && (1.93)\\
H_A^{03} &= -H_1 \frac{E_\gamma k_z}{m_P} + H_2 \frac{k_z (E_\gamma^2 - k^2)}{2m_P E_\gamma - k^2} - F_A \frac{(m_P - E_\gamma)\, k_z}{m_P} - f_P \frac{k_z\,(2m_P - E_\gamma)}{2m_P E_\gamma - k^2}\,, && (1.94)\\
H_A^{30} &= -H_1 \frac{E_\gamma k_z}{m_P} - H_2 \frac{k_z E_\gamma\,(m_P - E_\gamma)}{2m_P E_\gamma - k^2} + F_A \frac{k_z E_\gamma}{m_P} - f_P \frac{k_z\,(m_P - E_\gamma)}{2m_P E_\gamma - k^2}\,, && (1.95)\\
H_A^{33} &= -H_1 \frac{E_\gamma^2}{m_P} + H_2 \frac{E_\gamma k_z^2}{2m_P E_\gamma - k^2} - F_A \frac{E_\gamma\,(m_P - E_\gamma)}{m_P} - f_P \frac{E_\gamma\,(2m_P - E_\gamma)}{2m_P E_\gamma - k^2}\,, && (1.96)\\
H_A^{11} &= H_A^{22} = -H_1 \frac{k^2}{m_P} - F_A \frac{(m_P E_\gamma - k^2)}{m_P} - f_P\,. && (1.97)
\end{aligned}$$

Here and in the following we use continuum notation for the four-vectors but in lattice computations, in order to reduce the discretization uncertainties, the energy and momentum carried by the electromagnetic current can be understood by the following replacements:

$$k_z \to \hat{k}_z = \frac{2}{a}\sin\left(\frac{ak_z}{2}\right), \quad E_\gamma = \frac{2}{a}\sinh^{-1}\left[\frac{a}{2}\sqrt{\hat{k}_z^2 + \left(\frac{2}{a}\sinh\left(\frac{a\sqrt{k^2}}{2}\right)\right)^2}\,\right] \tag{1.98}$$

where k_z and $\sqrt{k^2}$ are the continuum, physical values for the photon's spatial momentum (which here is directed along the z-axis) and for the photon's virtuality respectively.

In order to extract the axial form factors, we need to combine these non-zero component of $H_A^{\mu\nu}$

into three independent expressions of F_A, H_1 and H_2, in which the point-like term proportional to f_P has been subtracted. We now address the delicate issue of subtracting the point-like term.

1.5.2 Subtraction of the point-like term

To determine the SD axial form factors from knowledge of the non-zero components of $H_A^{\mu\nu}$, it is necessary to subtract the point-like terms proportional to f_P. From the previous equations, it follows that the point-like terms become dominant in the infrared limit, $k \to 0$, where the SD part of the hadronic tensor vanishes. This is expected, since soft photons cannot probe the internal structure of the meson. However, this poses the problem for the numerical evaluation of the SD form factors at small k^2, that residual $\mathcal{O}(a^2)$ discretization effects in the subtraction of the point-like term contribute as enhanced artifacts in the determined values of the SD form factors. Moreover, these artifacts diverge as $k \to 0$. This problem has already been encountered in the previous work on $P \to \ell\bar{\nu}_\ell\gamma$ decays [6], where it was found that performing the subtraction using the value of f_P extracted from two-point correlation functions results in unphysically large values of F_A in the soft-photon limit. In the same paper, a solution to this problem was proposed. It has been showed that by exploiting the electromagnetic Ward Identity in the lattice theory, the subtraction of the point-like contribution can be performed non-perturbatively to all orders in the lattice spacing, thus avoiding infrared-divergent lattice artifacts in the resulting SD form factors. In particular, it has been demonstrated that, for the diagonal spatial components of the lattice correlation function, which are smooth in the limit $k \to 0$, this can be achieved by using the values of f_P obtained from the same components evaluated at zero photon momentum [6].

A similar situation occurs also when the final-state photon is virtual, albeit in this case the lepton masses provide an energy-momentum cut-off for the photon. Proceeding similarly, we define the subtracted quantities for the diagonal components as follows:

$$
\begin{aligned}
\tilde{H}_A^{33}(k_z,k^2) &\equiv H_A^{33}(k_z,k^2) - H_A^{33}(0,0)\frac{E_\gamma\,(2m_P - E_\gamma)}{2m_P E_\gamma - k^2} \\
&= -H_1\frac{E_\gamma^2}{m_P} + H_2\frac{E_\gamma k_z^2}{2m_P E_\gamma - k^2} - F_A\frac{E_\gamma\,(m_P - E_\gamma)}{m_P} \\
\tilde{H}_A^{11}(k_z,k^2) &\equiv H_A^{11}(k_z,k^2) - H_A^{11}(0,0) \\
&= -H_1\frac{k^2}{m_P} - F_A\frac{(m_P E_\gamma - k^2)}{m_P}\,.
\end{aligned}
\tag{1.99}
$$

Unfortunately, the same procedure cannot be used for the other components. The reason is that, in the limit $k \to 0$, the "excited" state consisting of a meson P with momentum $-\boldsymbol{k}$ and a photon with energy E_γ becomes degenerate with the "ground" state of the meson P at rest. As we have explicitly shown in Sec. 1.4.1, in the $k \to 0$ limit, the off-diagonal components, C_A^{30} and C_A^{03} go to zero; the contribution of the $P + \gamma$ state cancels that of the ground state. These components at zero photon momentum cannot therefore be used to subtract the contribution proportional to f_P. Instead, we define a linear combination of the two off-diagonal components, which in the continuum cancels the point-like term proportional to f_P, that is:

$$\begin{aligned} H_A^{[3,0]}(k_z,k^2) &\equiv H_A^{30}(k_z,k^2) - H_A^{03}(k_z,k^2)\left(\frac{m_P-E_\gamma}{2m_P-E_\gamma}\right) \\ &= -H_1\frac{E_\gamma k_z}{2m_P-E_\gamma} - H_2\frac{k_z(m_P-E_\gamma)}{2m_P-E_\gamma} + F_A\frac{k_z m_P}{2m_P-E_\gamma}\,. \end{aligned} \tag{1.100}$$

In the numerical study of $K\to\ell\,\nu_\ell\,\ell'^+\,\ell'^-$ decays, we also have an infrared cut-off on the photon virtuality k^2, given either by the non-negligible muon mass or by the experimental cut on the two-electron invariant mass $m_{ee}=\sqrt{k^2}>145$ MeV [9]. We observe that the form factors have a smooth behavior as a function of the photon momentum, without any anomalous increase in the infrared region caused by residual discretization errors in the subtraction of the point-like term.

An alternative possibility, one which we have not explored in this study, would be to compute the correlation function with the meson in motion ($\boldsymbol{p}\neq\mathbf{0}$) and to use different components of the correlation functions to extract the form factors.

1.5.3 Lattice estimators

Once we computed three independent linear combinations of the three axial form factors using lattice QCD, the form factors themselves are obtained by inverting the matrix of coefficients. Specifically, our estimators of the axial form factors, $\bar{H}_1(t,k^2,k_z), \bar{H}_2(t,k^2,k_z)$ and $\bar{F}_A(t,k^2,k_z)$, are obtained from the axial component of the lattice tensor $H^{\mu\nu}_{L,A}(t,k)\equiv H^{\mu\nu}_{L,A}(t,k,\mathbf{0})$ of Eq. (1.75) as follows:

$$\begin{pmatrix} \bar{H}_1(t,k^2,k_z) \\ \bar{H}_2(t,k^2,k_z) \\ \bar{F}_A(t,k^2,k_z) \end{pmatrix} \equiv \begin{pmatrix} -\frac{E_\gamma k_z}{2m_P-E_\gamma} & -\frac{k_z(m_P-E_\gamma)}{2m_P-E_\gamma} & \frac{k_z m_P}{2m_P-E_\gamma} \\ -\frac{E_\gamma^2+k^2}{m_P} & \frac{E_\gamma k_z^2}{2E_\gamma m_P-k^2} & \frac{E_\gamma^2-2E_\gamma m_P+k^2}{m_P} \\ \frac{k^2-E_\gamma^2}{m_P} & \frac{E_\gamma k_z^2}{2E_\gamma m_P-k^2} & \frac{E_\gamma^2-k^2}{m_P} \end{pmatrix}^{-1} \begin{pmatrix} H^{[3,0]}_{L,A}(t,k) \\ \tilde{H}^{33}_{L,A}(t,k)+\tilde{H}^{11}_{L,A}(t,k) \\ \tilde{H}^{33}_{L,A}(t,k)-\tilde{H}^{11}_{L,A}(t,k) \end{pmatrix} \tag{1.101}$$

We recall that the diagonal components $\tilde{H}^{33}_{L,A}$ and $\tilde{H}^{11}_{L,A}$ are defined in Eq. (1.99) after the subtraction of the point-like contributions proportional to $H^{33}_{A,L}(t,0)=H^{11}_{A,L}(t,0)=H^{22}_{A,L}(t,0)$. In the time region $0\ll t\ll T/2$, the estimators $\bar{H}_1(t,k^2,k_z), \bar{H}_2(t,k^2,k_z)$ and $\bar{F}_A(t,k^2,k_z)$, tend to the corresponding form factors.

In the limit $k_z\to 0$, two of the components of the vector on the right-hand side of Eq. (1.101), $H^{[3,0]}_{L,A}(t,k)$ and $\tilde{H}^{33}_{L,A}(t,k)-\tilde{H}^{11}_{L,A}(t,k)$, both go to zero for all values of k^2, see Eqs. (1.94) - (1.100). This fact can be used to define equivalent estimators of the form factors, obtained by making the following replacements in Eq. (1.101):

$$H^{[3,0]}_{L,A}(t,k)\to H^{[3,0]}_{L,A}(t,k)-H^{[3,0]}_{L,A}(t,(\sqrt{k^2},\mathbf{0})) \tag{1.102}$$

and

$$\tilde{H}^{33}_{L,A}(t,k) - \tilde{H}^{11}_{L,A}(t,k) \to \left(\tilde{H}^{33}_{L,A}(t,k) - \tilde{H}^{11}_{L,A}(t,k)\right) - \left(\tilde{H}^{33}_{L,A}(t,(\sqrt{k^2},\mathbf{0})) - \tilde{H}^{11}_{L,A}(t,(\sqrt{k^2},\mathbf{0}))\right) \; . \tag{1.103}$$

The correlated subtraction of the contribution coming from the kinematic point with the same value of k^2 but zero photon spatial momentum k_z, help to reduce the statistical noise of the estimators and improves the corresponding plateaux. The amount of improvement depends on the kinematic point and on the form factor being considered.

Finally, for the vector form factor F_V, we define the following estimator:

$$\bar{F}_V(t,k^2,k_z) = \frac{H^{12}_{L,V}(t,k) - H^{2,1}_{L,V}(t,k)}{2ik_z} \; , \tag{1.104}$$

which, again, for $0 \ll t \ll T/2$ tends to the F_V form factor.

Having explained our procedure for extracting the SD form factors from three-point lattice correlation functions, we now proceed to present our numerical results.

Chapter 2

Lattice numerical results and analysis for the form factors

In this chapter, we implement the procedure developed in the previous sections in order to obtain a theoretical prediction for the structure dependent form factors entering the $K \to \ell\, \nu_\ell\, \ell'^+ \ell'^-$ decays.

After showing the lattice results we obtained for the form factors, we compare our results with ChPT predictions, experimental data and real photon emission in lattice simulations. We remember to the reader that in Appendix B are explained in detail all the basic elements of lattice QCD calculations.

2.1 Simulation strategy

The simulations have been performed on the $A40.32$ ensemble generated by the ETMC [2] with $N_f = 2+1+1$ dynamical quark flavors, a space-time volume of $32^3 \times 64$ and a lattice spacing of $a = 0.0885(36)\,\mathrm{fm}$. The analysis was performed on 100 gauge configurations. The light quarks are heavier than the corresponding physical ones and correspond to $m_\pi \simeq 320\,\mathrm{MeV}$ and $m_K \simeq 530\,\mathrm{MeV}$. These meson masses satisfy the condition $m_K < 2m_\pi$ which, as discussed in Sec. 1.2, guarantees the absence of internal lighter states that would spoil the Wick rotation and thus the extraction of the physical hadronic tensor from Euclidean correlators.

We used smeared interpolating sources for the kaon field, obtained applying 128 steps of Gaussian smearing with step-size parameter $\epsilon = 0.1$. Moreover, we used four stochastic sources on each time slice when inverting the Dirac operator. On this ensemble, the values of the two renormalization constants are $Z_A = 0.731(8)$ and $Z_V = 0.587(4)$ [2]. The statistical analysis of the lattice data has been performed employing the jackknife resampling method in order to properly handle autocorrelation effects and cross-correlations among the different form factors in the computation of the branching ratios.

Below, we will compare our results for the form factors and branching ratios with those determined in experiments [9] and chiral perturbation theory. While these comparisons are interesting and instructive, it must be remembered that our computations were performed with unphysical quark masses, at a single value of the lattice spacing and on a single volume. Until the corre-

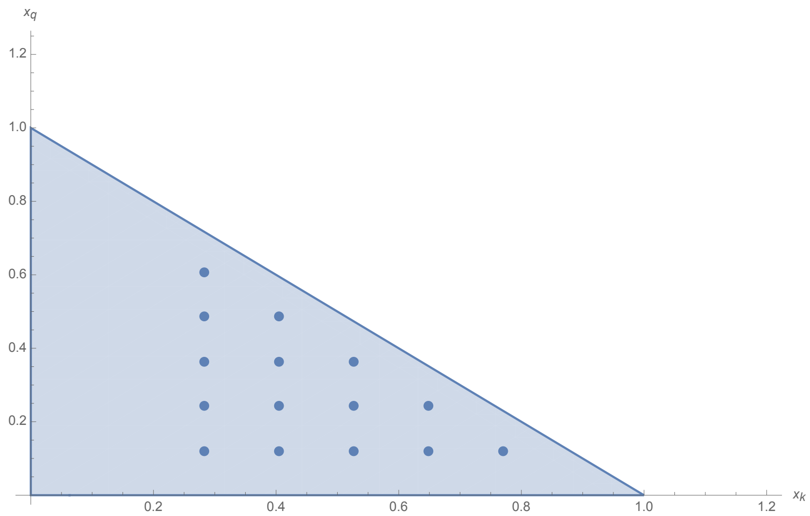

Figure 2.1: *The colored bands represent the range of allowed physical values of (x_k, x_q) when neglecting lepton masses, so that $0 < x_k < 1$ and $0 < x_q < 1 - x_k$. The points correspond to the 15 choices of (x_k, x_q) used in this analysis.*

sponding systematic uncertainties are studied in the future, the comparison with the experimental measurements may be indicative, but cannot be considered definitive.

2.1.1 Kinematics of the simulation

As already outlined in Sec. 1.3, we used twisted boundary conditions in order to evaluate the hadronic tensor for a range of values of the photon's spatial momentum $\boldsymbol{k}$. To probe the region of the phase-space relevant for the four $K \to \ell\, \nu_\ell\, \ell'^+ \ell'^-$ decay channels, with $\ell, \ell' = e, \mu$, we evaluate the Euclidean three-point functions $C^{\mu\nu}(t, E_\gamma, \boldsymbol{k}, \boldsymbol{p})$ for fifteen different values of $(E_\gamma, \boldsymbol{k})$, with $\boldsymbol{k} = (0, 0, k_z)$, and restricted our analysis to the kaon rest frame $\boldsymbol{p} = 0$. We find it convenient to parametrize the phase space in terms of the two dimensionless parameters x_k and x_q, defined as

$$x_k \equiv \sqrt{\frac{k^2}{m_K^2}}\,, \qquad x_q \equiv \sqrt{\frac{q^2}{m_K^2}}\,, \tag{2.1}$$

where q is the four-momentum of the lepton-neutrino pair created by the weak Hamiltonian. In terms of x_k and x_q the photon's four-momentum, $(E_\gamma, 0, 0, k_z)$, (in the kaon's rest frame) is given by

$$E_\gamma = \frac{m_K}{2}(1 + x_k^2 - x_q^2)\,, \qquad k_z = \frac{m_K}{2}\sqrt{(1 - x_k^2 - x_q^2)^2 - 4x_k^2 x_q^2}\,. \tag{2.2}$$

The allowed range of values of x_k and x_q is given in terms of the lepton masses, m_ℓ and $m_{\ell'}$, by

$$\frac{m_\ell}{m_K} \le x_q \le 1 - x_k\,; \qquad \frac{2m_{\ell'}}{m_K} \le x_k \le 1 - \frac{m_\ell}{m_K}, \tag{2.3}$$

so that the phase space has a triangular shape in the x_k - x_q plane.

In Fig. 2.1 we show the positions of the fifteen simulated kinematic configurations, which we take as equally spaced in the x_k - x_q plane. For completeness, the corresponding numerical values of x_k and x_q are reported in Tab. 2.1. In Tab.2.1, for each combination of x_k and x_q, we also reported the

x_k	x_q	off=$x_k \cdot am_K^L$	θ
0.28	0.12	0.074	0.60
0.28	0.24	0.074	0.56
0.28	0.36	0.074	0.50
0.28	0.48	0.074	0.41
0.28	0.61	0.074	0.29
0.41	0.12	0.11	0.54
0.41	0.24	0.11	0.50
0.41	0.36	0.11	0.42
0.41	0.48	0.11	0.30
0.53	0.12	0.14	0.46
0.53	0.24	0.14	0.41
0.53	0.36	0.14	0.30
0.65	0.12	0.17	0.36
0.65	0.24	0.17	0.28
0.77	0.12	0.20	0.23

Table 2.1: Values of (x_k, x_q) selected for the lattice calculation of the form factors. For each combination we also reported the offshellness $x_k \cdot (am_K^L)$ and the twisted angle θ to be assigned for the A40.32 ensemble.

corresponding parameters to be assigned to the lattice simulation for the $A40.32$ ensemble. They are the offshellness $x_k \cdot (am_K^L)$ and the twisted angle $\theta = \frac{L}{a\pi} \arcsin\left(a|\hat{k}|/2\right)$, where am_K^L is the kaon mass for the A40.32 ensemble in lattice units, a is the lattice spacing, L is the spatial length of the lattice and $a|\hat{k}|$ is the magnitude of the lattice spatial momentum in lattice unit. It should be noted that our computations are limited to $x_k \geq 0.28$. This choice is appropriate to describe both the cases in which a $\mu^+\mu^-$ or a e^+e^- pair is produced in the radiative decay of the kaon. Indeed, in the first case the lowest allowed value of x_k is given by $2m_\mu/m_K \simeq 0.428$, while for decays in which an e^+e^- pair is produced, although very low values of x_k are kinematically allowed, the experimental branching ratios have been determined with values of the electron-positron invariant mass $\sqrt{k^2} > 145\,\text{MeV}$ ($x_k > 0.294$) for $K^+ \to \mu^+\,\nu_\mu\,e^+\,e^-$ decays and $\sqrt{k^2} > 150\,\text{MeV}$ ($x_k > 0.304$) for $K^+ \to e^+\,\nu_e\,e^+\,e^-$ decays [9].

2.2 Form factor numerical results

For each kinematics, we compute on the lattice the correlators of Eq. (1.59) and we use the strategy explained in Sec. 1.5 to obtain the estimators of the structure dependent form factors. These are functions of the time t in which the weak current is placed, and when $0 \ll t \ll T/2$, if a plateau is reached, the value of the estimator will tend to the value of the relative form factor.

In Figs. 2.2, 2.3 and 2.4, we present the estimators $\bar{H}_1(t, x_k, x_q)$, $\bar{H}_2(t, x_k, x_q)$, $\bar{F}_A(t, x_k, x_q)$ and $\bar{F}_V(t, x_k, x_q)$ for selected values of x_k and x_q. In each figure, the shaded region indicates the result of a constant fit in the corresponding time interval. Figs. 2.2 and 2.3 illustrate the feature that for kinematics corresponding to small values of k_z (i.e. when $x_q + x_k \simeq 1$) the estimator of the axial

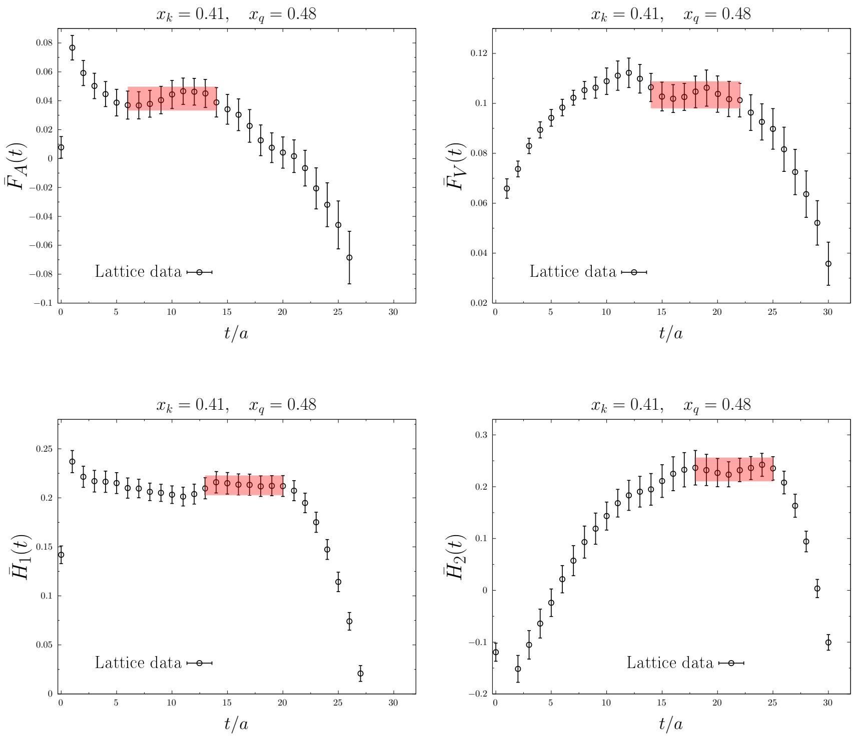

Figure 2.2: *Extraction of the form factors F_A, F_V, H_1, H_2 from the plateaux of the corresponding estimator. The data correspond to $x_k = 0.41$ and $x_q = 0.48$.*

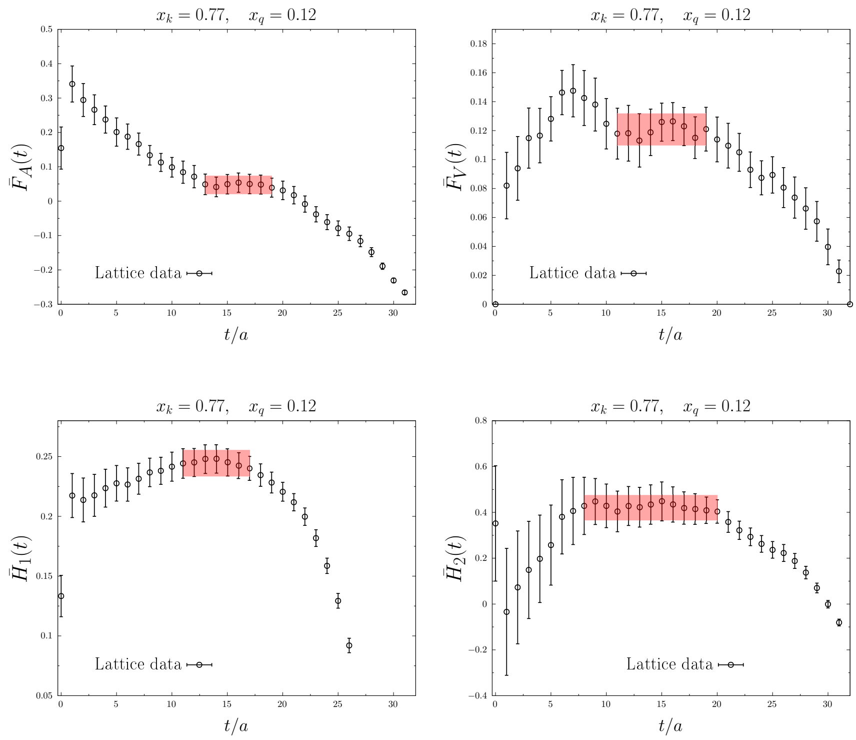

Figure 2.3: *Extraction of the form factors F_A, F_V, H_1, H_2 from the plateaux of the corresponding estimator. The data correspond to $x_k = 0.77$ and $x_q = 0.12$.*

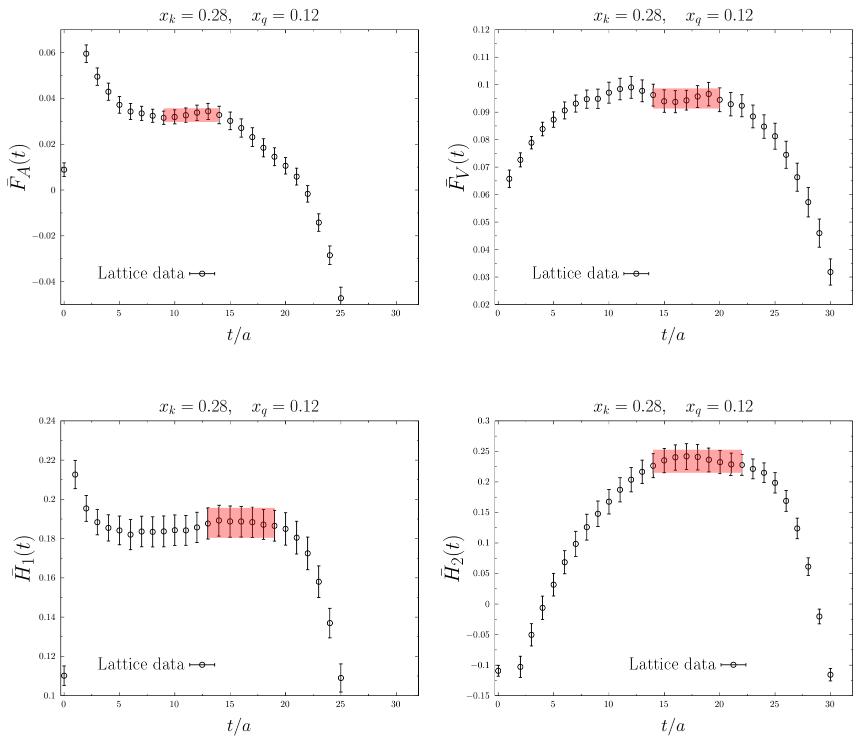

Figure 2.4: *Extraction of the form factors F_A, F_V, H_1, H_2 from the plateaux of the corresponding estimator. The data correspond to $x_k = 0.28$ and $x_q = 0.12$.*

form factor F_A becomes somewhat noisy, leading to increased uncertainties in its determination. On the other hand, for other values of (x_k, x_q) and for all other form factors, the precision achieved is very good and typically of the order of five to ten percent. To check the stability of our numerical results, we verified that the values of the form factors remain consistent within errors by changing the time interval adopted for the fits by a few units.

2.3 Form factor analysis

In the previous section, we presented our numerical results obtained for the structure dependent form factors at fifteen different kinematics. But in order to obtain a differential decay rate in momentum space, and then to integrate it in the phase space, we need an expression of the form factors as continuum functions of the two variables x_k and x_q. To do so, we fit the lattice form factors, using two different ansatzes to describe their dependence on x_k and x_q. The first is a simple polynomial in x_k^2 and x_q^2 given by

$$F_{\text{poly}}(x_k, x_q) = a_0 + a_k x_k^2 + a_q x_q^2\,, \tag{2.4}$$

where a_0, a_k and a_q are free fitting parameters. We find that this simple form represents our data very well, and the corresponding results presented in Chapter 3 for the branching ratios are obtained using Eq. (2.4). However, we have also performed fits using ansatzes which include additional terms which are quartic in x_k and x_q, i.e. terms proportional to $x_k^2 x_q^2$, x_k^4 and x_q^4. We find that including

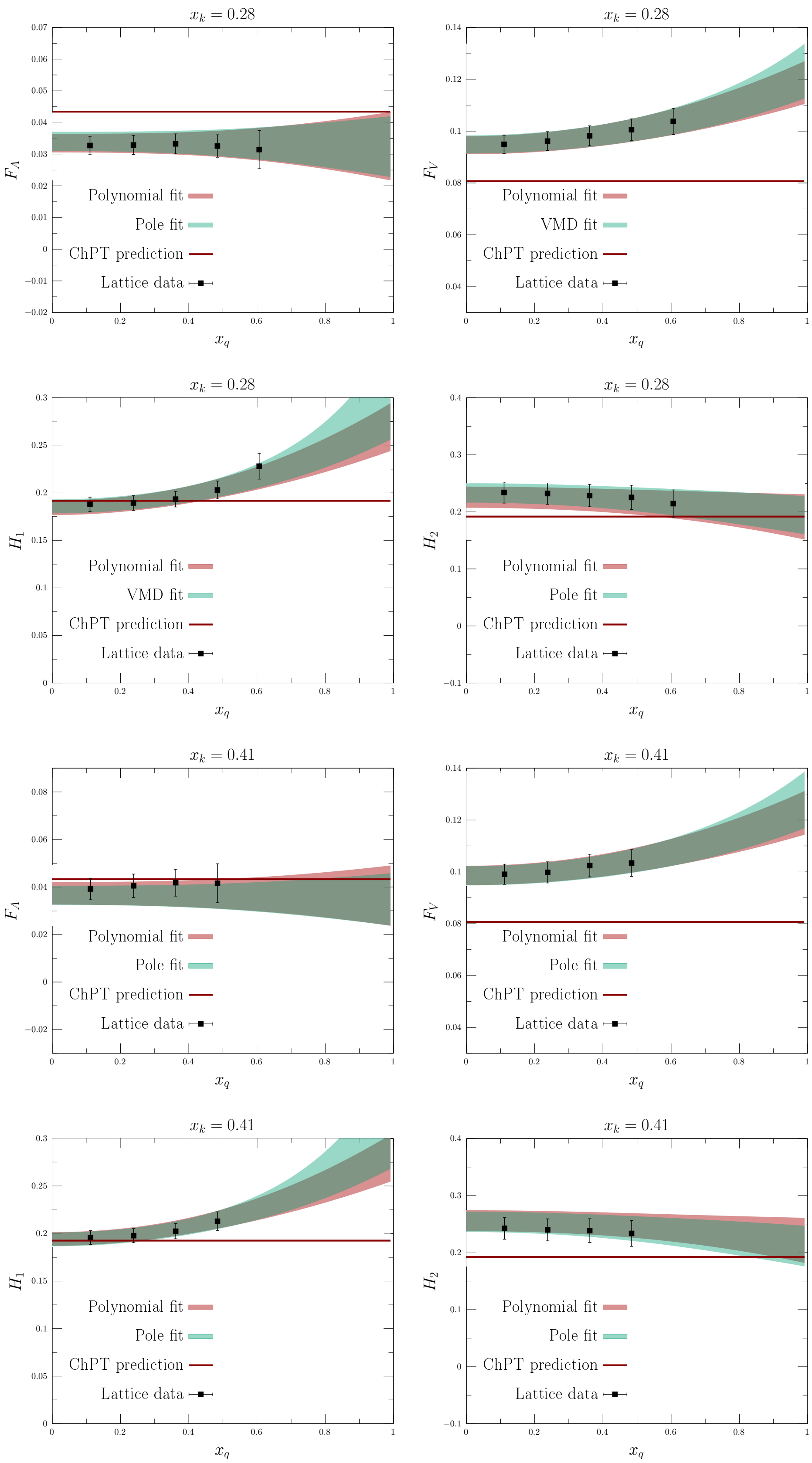

Figure 2.5: *The fitting functions corresponding to the polynomial and the pole-like fits of Eqs. (2.4) and(2.5) are plotted, along with the lattice data, as function of x_q and at a fixed value of $x_k = 0.28$ (panels 1-4) and $x_k = 0.41$ (panels 5-8) . The red line corresponds to the 1-loop ChPT prediction with $F = f_K/\sqrt{2}$.*

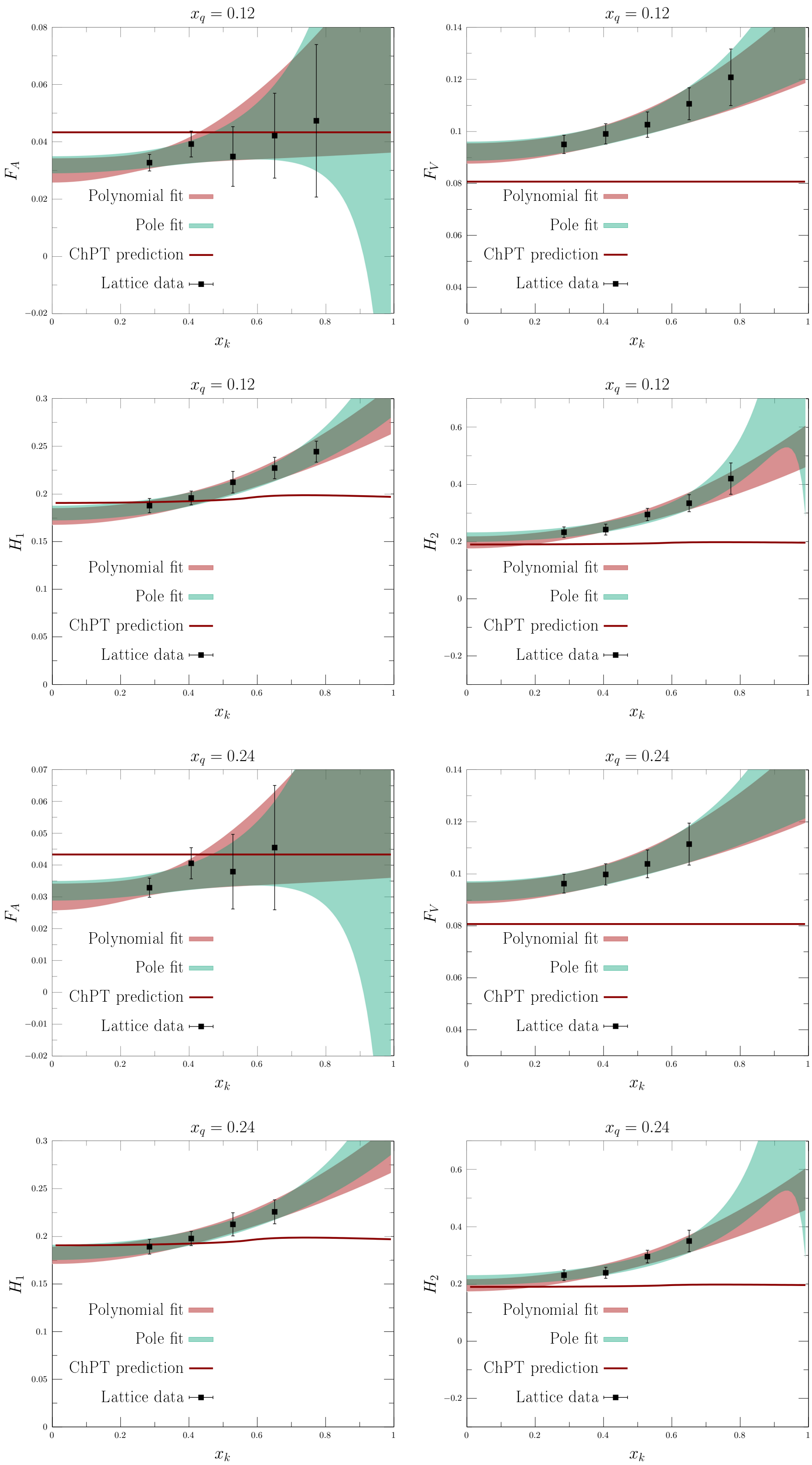

Figure 2.6: *The fitting functions corresponding to the polynomial and the pole-like fits of Eqs. (2.4) and(2.5) are plotted, along with the lattice data, as function of x_k and at a fixed value of $x_q = 0.12$ (panels 1-4) and $x_q = 0.24$ (panels 5-8). The red line corresponds to the 1-loop ChPT prediction with $F = f_K/\sqrt{2}$.*

all or some of such terms does not improve the fits, generally results in overfitting our data, and only negligibly changes the results for the form factors and decay rates.

The second ansatz has a pole-like structure of the form

$$F_{\text{pole}}(x_k, x_q) = \frac{A}{(1 - R_k x_k^2)\left(1 - R_q x_q^2\right)}\,, \tag{2.5}$$

where again A, R_k and R_q are free fitting parameters. The quality of the fit in all cases is very good, with the reduced χ^2 always smaller than one.

The results of both fits for each form factor are showed in the panels of Figs. 2.5 - 2.6. The two colored bands represent the result of the form factor interpolations obtained using either the polynomial or the pole-like ansatz (Eqs. (2.4) and (2.5) respectively). In each panel, we represent a form factor as a function of x_q at fixed x_k, or vice-versa. The red line represent the ChPT prediction for that form factor at next to leading order, which we discuss in detail in the next section. The parameters of both the polynomial and pole-like fits are collected in Tab. 2.2.

	a_0	a_k	a_q	A	R_k	R_q
H_1	0.1755(88)	0.113(30)	0.086(24)	0.1792(78)	0.453(88)	0.40(10)
H_2	0.199(21)	0.341(84)	-0.03(3)	0.217(17)	0.87(12)	-0.2(2)
F_A	0.0300(43)	0.04(4)	0.00(1)	0.0320(30)	0.74(50)	0.0(3)
F_V	0.0912(39)	0.044(18)	0.0246(59)	0.0921(38)	0.38(13)	0.233(49)

Table 2.2: *Values of the fit parameters for all the form factors, as obtained from the polynomial and pole-like fits of Eqs. (2.4) and (2.5).*

	a_{0,H_1}	a_{k,H_1}	a_{q,H_1}	a_{0,H_2}	a_{k,H_2}	a_{q,H_2}	a_{0,F_A}	a_{k,F_A}	a_{q,F_A}	a_{0,F_V}	a_{k,F_V}	a_{q,F_V}
a_{0,H_1}	1	-0.49	0.33	0.89	-0.58	-0.016	0.34	-0.79	-0.64	0.44	-0.18	0.18
a_{k,H_1}	-0.49	1	-0.40	-0.38	0.31	0.10	-0.65	0.60	0.19	0.076	-0.052	0.14
a_{q,H_1}	0.33	-0.40	1	0.30	-0.51	-0.66	-0.017	-0.081	-0.24	0.40	-0.56	0.27
a_{0,H_2}	0.89	-0.38	0.30	1	-0.76	-0.083	0.37	-0.75	-0.61	0.37	-0.28	0.27
a_{k,H_2}	-0.58	0.31	-0.51	-0.76	1	0.33	-0.31	0.54	0.45	-0.48	0.34	-0.44
a_{q,H_2}	-0.016	0.10	-0.66	-0.083	0.33	1	0.18	-0.24	-0.31	-0.46	0.11	-0.37
a_{0,F_A}	0.34	-0.65	-0.017	0.37	-0.31	0.18	1	-0.74	-0.10	-0.24	0.17	-0.20
a_{k,F_A}	-0.79	0.60	-0.081	-0.75	0.54	-0.24	-0.74	1	0.48	-0.16	0.00048	-0.14
a_{q,F_A}	-0.64	0.19	-0.24	-0.61	0.45	-0.31	-0.10	0.48	1	-0.17	0.53	0.14
a_{0,F_V}	0.44	0.076	0.40	0.37	-0.48	-0.46	-0.24	-0.16	-0.17	1	-0.22	0.76
a_{k,F_V}	-0.18	-0.052	-0.56	-0.28	0.34	0.11	0.17	0.00048	0.53	-0.22	1	-0.20
a_{q,F_V}	0.18	0.14	0.27	0.27	-0.44	-0.37	-0.20	-0.14	0.14	0.76	-0.20	1

Table 2.3: Correlation matrix for the fit parameters corresponding to the polynomial fit described in Eq. (2.4).

	A_{H_1}	R_{k,H_1}	R_{q,H_1}	A_{H_2}	R_{k,H_2}	R_{q,H_2}	A_{F_A}	R_{k,F_A}	R_{q,F_A}	A_{F_V}	R_{k,F_V}	R_{q,F_V}
A_{H_1}	1	−0.57	0.13	0.87	−0.69	0.25	−0.48	−0.63	−0.58	0.49	−0.26	0.20
R_{k,H_1}	−0.57	1	−0.45	−0.48	0.46	−0.075	−0.10	0.70	0.25	−0.094	0.0058	0.034
R_{q,H_1}	0.13	−0.45	1	−0.0030	−0.37	−0.58	−0.019	0.038	−0.15	0.17	−0.51	0.24
A_{H_2}	0.87	−0.48	−0.0030	1	−0.62	0.34	−0.36	−0.61	−0.52	0.21	−0.25	0.12
R_{k,H_2}	−0.69	0.46	−0.37	−0.62	1	−0.053	0.25	0.49	0.48	−0.41	0.42	−0.45
R_{q,H_2}	0.25	−0.075	−0.58	0.34	−0.053	1	−0.096	−0.45	−0.47	−0.31	0.042	−0.27
A_{F_A}	−0.48	−0.10	−0.019	−0.36	0.25	−0.096	1	−0.15	0.43	−0.52	0.37	−0.40
R_{k,F_A}	−0.63	0.70	0.038	−0.61	0.49	−0.45	−0.15	1	0.25	−0.069	−0.089	−0.080
R_{q,F_A}	−0.58	0.25	−0.15	−0.52	0.48	−0.47	0.43	0.25	1	−0.049	0.57	0.17
A_{F_V}	0.49	−0.094	0.17	0.21	−0.41	−0.31	−0.52	−0.069	−0.049	1	−0.17	0.67
R_{k,F_V}	−0.26	0.0058	−0.51	−0.25	0.42	0.042	0.37	−0.089	0.57	−0.17	1	−0.37
R_{q,F_V}	0.20	0.034	0.24	0.12	−0.45	−0.27	−0.40	−0.080	0.17	0.67	−0.37	1

Table 2.4: Correlation matrix for the fit parameters corresponding to the pole fit described in Eq. (2.5).

For completeness, in Tabs. 2.3 - 2.4 we also give the correlation matrices for the form factor fit parameters. Since we adopted two different fitting ansatzes, given in Eq. (2.4) and Eq. (2.5), we have two different matrices. Each one is a 12×12 matrix, since there are four form factors, each one described by a function defined through three parameters, and so there are twelve different parameters for each ansatz. Given two different parameters A and B, the correlation between them has been computed according to

$$\rho_{A,B} = \frac{\sum_i (A_i - \mu_A)(B_i - \mu_B)}{\sqrt{\sum_i (A_i - \mu_A)^2}\sqrt{\sum_i (B_i - \mu_B)^2}}\,, \quad \mu_A = \frac{1}{N}\sum_i A_i\,, \quad \mu_B = \frac{1}{N}\sum_i B_i\,, \tag{2.6}$$

where A_i and B_i are the jackknife samples for two parameters and the sum runs over all the jackknifes.

2.4 Comparison with ChPT predictions

Before our lattice calculation, the only theoretical prediction for the structure dependent form factors entering the processes $K \to \ell\, \nu_\ell\, \ell'^+ \ell'^-$ have been obtained with Chiral Perturbation Theory (ChPT). ChPT is an effective theory which describes QCD at low energy making use of the spontaneously broken Chiral symmetry of QCD for massless quarks, which is a good approximation for the light quark sector of the theory, that includes up, down and, to a smaller extent, strange quarks. Thus, ChPT provides an effective theory to compute a prediction for the structure dependent form factors and so for the branching ratios, when the decaying meson P^+ is a light pseudoscalar meson, like a kaon or a pion.

The 1-loop ChPT predictions for the form factors H_1, H_2, F_A and F_V of the K^+-meson read [23]

$$
\begin{aligned}
H_1(k^2) &= H_2(k^2) = 2\sqrt{2}\,F\,m_K \frac{\left(F^K_{\rm em}(k^2)-1\right)}{k^2}\,, && (2.7)\\
F_V &= \frac{\sqrt{2}\,m_K}{4\pi^2\,F}\,, && (2.8)\\
F_A &= \frac{8\sqrt{2}\,m_K}{F}(L_9^r+L_{10}^r)\,. && (2.9)
\end{aligned}
$$

where F is the ChPT leading-order low-energy constant (LEC), while L_9^r and L_{10}^r are ChPT LECs at next-to-leading order.

The 1-loop ChPT prediction for the kaon electromagnetic form factor $F^K_{\rm em}(k^2)$ reads

$$
F^K_{\rm em}(k^2) = 1 + H_{\pi\pi}(k^2) + 2H_{KK}(k^2)\,, \tag{2.10}
$$

where the function $H(k^2)$ is given by

$$
\begin{aligned}
H(t) &= \frac{4}{3}\frac{L_9^r}{F^2}\,t + \frac{2}{F^2}\,t\,M^r(t)\,, && (2.11)\\
M^r(t) &= \frac{1}{12t}\left(t-4M^2\right)\bar{J}(t) + \frac{1}{288\pi^2} - \frac{\kappa}{6}\,, && (2.12)\\
\bar{J}(t) &= -\frac{1}{16\pi^2}\int_0^1 dx \log\left(1-\frac{t}{M^2}\,x\,(1-x)\right), && (2.13)\\
\kappa(M,\mu) &= \frac{1}{32\pi^2}\left[1+\log\frac{M^2}{\mu^2}\right]\,, && (2.14)
\end{aligned}
$$

where μ is the renormalization scale that we set to the ρ^+ mass $M_{\rho^+} \sim 0.775$ GeV. For the LECs L_9^r and L_{10}^r, we use the values

$$
L_9^r = 6.9\times10^{-3} \qquad L_{10}^r = -5.2\times10^{-3}\,, \tag{2.15}
$$

taken from [44].

The low energy constant $F = f_P/\sqrt{2}$ represents the value of the meson decay constant at leading order in Chiral Perturbation Theory, that is, in the limit of massless quarks. In this limit, there is no distinction between the pion or kaon decay constant. In other words, the difference between f_π, f_K and $\sqrt{2}F$ is generated only at the next to leading order in the chiral expansion. When evaluating the branching ratios using the ChPT predictions for the form factors, we accounted for this ambiguity to estimate the uncertainty of the numerical results. We evaluated the ChPT predictions for the form factors using the physical charged kaon and pion masses and setting either $F = f_\pi/\sqrt{2}$ or $F = f_K/\sqrt{2}$, where f_π and f_K are the physical values of these decays constants. We label these two determinations as ChPT(f_π) and ChPT(f_K), respectively. Their difference is taken as the uncertainty of the ChPT prediction at this order.

Finally, notice that at this order, the 1-loop prediction for the form factors does not depend on q^2. Moreover, the dependence on the virtuality k^2 is very mild as well, and only enters the prediction for the form factors H_1 and H_2, through the $O(k^4)$ corrections to the parametrization of the electromagnetic form factor

$$F^K_{\mathrm{em}}(k^2) = 1 + \frac{\langle r_K^2 \rangle}{6} k^2 + \mathcal{O}(k^4)\,, \tag{2.16}$$

where $\langle r_K^2 \rangle$ is the kaon's mean-square radius. We also notice that, with our definition of the form factors, one has $H_1 = H_2$ at 1 loop.

From Figs. 2.5 - 2.6 it can be seen that our results are reasonably consistent with the ChPT predictions. Note, however, that, since at NLO ChPT does not include any momentum dependence of the form factors, the comparison should be made with their values at $x_k = 0$ and $x_q = 0$, that is with the parameters a_0 or A. Moreover, even at zero momenta, the comparison can only be approximate due to the fact that the ChPT prediction is exactly valid only at zero momenta and in the chiral limit. Finally, we remind that our lattice results are affected by systematic errors, such as the continuum, chiral and infinite-volume extrapolations, that will be studied in the future.

2.5 Experimental data and VMD description of the form factors

In Ref. [9], the authors presented the first experimental measure for the branching ratios of the processes $K^+ \to e^+e^-e^+\nu_e$ and $K^+ \to e^+e^-\mu^+\nu_\mu$. Then they used the experimental data to extract information about the structure dependent form factors.

In particular, a Vector Meson Dominance (VMD) ansatz has been used in order to describe the momentum behavior of the form factors H_1, F_A, F_V, and has been then used in order to reproduce the experimental data. The authors of Ref. [9] expressed H_2 only in terms of the kaon electromagnetic form factor, as the NLO ChPT prediction of Eq. (2.7). Thus their analysis of the SD form factors is restricted to F_A, F_V and H_1. Within the VMD framework, the momentum dependence of the form factors is assumed to be determined by the masses of the low-lying resonances created by the electromagnetic and weak currents. In Ref. [9], for each of the three form factors, the fitting function has been taken to be of the form

$$F_{\mathrm{VMD}}\,(x_k, x_q) = \frac{F(0,0)}{\left(1 - x_k^2\, m_K^2/m_\rho^2\right)\left(1 - x_q^2\, m_K^2/m_{K^*}^2\right)}\,, \tag{2.17}$$

where $F(0,0)$ is the only free fitting parameter. In Eq. (2.17), m_ρ is the mass of the ρ meson, while m_{K^*} is the mass of the $K^*(1270)$ in the axial channel, and that of the $K^*(892)$ in the vector one. Thus, the VMD model corresponds to fixing, in the pole-like fit of Eq. (2.5), $R_k = (m_K/m_\rho)^2 \simeq 0.4116$, and $R_q = (m_K/m_{K^*}(1270))^2 \simeq 0.1513$ for the axial channel and $R_q = (m_K/m_{K^*}(892))^2 \simeq 0.3064$ for the vector one.

We notice that the fitted values of R_k and R_q reported in Tab. 2.2, are in qualitative agreement with the values predicted by VMD, albeit with large errors. In particular, we are not able to see a clear x_k and x_q dependence in the lattice data for F_A, while the value of the fit parameter R_q, for the form factor H_1, seems to be larger than the expectation based on VMD. Concerning the form factor H_2, the dominant contribution from the low-lying intermediate state comes from the virtual

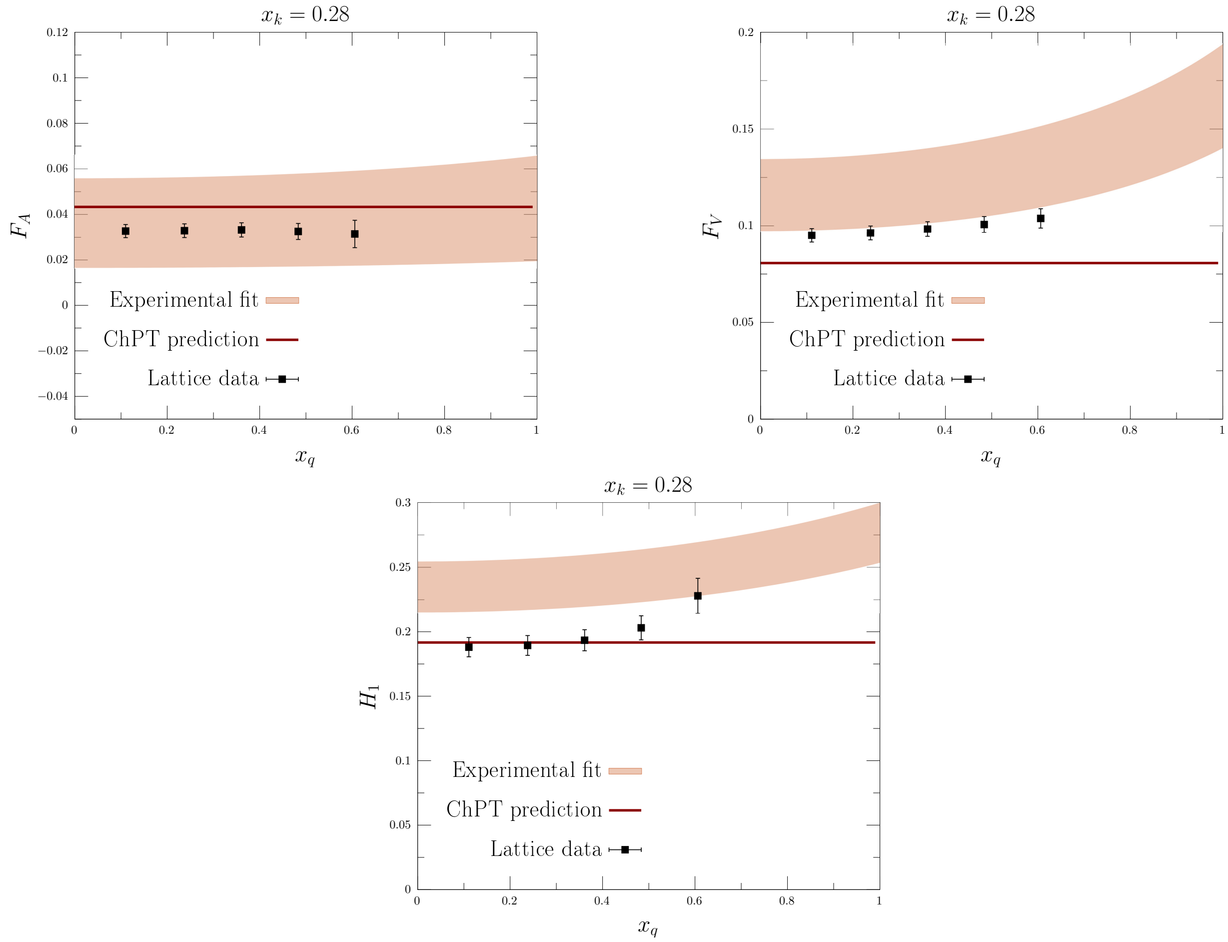

Figure 2.7: *The experimental VMD fits for the form factors H_1, F_A and F_V performed in [9] are plotted, together with our lattice data, as a function of x_q at a fixed value of $x_k = 0.28$. The red line corresponds to the 1-loop ChPT prediction with $F = f_K/\sqrt{2}$.*

K^+ state created by the weak current ($|n_f\rangle = |K^+\rangle$ in Eq. (1.35)). The resulting contribution $H_{2;K^+}$ to H_2 is then proportional to the electromagnetic kaon form factor $F^K_{\rm em}(x_k)$ [23]

$$H_{2;K^+} = \frac{2f_K}{m_K}\,\frac{F^K_{\rm em}(x_k) - 1}{x_k^2}\,, \tag{2.18}$$

as also shown by the prediction from ChPT presented in Eq. (2.7). As shown in Tab. 2.2 and in Fig. 2.5, we do not see any clear x_q dependence in our lattice data for H_2 in agreement with the prediction of Eq. (2.18)[1]. Moreover, making use of Eq. (2.16) one has that the contribution from the intermediate kaon to H_2 at $x_k = 0$ is given by

$$H_{2;K^+}(x_k = 0) = f_K m_K \frac{\langle r_K^2\rangle}{3}\ . \tag{2.19}$$

Using the value from the PDG, $\langle r_K^2\rangle = (0.560 \pm 0.031\ \text{fm})^2$ [8] and the physical values of

[1]This depends on the choice we had made in Eq. (1.21) for the kinematic prefactor in the definition of H_2 in the decomposition of the hadronic tensor in terms of form factors. If instead we had employed the same parametrization as in Refs. [23] or [37], we would have had a pole $1/(1-x_q^2)$ in the expression in Eq. (2.18).

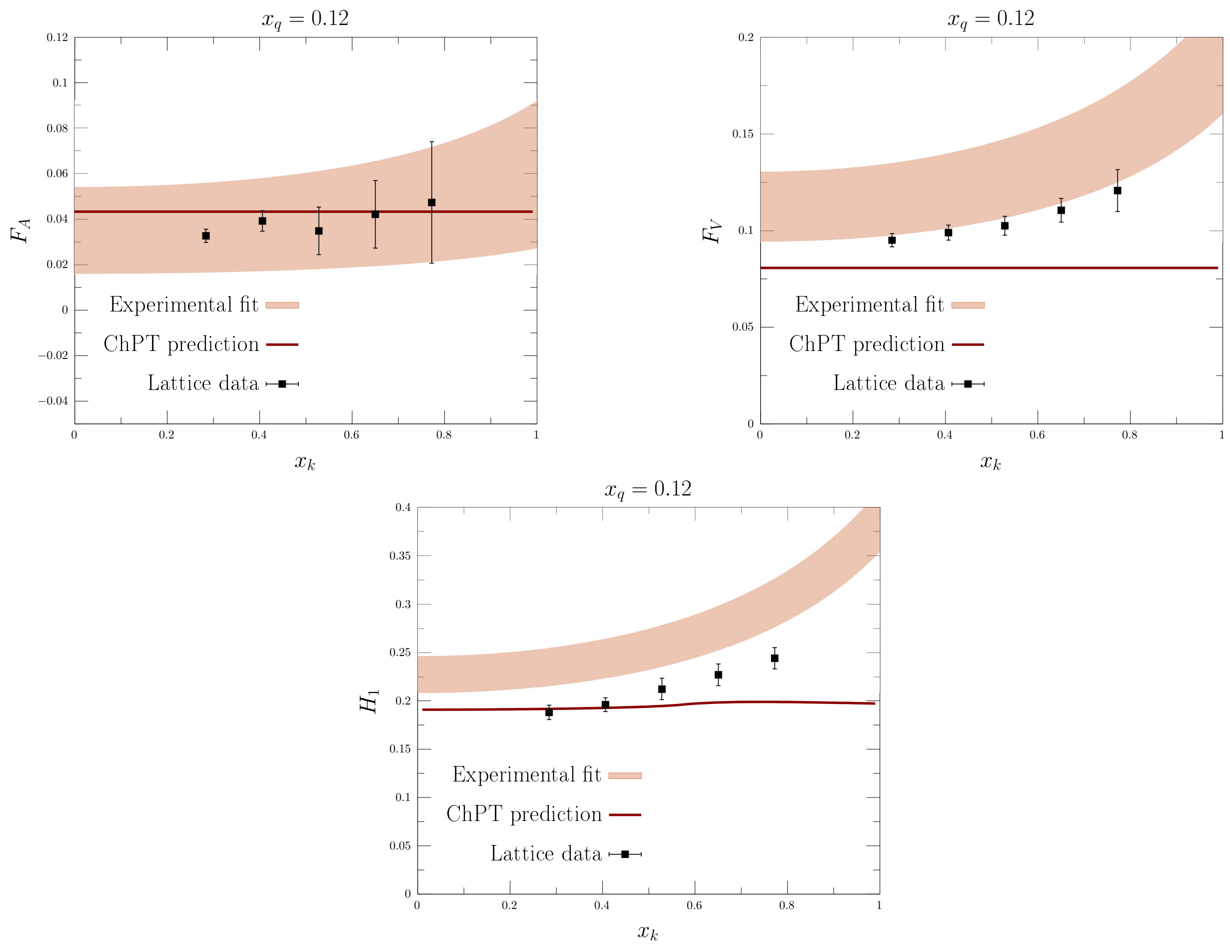

Figure 2.8: *The experimental VMD fits for the form factors H_1, F_A and F_V performed in [9] are plotted, together with our lattice data, as function of x_k at a fixed value of $x_q = 0.12$. The red line corresponds to the 1-loop ChPT prediction with $F = f_K/\sqrt{2}$.*

the kaon mass and decay constant, one obtains $H_{2;K^+}(x_k = 0) = 0.206(23)$, which nicely agrees with the value we obtained for the parameter A in the pole-like fit of H_2 presented in Tab. 2.2. Assuming the dominance of the rho-meson pole in the electromagnetic form factor $F^K_{\rm em}$, one has that $H_2 \propto 1/(1 - R_k x_k^2)$ with $R_k = (m_K/m_\rho)^2 \simeq 0.4116$. In this case, our fitted value of R_k turns out to be larger than the value predicted by VMD.

In Tab. 2.5 we compare the values of $F(0,0)$ obtained from experiments by assuming VMD and presented in Ref. [9], with the corresponding values of the form factors at zero x_k and x_q that we obtained from our lattice data by using the pole fit of Eq. (2.5), i.e. the values for the parameter A reported in Tab. 2.2. Despite the systematic uncertainties affecting our lattice computation, the results are in reasonably good agreement. The largest discrepancy that we observe, which is of $\mathcal{O}(20\%)$, is for the form factor H_1. In Figs. 2.7 and 2.8 we compare our lattice data for the form factors H_1, F_A, F_V, with the result of the experimental VMD fits performed in [9]. The figures show that the lattice computation for the form factors F_A and F_V is consistent, within errors, with the experimental fit performed by assuming VMD, while the lattice determination of H_1 deviates significantly from the experimental fit.

	$H_1(0,0)$	$F_A(0,0)$	$F_V(0,0)$
This work	0.1792(78)	0.0320(30)	0.0921(38)
Experiment [9]	0.227(19)	0.035(19)	0.112(18)

Table 2.5: *Comparison of the values of the VMD fit parameters $F(0,0)$ for the form factors H_1, F_A and F_V as obtained in Ref. [9] with the lattice results from this work (using the pole fit in Eq. (2.5)).*

2.6 Comparison with previous lattice results on real photon emission

We end this chapter by comparing the results for the form factors F_V and F_A obtained in this work, and extrapolated to $x_k = 0$ using Eqs. (2.4) and (2.5), with those reported on the same configurations in the earlier lattice study on real photon emission [6], i.e. for the decays $K \to \ell\nu_\ell\gamma$ [2]. The comparison is shown in Fig. 2.9 and shows good agreement, in spite of the fact that the ansatzes and parameters in Eqs. (2.4) and (2.5) were obtained from fits to data with $x_k \geq 0.28$.

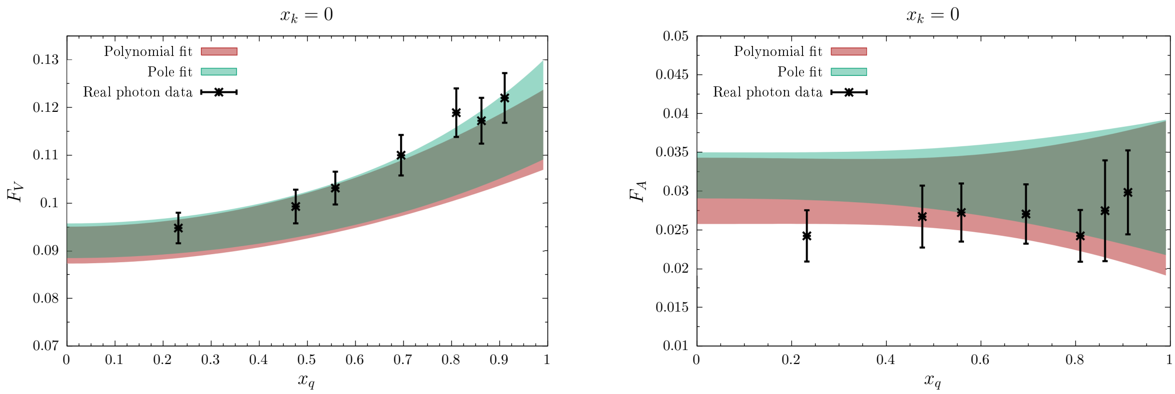

Figure 2.9: *Extrapolation of our lattice results for F_V (left) and F_A (right) to $x_k = 0$ using the polynomial and pole fit ansatzes defined in Eqs. (2.4) and (2.5) (colored bands). The black points correspond to the lattice results for F_V and F_A obtained directly at $x_k = 0$ in the lattice study of $K \to \ell\nu_\ell\gamma$ decays [6].*

[2]The form factors H_1 and H_2 do not contribute to the amplitude for $K \to \ell\nu_\ell\gamma$ decays.

Chapter 3

Numerical results for differential decay rate and branching ratios

In this chapter, we discuss the theoretical predictions for the decay rates and branching ratios of the processes $K^+ \to \ell^+ \, \nu_\ell \, \ell'^+ \, \ell'^-$, coming from the lattice determinations of the structure dependent form factors. From the knowledge of the hadronic tensor $H^{\mu\nu}$, the $K^+ \to \ell^+ \nu_\ell \, \ell'^+ \ell'^-$ decay rate is obtained by integrating the square of the unpolarised amplitude, $\sum_{\rm spins} |\mathcal{M}|^2$, over the phase space of the final-state charged leptons and neutrino. We derived in Section 1.1.3 that, when the two positively-charged leptons are different, i.e. when $\ell \neq \ell'$, the amplitude $\mathcal{M}$ is given by

$$\mathcal{M} = -\frac{G_F}{\sqrt{2}} \, V_{us}^* \, \frac{e^2}{k^2} \; \bar{u}(p_{\ell'^-})\gamma_\mu v(p_{\ell'^+}) \; \Big[f_K L^\mu(p_{\ell'^+}, p_{\ell'^-}, p_{\ell^+}, p_{\nu_\ell}) - H^{\mu\nu}_{\rm SD}(p,q) \, l_\nu(p_{\ell^+}, p_{\nu_\ell}) \Big] \, , \tag{3.1}$$

where the leptonic vectors are given by

$$\begin{aligned} L^\mu(p_{\ell'^+}, p_{\ell'^-}, p_{\ell^+}, p_{\nu_\ell}) &= m_\ell \, \bar{u}(p_{\nu_\ell})(1+\gamma_5) \left\{ \frac{2p^\mu - k^\mu}{2p\cdot k - k^2} - \frac{2p^\mu_{\ell^+} + \not{k}\gamma^\mu}{2p_{\ell^+}\cdot k + k^2} \right\} v(p_{\ell^+}) \, , && (3.2) \\ l^\mu(p_{\ell^+}, p_{\nu_\ell}) &= \bar{u}(p_{\nu_\ell})\gamma^\mu(1-\gamma_5) v(p_{\ell^+}) \, . && (3.3) \end{aligned}$$

In Eqs. (3.1) - (3.3), p is the four-momentum of the kaon, $k = p_{\ell'^+} + p_{\ell'^-}$, and $q = p_{\ell^+} + p_{\nu_\ell}$. In Eq. (3.1), the first term in the square parentheses gives the decay rate in the approximation in which the decaying kaon is treated as a point-like particle and includes the radiation from both the meson and charged lepton [1]. Except for the kaon decay constant f_K, the non-perturbative contribution to the rate is entirely contained in the second term of Eq. (3.1). The SD part of the hadronic tensor $H^{\mu\nu}_{\rm SD}$ is defined in Eq. (1.21).

When $\ell = \ell'$, since the final-state positively-charged leptons are indistinguishable, the exchange contribution, in which the momenta $p_{\ell'^+}$ and p_{ℓ^+} are interchanged, must be added to the amplitude $\mathcal{M}$ resulting in the replacement

$$\mathcal{M}(p_{\ell'^+}, p_{\ell'^-}, p_{\ell^+}, p_{\nu_\ell}) \to \mathcal{M}(p_{\ell'^+}, p_{\ell'^-}, p_{\ell^+}, p_{\nu_\ell}) - \mathcal{M}(p_{\ell^+}, p_{\ell'^-}, p_{\ell'^+}, p_{\nu_\ell}) \, . \tag{3.4}$$

[1] This term is frequently referred to as the *inner-bremsstrahlung* contribution.

The branching ratio for $K^+ \to \ell^+ \nu_\ell \ell'^+ \ell'^-$ decays is given by

$$\mathrm{BR}\left[K^+ \to \ell^+ \nu_\ell \ell'^+ \ell'^-\right] =$$

$$\frac{\mathcal{S}}{2m_K \Gamma_K (2\pi)^8} \int \sum_{\mathrm{spins}} |\mathcal{M}|^2 \, \delta\left(p - p_{\ell^+} - p_{\nu_\ell} - p_{\ell'^+} - p_{\ell'^-}\right) \frac{d^3 p_{\ell^+}}{2E_{\ell^+}} \frac{d^3 p_{\nu_\ell}}{2E_{\nu_\ell}} \frac{d^3 p_{\ell'^+}}{2E_{\ell'^+}} \frac{d^3 p_{\ell'^-}}{2E_{\ell'^-}} \, , \tag{3.5}$$

where $\Gamma_K = 5.3167(86) \times 10^{-17}$ GeV is the total decay rate of the K^+ meson [8] and $\mathcal{S}$ is a symmetry factor that takes the value $\mathcal{S} = 1$ for $\ell \neq \ell'$ and $\mathcal{S} = 1/2$ for $\ell = \ell'$. Since the phase-space integration is considerably easier for the case $\ell \neq \ell'$, in which a significant part of the integration can be performed analytically, we will discuss the two cases separately.

3.1 Decay rates formulae for $\ell \neq \ell'$

When the final state leptons have different flavors, the integral over the spatial momenta of the final-state particles can be partially performed analytically using invariance arguments and the fact that in $\sum_{\mathrm{spins}} |\mathcal{M}|^2$ the form factors only depend on $k^2 = (p_{\ell'^+} + p_{l'^-})^2$ and $q^2 = (p_{\ell^+} + p_{\nu_\ell})^2$ [45]. This leads to the following simplified expression for the differential decay rate [23]

$$d\Gamma\left[K^+ \to \ell^+ \nu_\ell \ell'^+ \ell'^-\right] = \alpha^2 G_F^2 |V_{us}|^2 m_K^5 \, G(x_k, r_{\ell'}) \left\{ -\sum_{\mathrm{spins}} T_\mu^* T^\mu \right\} dx_k \, dx_q \, dy \, , \tag{3.6}$$

where

$$r_\ell = \frac{m_\ell^2}{m_K^2} \, , \qquad r_{\ell'} = \frac{m_{\ell'}^2}{m_K^2} \, , \qquad y = \frac{2p_\ell \cdot p}{m_K^2},$$

$$G(x_k, r_{\ell'}) = \frac{2x_q}{192\pi^3 x_k} \left(1 + \frac{2r_{\ell'}}{x_k^2}\right) \sqrt{1 - \frac{4r_{\ell'}}{x_k^2}} \, , \tag{3.7}$$

$$T^\mu = \frac{\sqrt{2}}{m_K^2} \left\{ f_K L^\mu - H_{SD}^{\mu\nu} \, l_\nu \right\} \, .$$

The dimensionless integration variables x_k and x_q have been defined in Eq. (2.1). The integration domain for the variable y is given by

$$A - B \ \leq \ y \ \leq A + B \, , \tag{3.8}$$

where

$$A = \frac{(2 - x_\gamma)(1 + x_k^2 + r_\ell - x_\gamma)}{2(1 + x_k^2 - x_\gamma)}, \qquad B = \frac{(1 + x_k^2 - x_\gamma - r_\ell)\sqrt{x_\gamma^2 - 4x_k^2}}{2(1 + x_k^2 - x_\gamma)} \tag{3.9}$$

$$x_\gamma \equiv \frac{2p \cdot k}{m_K^2} = 1 + x_k^2 - x_q^2 \, , \tag{3.10}$$

and the limits of integration for x_k and x_q are given in Eq. (2.3). Since the form factors only depend on the invariant mass of the lepton-antilepton pair ($x_k m_K$) and on the invariant mass of the lepton-neutrino pair ($x_q m_K$), the integral over the variable y can also be performed analytically, leading to the following expression for the double differential decay rate:

$$\frac{\partial^2 \Gamma}{\partial x_k \, \partial x_q} = \alpha^2 \, G_F^2 \, |V_{us}|^2 \, m_K^5 \, \left[\Gamma''_{\rm pt}(x_k, x_q) \; + \; \Gamma''_{\rm int}(x_k, x_q) \; + \; \Gamma''_{\rm SD}(x_k, x_q) \right] . \tag{3.11}$$

The differential rate is written as a sum of three different contributions. The first term, $\Gamma''_{\rm pt}(x_k, x_q)$, is the point-like contribution proportional to f_K^2 and gives the total differential decay rate in absence of any SD terms (i.e. if $H_{\rm SD}^{\mu\nu} = 0$). The third term, $\Gamma''_{\rm SD}(x_k, x_q)$, is the contribution to the decay rate coming entirely from $H_{\rm SD}^{\mu\nu}$, and corresponds to a quadratic expression of the form factors $H_1, \; H_2, \; F_A, \; F_V$. Finally, $\Gamma''_{\rm int}(x_k, x_q)$ is the interference term between the point-like and SD components of the amplitude. It arises from contributions of the form $H_{\rm SD}^{\mu\nu} L_\mu l_\nu$ in $T_\mu^* T^\mu$ and is proportional to f_K and depends linearly on the form factors. Clearly, all the information from the internal structure of the kaon (i.e. from $H_{\rm SD}^{\mu\nu}$) is contained in $\Gamma''_{\rm int}(x_k, x_q)$ and $\Gamma''_{\rm SD}(x_k, x_q)$.

The Γ'' functions are all dimensionless quantities which can be evaluated directly from the knowledge of the form factors and of the dimensionless ratio f_K/m_K, for which we use our lattice value $f_K/m_K = 0.3057(11)$. Their explicit expressions in terms of $H_1, \; H_2, \; F_A, \; F_V$, and f_K/m_K are presented in Appendix C. Using these formulae and the form factors obtained from the polynomial and pole-like fits described in the previous chapter, we are able to evaluate each of the terms on the right-hand side of Eq. (3.11). In order to obtain the total decay rates, we rely on numerical integration using Gaussian quadrature rules.

3.2 Decay rates formulae for $\ell = \ell'$

When the final state leptons have the same flavor, the exchange contribution must be added as shown in Eq. (3.4). In this case $\sum_{\rm spins} |\mathcal{M}|^2$, depends on products of form factors evaluated at $k^2 = (p_{\ell'^+} + p_{\ell'^-})^2$ and $q^2 = (p_{\ell^+} + p_{\nu_\ell})^2$ as before, but also at the exchanged invariant masses $k'^2 = (p_{\ell^+} + p_{\ell'^-})^2$ and $q'^2 = (p_{\ell'^+} + p_{\nu_\ell})^2$. It is not possible to integrate analytically as many variables as before. For the decay $K^+ \to \ell^+ \nu_\ell \ell'^+ \ell'^-$, the four-body phase space $d\Phi_4$ can be written in terms of five Lorentz invariant quantities $x_k, \; x_q, \; y_{12}, \; y_{34}, \; \phi$ as [22]

$$d\Phi_4 = \frac{\mathcal{S} \, \lambda \, \omega \, m_K^4}{2^{14} \, \pi^6} \; dx_k \, dx_q \, dy_{12} \, dy_{34} \, d\phi \; , \tag{3.12}$$

where $\omega = 2 x_k x_q$, the symmetry factor $\mathcal{S} = \frac{1}{2}$ for the case $\ell = \ell'$, $\lambda = \sqrt{(1 - x_k^2 - x_q^2)^2 - 4 x_k^2 x_q^2}$ and the three additional integration variables $y_{12}, \; y_{34}$ and ϕ, are defined as

$$\begin{aligned} y_{12} &\equiv \frac{2}{m_K^2 \, \lambda} \; (p_{\ell'^-} - p_{\ell'^+}) \cdot (p_{\ell^+} + p_{\nu_\ell}) \, , \\ y_{34} &\equiv \frac{2}{m_K^2 \, \lambda} \; \left(\left(1 + \frac{r_\ell}{x_q^2} \right) p_{\nu_\ell} - \left(1 - \frac{r_\ell}{x_q^2} \right) p_{\ell^+} \right) \cdot (p_{l'^+} + p_{\ell'^-}) \; , \end{aligned} \tag{3.13}$$

$$\sin\phi \equiv -\frac{16}{\lambda\,\omega\,m_K^4}\;\frac{1}{\sqrt{(\lambda_{12}^2-y_{12}^2)(\lambda_{34}^2-y_{34}^2)}}\;\epsilon_{\mu\nu\rho\sigma}\;p^{\mu}_{\ell'-}\,p^{\nu}_{\ell'+}\,p^{\rho}_{\nu_\ell}\,p^{\sigma}_{\ell+}$$

where

$$\lambda_{12}=\sqrt{1-4\frac{r'_\ell}{x_k^2}}\;,\qquad \lambda_{34}=1-\frac{r_\ell}{x_q^2}\;. \tag{3.14}$$

The integration domain is given by

$$-\lambda_{12}\le y_{12}\le\lambda_{12},\qquad -\lambda_{34}\le y_{34}\le\lambda_{34},\qquad \phi\in[0,2\pi]\;, \tag{3.15}$$

while for x_k and x_q the limits of integration are as defined in Eq. (2.3).

In order to determine the decay rate, we have evaluated the square of the unpolarised amplitude, $\sum_{\rm spins}|\mathcal{M}|^2$, in terms of the five integration variables using FeynCalc [46]. As for the case when $\ell\neq\ell'$, we decompose the differential rate as a sum of a point-like, an interference and a quadratic term (SD) in the form factors, i.e. as

$$\begin{aligned}\frac{\partial^5\Gamma}{\partial x_k\,\partial x_q\,\partial y_{12}\,\partial y_{34}\,\partial\phi} &= \alpha^2\,G_F^2\,|V_{us}|^2\,m_K^5\Big[\,\Gamma^{(5)}_{\rm pt}(x_k,x_q,y_{12},y_{34},\phi)\;+\;\Gamma^{(5)}_{\rm int}(x_k,x_q,y_{12},y_{34},\phi)\\ &\qquad +\;\Gamma^{(5)}_{\rm SD}(x_k,x_q,y_{12},y_{34},\phi)\Big]\,.\end{aligned} \tag{3.16}$$

The explicit, very lengthy, expressions for the three contributions $\Gamma^{(5)}_{\rm pt}$, $\Gamma^{(5)}_{\rm int}$ and $\Gamma^{(5)}_{\rm SD}$, written in terms of the five integration variables and the form factors, are not presented here but are available on request from the author. The total rate can be obtained through standard Monte Carlo integration of these expressions over the five-dimensional phase space. This has been done employing the GSL implementation of the VEGAS algorithm of G.P. Lepage [47].

3.3 Numerical results and comparison with experiments and other predictions

In this section, we give our final theoretical predictions for the different channels of $K^+\to\ell^+\,\nu_\ell\,\ell'^+\,\ell'^-$ decays. In each subsection we also compare our results to experimental measurements (whenever available), ChPT predictions and the lattice predictions coming from the very recent work [22].

In [22], a different lattice strategy was presented and implemented to compute the branching ratio for the decays $K^+\to\ell^+\,\nu_\ell\,\ell'^+\,\ell'^-$, but without determining the SD form factors themselves and also without separating the point-like contribution from the structure dependent one at any stage of the computation. The simulation in Ref. [22] was performed on a single gauge ensemble on a $24^3\times 48$ lattice with $a\simeq 0.093$ fm and with quark masses corresponding to $m_\pi\simeq 352$ MeV and $m_K\simeq 506$ MeV.

Concerning the ChPT predictions, they have been obtained by computing the branching ratios employing the next to leading formulae for the form factors that we reported in Section 2.4. As discussed in that section, in the following we will evaluate the ChPT predictions for the form factors setting either $F = f_\pi/\sqrt{2}$ or $F = f_K/\sqrt{2}$, and label these two determinations as ChPT(f_π) and ChPT(f_K), respectively.

We address now each of the four possible channels of $K^+ \to \ell^+ \nu_\ell \ell'^+ \ell'^-$ decays in a different subsection.

3.3.1 $K^+ \to e^+ \nu_e \mu^+ \mu^-$ decay

For the decay $K^+ \to e^+\nu_e \mu^+\mu^-$, the differential decay rate is completely dominated by the SD terms, since the point-like contribution is helicity suppressed ($L_\mu \propto m_e$). This is shown in Fig. 3.1, where we plot, as functions of x_k, the contributions from $\Gamma''_{\rm pt}$, $\Gamma''_{\rm int}$ and from $\Gamma''_{\rm SD}$ to the partially-integrated differential decay rate $\partial\Gamma(x_k)/\partial x_k = \int dx_q\, \partial^2\Gamma/\partial x_k \partial x_q$.

Furthermore, we find that the dominant term in the integral of $\Gamma''_{\rm SD}$ is the one proportional to H_1^2, while the contribution to the rate coming from the form factor H_2 turns out to be negligible. The remaining linear and quadratic terms in the form factors give subdominant contributions to the branching ratio of about 5% in total. Integrating the double differential decay rate of Eq. (3.11), we obtain the following value for the branching ratio

$$\mathrm{BR}\left[K^+ \to e^+ \nu_e \mu^+ \mu^-\right] = 0.762\ (49) \times 10^{-8}\,. \tag{3.17}$$

In Tab. 3.1 we compare this result with the recent lattice value from Ref. [22], with the prediction from ChPT, and with the measurement from the E865 experiment at the Brookhaven AGS [10]. As the table shows, our value of the branching ratio is in agreement with the updated determination of Ref. [22], while there is a tension with the experimental measurement at the level of about 2σ. However, it should be noted that both our computation and that of Ref. [22] are limited to a single value of the lattice spacing, a single volume and to unphysically large light-quark masses. Given that the branching ratio is dominated by the quadratic term proportional to H_1^2, an increase of about 25% in the value of H_1, due to the missing continuum, chiral and infinite-volume extrapolations, would reduce the tension between our result and the experimental measurement to about 1σ. It will be very interesting in the future, once these extrapolations have been performed, to learn whether H_1 does indeed increase.

We also note, however, that there is a 1.6σ difference between the values of $H_1(0,0)$ obtained in Refs. [9] and [10]. The value of $H_1(0,0)$ deduced by the E865 collaboration from the experimental study of the decay $K^+ \to e^+\nu_e \mu^+\mu^-$ is $H_1(0,0) = 0.303 \pm 0.043$ [10] [2]. This value is somewhat higher than the one obtained from studies of the decays $K^+ \to e^+\nu_e e^+e^-$ and $K^+ \to \mu^+\nu_\mu e^+e^-$ also in the E865 experiment, $H_1(0,0) = 0.227 \pm 0.019$ [9], which is quoted in Tab. 2.5.

3.3.2 $K^+ \to \mu^+ \nu_\mu e^+ e^-$ decay

For the decay channel $K^+ \to \mu^+\nu_\mu e^+e^-$, the point-like contribution is not helicity suppressed ($L_\mu \propto m_\mu$), and gives the dominant contribution to the differential decay rate at small values of the e^+e^- invariant mass. This is illustrated in Fig. 3.2, where we plot the contributions of $\Gamma''_{\rm pt}$, $\Gamma''_{\rm int}$ and

[2] We have combined the errors quoted in Eq. (7) of Ref. [10] in quadrature.

BR $[K^+ \to e^+ \nu_e \mu^+ \mu^-]$					
This work	point-like approximation	Tuo et al. [22]	ChPT(f_π)	ChPT(f_K)	experiment [10]
$0.762(49) \times 10^{-8}$	3.0×10^{-13}	$0.72(5) \times 10^{-8}$	1.19×10^{-8}	0.62×10^{-8}	$1.72(45) \times 10^{-8}$

Table 3.1: *Comparison of our result for the branching ratio $BR[K^+ \to e^+ \nu_e \mu^+ \mu^-]$ with the one coming from the point-like approximation, the result from Ref. [22] and with the results for the branching ratio obtained using the NLO ChPT predictions for the SD form factors (Eq. (2.7)) setting either $F = f_\pi/\sqrt{2}$ or $F = f_K/\sqrt{2}$ (denoted by ChPT(f_π) and ChPT(f_K) respectively). In the last column, we show the experimental result from the E865 experiment [10].*

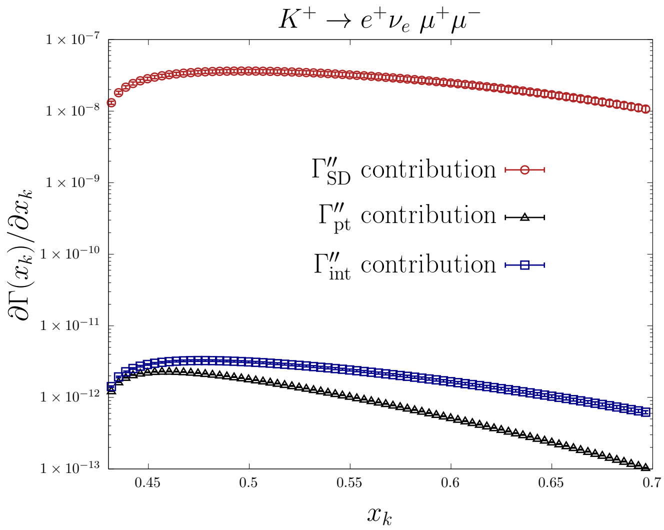

Figure 3.1: *The contributions from $\Gamma''_{\rm pt}$, $\Gamma''_{\rm int}$ and $\Gamma''_{\rm SD}$ to the differential rate $\partial\Gamma(x_k)/\partial x_k$, are shown for the decay channel $K^+ \to e^+\nu_e\mu^+\mu^-$. Although not shown in the figure, all contributions to $\partial\Gamma(x_k)/\partial x_k$ are zero at $x_k = 2\sqrt{r_\ell} \simeq 0.4280$ but grow rapidly as x_k is increased.*

$\Gamma''_{\rm SD}$ to the partially integrated differential decay rate $\partial\Gamma(x_k)/\partial x_k$. The contributions from $\Gamma''_{\rm pt}$ and $\Gamma''_{\rm int} + \Gamma''_{\rm SD}$ become of similar size at values of $x_k \simeq 0.3 - 0.4$, which corresponds approximately to the cut on the e^+e^- invariant mass $\sqrt{k^2} > 145, 150\,\text{MeV}$ ($x_k > 0.294, 0.304$) adopted in the E865 experiment [9]. For such values of the cut on x_k, we find that the contribution to the decay rate from $\Gamma''_{\rm int}$ is greater than that of $\Gamma''_{\rm SD}$ and that the contribution from the form factor H_2 is again negligible.

Imposing a cut on the e^+e^- invariant mass of $x_k > 0.284$, we obtain the following value for the branching ratio

$$\text{BR}\left[K^+ \to \mu^+ \nu_\mu e^+ e^-\right] = 8.26\ (13) \times 10^{-8}\,. \tag{3.18}$$

In Tab. 3.2 we compare our result for the branching ratio with the lattice determination of Ref. [22], with the ChPT prediction and with the experimental result of Ref. [9].

For this channel we find a remarkable agreement with both the experimental result and the ChPT prediction, while the lattice result of Ref. [22] is a little larger than ours. In this case, since the interference term dominates over $\Gamma''_{\rm SD}$, systematic effects in our determination of the form factors, due to lattice artifacts and to the unphysical quark masses, will only reflect linearly in the result for

BR $[K^+ \to \mu^+ \nu_\mu e^+ e^-]$ for $x_k > 0.284$					
This work	point-like approximation	Tuo et al. [22]	ChPT(f_π)	ChPT(f_K)	experiment [9]
$8.26(13) \times 10^{-8}$	4.8×10^{-8}	$10.59(33) \times 10^{-8}$	9.82×10^{-8}	8.25×10^{-8}	$7.93(33) \times 10^{-8}$

Table 3.2: *Comparison of our result for the branching ratio BR $[K^+ \to \mu^+ \nu_\mu e^+ e^-]$ with the one coming from the point-like approximation, the result from Ref. [22] and with the results for the branching ratio obtained using the NLO ChPT predictions for the SD form factors (Eq. (2.7)) setting either $F = f_\pi/\sqrt{2}$ or $F = f_K/\sqrt{2}$ (denoted by ChPT(f_π) and ChPT(f_K) respectively). In the last column, we show the experimental result from the E865 experiment [9], which has been extrapolated from $x_k > 0.294$ to $x_k > 0.284$ using the formula presented in Ref [9].*

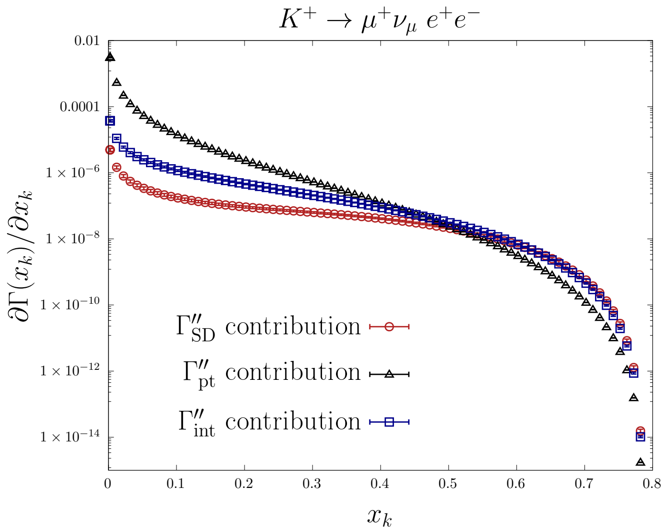

Figure 3.2: *The contributions from $\Gamma''_{\rm pt}$, $\Gamma''_{\rm int}$ and $\Gamma''_{\rm SD}$ to the differential rate $\partial\Gamma(x_k)/\partial x_k$, are shown for the decay channel $K^+ \to \mu^+\nu_\mu e^+e^-$. Even if not shown in the figure, all contributions to $\partial\Gamma(x_k)/\partial x_k$ are zero at $x_k = 2\sqrt{r_\ell} \simeq 0.00207$ but grow rapidly as x_k is increased.*

the branching ratio; for example an increase in H_1 of 20% would increase the branching ratio by about 7%.

3.3.3 $K^+ \to \mu^+ \nu_\mu \mu^+ \mu^-$ decay

For the decay channel $K^+ \to \mu^+ \nu_\mu \mu^+ \mu^-$, we find that the point-like contribution corresponds to about 30% of the total rate. This is shown in Fig. 3.3, where we plot the contributions to the decay rate as a function of the lower cutoff on the invariant mass of the $\mu^+\mu^-$ pair, from $\Gamma^{(5)}_{\rm pt}$ alone and from $\Gamma^{(5)}_{\rm int} + \Gamma^{(5)}_{\rm SD}$. For decays into identical leptons, the same cuts are always applied to both invariant masses

$$\sqrt{k^2} = m_K x_k = \sqrt{(p_{\ell'^+} + p_{\ell'^-})^2}\,, \qquad \sqrt{k'^2} \equiv m_K x'_k = \sqrt{(p_{\ell^+} + p_{\ell'^-})^2}\,. \tag{3.19}$$

We find that the contribution from the form factor H_2 is again negligible and that the contribution from the vector form factor F_V is also very small. For the total branching ratio, we obtain the value

$$\mathrm{BR}\left[K^+ \to \mu^+ \nu_\mu \mu^+ \mu^-\right] = 1.178\ (35) \times 10^{-8}\,. \tag{3.20}$$

BR $[K^+ \to \mu^+ \nu_\mu \mu^+ \mu^-]$					
This work	point-like approximation	Tuo et al. [22]	ChPT(f_π)	ChPT(f_K)	experiment
$1.178(35) \times 10^{-8}$	3.7×10^{-9}	$1.45(6) \times 10^{-8}$	1.51×10^{-8}	1.10×10^{-8}	–

Table 3.3: *Comparison of our result for the branching ratio BR $[K^+ \to \mu^+ \nu_\mu \mu^+ \mu^-]$ with the one coming from the point-like approximation, the result from Ref. [22] and with the results for the branching ratio obtained using the NLO ChPT predictions for the SD form factors (Eq. (2.7)) setting either $F = f_\pi/\sqrt{2}$ or $F = f_K/\sqrt{2}$ (denoted by ChPT(f_π) and ChPT(f_K) respectively).*

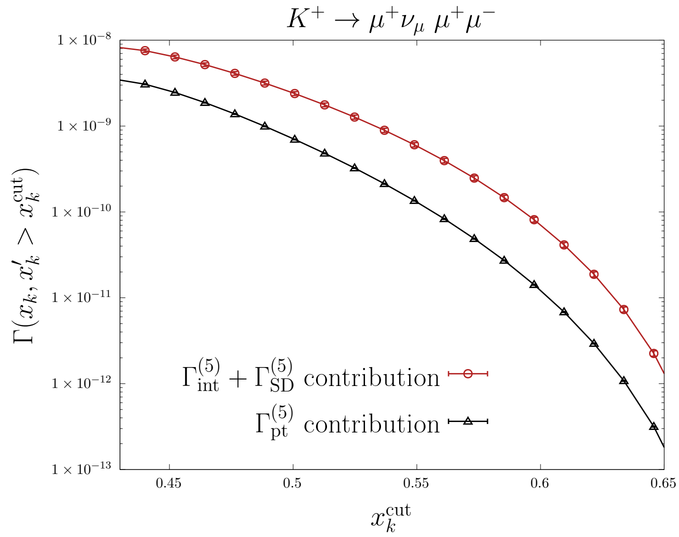

Figure 3.3: *The contributions from $\Gamma^{(5)}_{\mathrm{pt}}$, and $\Gamma^{(5)}_{\mathrm{int}} + \Gamma^{(5)}_{\mathrm{SD}}$ to the integrated decay rate $\Gamma(x_k, x_{k'} > x_k^{\mathrm{cut}})$ are shown for the decay channel $K^+ \to \mu^+\nu_\mu\mu^+\mu^-$, as a function of the common lower cut, x_k^{cut}, on the values of x_k and x'_k.*

Since for this decay channel there is no experimental measurement available, our result can only be compared with the lattice determination of Ref. [22] and with the ChPT prediction (Tab. 3.3). As the table shows, our result is in reasonably good agreement with the value predicted by ChPT, while at this stage the observed discrepancy with the result obtained by Tuo et al. [22], which is of O(25%) may be attributed to the unknown systematics associated to the missing chiral, continuum and infinite-volume extrapolations.

3.3.4 $K^+ \to e^+ \nu_e e^+ e^-$ decay

Finally, for the decay channel $K^+ \to e^+\nu_e e^+ e^-$, we find again that the point-like contribution is much suppressed compared to that from the SD terms. This is shown in Fig. 3.4, where we have plotted, as in the previous case, the contribution from $\Gamma^{(5)}_{\mathrm{pt}}$ and from $\Gamma^{(5)}_{\mathrm{int}} + \Gamma^{(5)}_{\mathrm{SD}}$ to the total decay rate, as a function of the lower cutoff on the e^+e^- invariant masses.

Similarly to the case of the decay $K^+ \to \mu^+\nu_\mu e^+ e^-$, we find that the dominant contribution to the rate is given by the term proportional to H_1^2, while the contributions from the form factors H_2 and F_V are very small.

BR $\left[K^+ \to e^+\,\nu_e\,e^+\,e^-\right]$ for $x_k > 0.284$					
This work	point-like approximation	Tuo et al. [22]	ChPT(f_π)	ChPT(f_K)	experiment [9]
$1.95(11) \times 10^{-8}$	2.0×10^{-12}	$1.77(16) \times 10^{-8}$	3.34×10^{-8}	1.75×10^{-8}	$2.91(23) \times 10^{-8}$

Table 3.4: *Comparison of our result for the branching ratio BR $[K^+ \to e^+\,\nu_e\,e^+\,e^-]$ with the one coming from the point-like approximation, the result from Ref. [22] and with the results for the branching ratio obtained using the NLO ChPT predictions for the SD form factors (Eq. (2.7)) setting either $F = f_\pi/\sqrt{2}$ or $F = f_K/\sqrt{2}$ (denoted by ChPT(f_π) and ChPT(f_K) respectively). In the last column, we show the experimental result from the E865 experiment [9], which has been extrapolated from $x_k > 0.304$ to $x_k > 0.284$ using the formula presented in Ref. [9].*

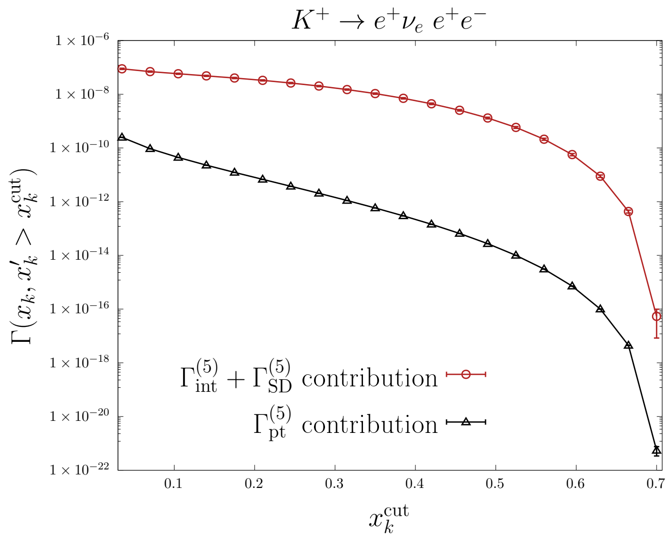

Figure 3.4: *The contributions from $\Gamma^{(5)}_{\rm pt}$, and $\Gamma^{(5)}_{\rm int} + \Gamma^{(5)}_{\rm SD}$ to the integrated decay rate $\Gamma(x_k, x_{k'} > x_k^{\rm cut})$ are shown for the decay channel $K^+ \to e^+\nu_e e^+ e^-$, as a function of the common lower cut $x_k^{\rm cut}$ on the values of x_k and x'_k.*

Employing the cutoffs $x_k, x'_k > 0.284$, we obtain the following value for the branching ratio

$$\text{BR}\left[K^+ \to e^+\,\nu_e\,e^+\,e^-\right] = 1.95\ (11) \times 10^{-8}\,. \tag{3.21}$$

In Tab. 3.4 we compare our determination with the experimental measurement of Ref. [9], with the lattice result of Ref. [22], and with the ChPT prediction. Our result appears to be significantly smaller than the experimental measurement, as in the case of the $K^+ \to \mu^+\nu_\mu e^+ e^-$ decay, while being consistent with the updated determination of Ref. [22]. Since the term proportional to H_1^2 is also the dominant one in this case, this finding is consistent with possible systematic effects of about 20% on our lattice value.

Conclusions

In this thesis we have presented a strategy to compute, using Lattice QCD, the amplitudes and branching ratios for the decays $P^+ \to \ell^+\,\nu_\ell\,\ell'^+\,\ell'^-$, where P^+ is a pseudoscalar meson and ℓ and ℓ' are charged leptons. In particular, we explain how the four structure-dependent (SD) form factors can be determined and separated from the point-like ("inner-bremsstrahlung") contribution. Apart from the leptonic decay constant f_P, the point-like contribution to the amplitude can be calculated in perturbation theory, whereas the SD form factors are non-perturbative and describe the interaction of the off-shell photon with the internal hadronic structure of the meson. We apply the formalism developed in Chapter 1 to the four channels of $K^+ \to \ell^+\,\nu_\ell\,\ell'^+\,\ell'^-$ decays, where ℓ and $\ell' = \mu$ or e, in an exploratory Lattice QCD computation at a single lattice spacing and unphysical light-quark masses. We demonstrate that all four SD form factors, F_V, F_A, H_1 and H_2 can be determined with good precision and used to calculate the corresponding branching ratios. In spite of the unphysical quark masses used in this simulation (our pion and kaon masses are about 320 MeV and 530 MeV respectively) it has been interesting and instructive to compare our results with those from experiment (where available) and from NLO ChPT. As can be seen from Tabs. 3.1 - 3.4, the results are generally in reasonable semi-quantitative agreement.

The comparison of our results with those from experimental measurements results in an interesting observation to be investigated further in the future. For the decays $K^+ \to e^+\nu_e\,\mu^+\mu^-$ and $K^+ \to e^+\nu_e\,e^+e^-$ the point-like contribution is negligible as a result of the chiral suppression due to the small electron mass, and the decay rate is dominated by the form factor H_1. In both cases our results are somewhat below the experimental measurement (see Tabs. 3.1 and 3.4) and it would require an increase of order 20% in the value of H_1 to recover consistency. It will be interesting to see whether such an increase will result after the continuum, chiral and infinite-volume extrapolations have been performed in the future. It should be also noted, however, the discrepancy in the values of $H_1(0,0)$ in Refs. [9] and [10] obtained in the E865 experiment from different channels, which is discussed in Sec. 3.3.1.

A complementary exploratory lattice computation of the branching ratios has been performed by Tuo et al. [22] on a $24^3 \times 48$ lattice, with lattice spacing $a = 0.093$ fm and with quark masses similar to our ($m_\pi = 352$ MeV and $m_K = 506$ MeV). The lattice action with Wilson-Clover Twisted Mass Fermions is different from the one we use, which does not include the clover term. The methodology in Ref. [22] is also different from ours in that the individual form factors are not extracted and the point-like contribution is not separated from structure dependent terms. The aim of this thesis, on the other hand, is to determine explicitly the (non-perturbative) structure dependent contributions to the decay rate. In Tabs. 3.1 - 3.4 we also compare our results with those of Ref. [22], but given the different systematics, and in particular the finite-volume effects, we do not speculate on the origin of any differences.

Having demonstrated the feasibility of the method, our future work will focus on controlling and reducing the systematic uncertainties and in particular those resulting from the current absence of continuum, chiral and infinite-volume extrapolations. We will also work to extend the method to heavier pseudoscalar mesons, for which the analytic continuation to Euclidean space gives rise to enhanced finite-volume effects due to the presence of internal lighter states. Given the recent results suggesting the violation of lepton-flavour universality and potential new interactions involving leptons (see e.g. Ref. [13] for a brief introduction), we believe that reliable non-perturbative, model-independent theoretical predictions of decays such as those studied here will be very useful in unraveling the underlying theory beyond the Standard Model. In particular, experimental measurements of ratios of decay rates of heavy mesons into different final-state leptons, together with the corresponding lattice calculations, would be a significant contribution to the general investigation of lepton-flavour universality.

Appendix A

Notations

In this appendix we show the notations and the conventions used in the thesis, the information here reported can be found in [48, 49].

We use the metric tensor defined as

$$g_{\mu\nu} = g^{\mu\nu} = \begin{pmatrix} 1 & 0 & 0 & 0 \\ 0 & -1 & 0 & 0 \\ 0 & 0 & -1 & 0 \\ 0 & 0 & 0 & -1 \end{pmatrix} . \tag{A.1}$$

If not specified, the Greek indices assume the values $\alpha = 0, 1, 2, 3$ while the Latin ones stand for $i = 1, 2, 3$.

A.1 The generators of $SU(N)$

Every element of the Lie group $U(N)$ can be written in the exponential representation as

$$U = \exp\left[\sum_{a=0}^{N^2-1} iT^a\omega^a\right] , \tag{A.2}$$

where $\omega^a \in \mathbb{R}$, $T^0 = \frac{1}{\sqrt{N}}\mathbb{I}$ and the others T^a are the generators of the Lie group $SU(N)$. The generators are the basis of the corresponding Lie algebra, which is the space of the Hermitian, traceless, $N \times N$ matrices. That is, they are $N^2 - 1$ linearly independent matrices which respect the relations

$$\mathrm{Tr}T^a = 0\,, \quad T^{a\dagger} = T^a\,. \tag{A.3}$$

As convention, the generators are normalized through the relation

$$\mathrm{Tr}[T^aT^b] = \frac{1}{2}\delta^{ab}\,. \tag{A.4}$$

The algebra is closed under the multiplication between matrices, so the commutator, and the anti-commutator, of two generators can be expressed as a linear combination of the generators, that is (we use a summation convention over repeated indices)

$$[T^a, T^b] = if^{abc}T^c\,, \tag{A.5}$$

$$\{T^a, T^b\} = d^{abc}T^c + \frac{\delta^{ab}}{N}\mathbb{I}\,. \tag{A.6}$$

The structure constants f^{abc} are completely antisymmetric and real, instead d^{abc} are symmetric real coefficients.

Now we show some actual expressions for the generators T^a in the typical cases $N = 2$ and $N = 3$. For $SU(2)$ we have 3 generators

$$T^a = \frac{\sigma_a}{2}, \quad a = 1, 2, 3, \tag{A.7}$$

where σ_a are the Pauli matrices

$$\sigma_1 = \begin{pmatrix} 0 & 1 \\ 1 & 0 \end{pmatrix}, \quad \sigma_1 = \begin{pmatrix} 0 & -i \\ i & 0 \end{pmatrix}, \quad \sigma_2 = \begin{pmatrix} 1 & 0 \\ 0 & -1 \end{pmatrix}. \tag{A.8}$$

By computing the structure constants we found

$$f^{abc}) = \epsilon^{abc}, \quad d^{abc} = 0\,, \tag{A.9}$$

where ϵ^{abc} is the completely antisymmetric tensor with $\epsilon^{123} = 1$.

For $SU(3)$ we have

$$T^a = \frac{\lambda_a}{2}, \quad a = 1, 2, ..., 8, \tag{A.10}$$

where λ_a are the Gell-Mann matrices

$$\begin{aligned}
\lambda_1 &= \begin{pmatrix} 0 & 1 & 0 \\ 1 & 0 & 0 \\ 0 & 0 & 0 \end{pmatrix}, \quad \lambda_2 = \begin{pmatrix} 0 & -i & 0 \\ i & 0 & 0 \\ 0 & 0 & 0 \end{pmatrix}, \quad \lambda_3 = \begin{pmatrix} 1 & 0 & 0 \\ 0 & -1 & 0 \\ 0 & 0 & 0 \end{pmatrix}, \\
\lambda_4 &= \begin{pmatrix} 0 & 0 & 1 \\ 0 & 0 & 0 \\ 1 & 0 & 0 \end{pmatrix}, \quad \lambda_5 = \begin{pmatrix} 0 & 0 & -i \\ 0 & 0 & 0 \\ i & 0 & 0 \end{pmatrix}, \quad \lambda_6 = \begin{pmatrix} 0 & 0 & 0 \\ 0 & 0 & 1 \\ 0 & 1 & 0 \end{pmatrix}, \\
\lambda_7 &= \begin{pmatrix} 0 & 0 & 0 \\ 0 & 0 & -i \\ 0 & i & 0 \end{pmatrix}, \quad \lambda_8 = \frac{1}{\sqrt{3}} \begin{pmatrix} 1 & 0 & 0 \\ 0 & 1 & 0 \\ 0 & 0 & -2 \end{pmatrix},
\end{aligned} \tag{A.11}$$

A.2 Dirac matrices

The four Dirac matrices γ_μ, $\mu = 0, ..., 3$, are defined in Minkowski space by the anti-commutation relations

$$\{\gamma^\mu, \gamma^\nu\} = 2g^{\mu\nu}, \quad \gamma_\mu = g_{\mu\nu}\gamma^\nu \,, \tag{A.12}$$

and they satisfy the Hermiticity conditions

$$\gamma^{\mu\dagger} = \gamma^0\gamma^\mu\gamma^0 \,. \tag{A.13}$$

It is possible to define a fifth anti-commuting Dirac matrix, it is defined by

$$\gamma^5 = i\gamma^0\gamma^1\gamma^2\gamma^3 = \frac{i}{4!}\epsilon_{\mu\nu\rho\sigma}\gamma^\mu\gamma^\nu\gamma^\rho\gamma^\sigma \,, \tag{A.14}$$

and it obeys the relations

$$\{\gamma^\mu, \gamma^5\} = 0, \quad (\gamma^5)^2 = \mathbb{I}, \quad \gamma^{5\dagger} = \gamma^5 \,. \tag{A.15}$$

Other important Dirac matrices are given by the commutators of the γ-matrices, which are denoted by

$$\sigma^{\mu\nu} = \frac{i}{2}[\gamma^\mu, \gamma^\nu] \,, \tag{A.16}$$

and satisfy

$$\sigma^{\mu\nu\dagger} = \gamma^0\sigma^{\mu\nu}\gamma^0 \,. \tag{A.17}$$

By using γ^5, we can define the projection operators on left- and right-handed chirality as

$$P_L = \frac{1}{2}(\gamma^5), \quad P_R = \frac{1}{2}(1+\gamma^5) \,. \tag{A.18}$$

Then the left- and right-handed chiral components of the fermion fields ψ, $\overline{\psi}$ are defined through the relations

$$\psi_{L,R} = P_{L,R}\psi, \quad \overline{\psi}_{L,R} = \overline{\psi}P_{R,L} \,. \tag{A.19}$$

Usually, the explicit representation of the Dirac matrices is given by

$$\gamma^i = \begin{pmatrix} 0 & \sigma_i \\ -\sigma_i & 0 \end{pmatrix} \,, \tag{A.20}$$

and

$$\gamma^0 = \begin{pmatrix} 0 & 1 \\ 1 & 0 \end{pmatrix}, \quad \gamma^5 = \begin{pmatrix} -1 & 0 \\ 0 & 1 \end{pmatrix}. \tag{A.21}$$

Until now, we have considered the Dirac matrices in Minkowski space, but sometimes the theories have to be formulated in Euclidean space. In that case, one has to use the Dirac matrices in Euclidean space, which are defined by

$$\begin{aligned} \gamma_i^E &= -i\gamma_i^M, \\ \gamma_4^E &= \gamma_0^M, \\ \gamma_5^E &= -\gamma_5^M = \gamma_1^E\gamma_2^E\gamma_3^E\gamma_4^E. \end{aligned} \tag{A.22}$$

The Euclidean Dirac matrices are Hermitian

$$\gamma_\mu^{E\dagger} = \gamma_\mu^E, \quad \gamma_5^{E\dagger} = \gamma_5^E, \tag{A.23}$$

and they have different anti-commutation relations, which are

$$\{\gamma_\mu^E, \gamma_\nu^E\} = 2\sigma_{\mu\nu}, \quad \{\gamma_\mu^E, \gamma_5^E\} = 0. \tag{A.24}$$

A.3 Grassmann algebra

In this section, we collect the basic definitions of the Grassmann Algebra and some useful relations. Grassmann variables are defined by the condition that they anti-commute among each other. Given the variables $\eta_1, ..., \eta_N$ we have

$$\{\eta_i, \eta_j\} = 0, \quad i, j = 1, ..., N, \tag{A.25}$$

and so it follows that

$$\eta_i^2 = 0. \tag{A.26}$$

Eq. (A.26) is a fundamental property which implies that any function of Grassmann variables can be expanded as a power series with only a finite number of terms. An important example is given by

$$e^\eta = 1 + \eta, \tag{A.27}$$

which can be generalized to the more useful case of $2N$-Grassmann variables. Denoting them by $\eta_1, \dots, \eta_N, \overline{\eta}_1, \dots, \overline{\eta}_N$, we have

$$e^{-\sum_{i,j} \overline{\eta}_i M_{ij} \eta_j} = \prod_{i,j=1}^{N} \left(1 - \overline{\eta}_i M_{ij} \eta_j\right) . \tag{A.28}$$

To introduce the derivative of a function of the Grassmann variables, it is sufficient the rule

$$\frac{\partial}{\partial \eta_i} \eta_i = 1 \,, \tag{A.29}$$

since in a generic function $f(\eta)$, any Grassmann variable can appear only to the first power, at most.

The relevant property to keep in mind is that the partial derivative of Grassmann variables anti-commute as well:

$$\left\{ \frac{\partial}{\partial \eta_i}, \frac{\partial}{\partial \eta_j} \right\} = 0 \,. \tag{A.30}$$

Given a generic function $f(\eta)$ we indicate the integral on the Grassman variables as

$$\int \prod_{i=1}^{N} d\eta_i f(\eta) \,, \tag{A.31}$$

which is defined by the following rules

$$\begin{aligned} \int d\eta_i &= 0 \,, \quad \int d\eta_i \eta_i = 1 \,, & \text{(A.32)} \\ \{d\eta_i, d\eta_j\} &= 0 \,. & \text{(A.33)} \end{aligned}$$

Even in this case, the previous rules are sufficient to compute every integral of every function $f(\eta)$.

A very important integral is

$$I[M] = \int \prod_{n=1}^{N} d\overline{\eta}_n d\eta_n \exp \left\{ - \sum_{i,j=1}^{N} \overline{\eta}_i M_{ij} \eta_j \right\} . \tag{A.34}$$

From the applications of the rules in Eqs.(A.32), and from the anti-commuting properties of the Grassmann variables, it follows that the only term of the exponential which contributes to the integral is

$$\eta_1 \overline{\eta}_1 \eta_2 \overline{\eta}_2 \dots \eta_N \overline{\eta}_N \sum_{i_1 \dots i_N} \epsilon_{i_1 i_2 \dots i_n} M_{1 i_1} M_{2 i_2} \dots M_{N i_N} \,, \tag{A.35}$$

where $\epsilon_{i_1 i_2 \dots i_n}$ is the N-dimensional total antisymmetric tensor.

Thus, we have

$$\begin{aligned} I[M] &= \int \prod_{n=1}^{N} d\overline{\eta}_n d\eta_n \exp\left\{ - \sum_{i,j=1}^{N} \overline{\eta}_i M_{ij} \eta_j \right\} \\ &= \left[\prod_{n=1}^{N} \int d\overline{\eta}_n d\eta_n \eta_n \overline{\eta}_n \right] \mathrm{det} M = \mathrm{det} M \, . \end{aligned} \tag{A.36}$$

The previous result represents a typical feature of the Grassmann algebra, since for ordinary, commuting, variables we would have instead

$$\int \prod_{n=1}^{N} d\overline{z}_n dz_n \exp\left\{ - \sum_{i,j=1}^{N} \overline{z}_i M_{ij} z_j \right\} \propto (\mathrm{det} M)^{-1} \, . \tag{A.37}$$

Appendix B

Introduction to Lattice QCD

Quantum Chromodynamics (QCD) is the non-Abelian gauge field theory describing the strong interactions of colored quarks and gluons, and it is the $SU(3)$ component of the $SU(3) \otimes SU(2) \otimes U(1)$ Standard Model of Particle Physics. The main difference with respect to the Quantum Electrodynamics (QED) is that the photon is replaced by eight gluons (the gauge fields), that can interact either with the quarks (the matter fields) and with each other, while the photon can interact only with matter fields. This is a peculiar characteristic of non-Abelian gauge theories, and it affects also the trend of the strong coupling α_s with the energy.

Indeed, computing the β function, which gives information about the evolution of the coupling constant with respect to the energy scale, one finds that at high energies, $\mu \gg \Lambda_{QCD} \simeq 0.3\ GeV$, $\alpha_s < 1$ and the theory can be handled perturbatively, this phenomenon is the so-called *asymptotic freedom* [50]. On the contrary at low energies α_s becomes large, the dynamics of the strong interactions is non-perturbative, and so the spectrum of the theory cannot be studied in perturbation theory and can not be expressed in terms of free quark fields. This behavior justifies the *confinement* phenomenon due to which quarks don't exist as free colored particles but are bounded into hadrons [51].

Since the coupling constant increases at low energy, it is necessary the use of a non-perturbative approach to determine the infrared properties of QCD, i.e. its mass spectrum and the matrix elements of generic operators between hadronic states. This is indispensable in order to perform a reliable study of hadron decays. The quantization of the QCD theory through the generating functional formalism provides a suitable non-perturbative approach. As in every quantum field theory, in order to calculate the quantities of interest, we have to introduce a regulator. In the generating functional formalism, the Lattice arises like a natural regulator of the quantized QCD theory. This approach lead to lattice gauge theory, as proposed by K. Wilson in 1974 [52]. Since then much progress have been made and its application is neither straightforward nor unique. In this appendix, we review the basic concepts of modern lattice QCD [53, 54] and travel through several issues which will naturally arise.

B.1 The Lagrangian of QCD

QCD is based on the Special Unitary Lie color group, $SU(N_c)$, with $N_c = 3$ number of colors; the fundamental degrees of freedom of the theory are quarks and gluons. The quarks are massive fermions of spin 1/2, which transform as the fundamental representation of $SU(3)$, i.e. the triplet representation (anti-triplet for anti-quarks). They are described by the Dirac spinors

$$q_f^{\alpha,c}(x),\ \overline{q}_f^{\alpha,c}(x)\,. \tag{B.1}$$

These quark fields carry several indices and arguments. The space–time position is denoted by x, the Dirac index by $\alpha = 1, 2, 3, 4$, and the color index by $c = 1, 2, 3$. In general, we will use Greek letters for Dirac indices and letters a, b, c, ... for color ones. Each field $q_f(x)$ thus has 12 independent components.

In addition, the quarks come in several flavors called up (u), down (d), strange (s), charm (c), bottom (b) and top (t), which we indicate by a flavor index $f = 1, 2, ..., 6$. We remark that often we omit the indices and use matrix/vector notation instead. In the Minkowskian space-time, the quark and the antiquark fields are related by $\overline{q} = q^\dagger\gamma_0$, where γ_0 is the Dirac matrix associated to the time-component of a four-vector.

Then there are the gluons, which are massless gauge bosons of spin 1,

$$A_\mu(x)_{ab}\,. \tag{B.2}$$

The gluons have the space-time argument x like the quarks, but have also a Lorentz index, μ which labels the four different directions in space-time. Moreover, they are 3×3 traceless hermitian matrices i.e. they are elements of the algebra of the gauge group, and so they can be expanded in the basis of the eight generators of $SU(3)$ as

$$A_\mu(x) = \sum_{a=1}^{8} \frac{\lambda^a}{2} A_\mu^a(x), \tag{B.3}$$

where we have omitted (as we will usually do in this thesis) the color indices carried by the gluon field $A_\mu(x)$ and by the generators $\lambda^a/2$, while the eight fields $A_\mu^a(x)$ don't carry any color index. The matrices λ^a are the Gell-Mann matrices, which are defined in Appendix A together with their relevant relations.

The Lagrangian of QCD for quark and gluon fields is built requiring its invariance (gauge symmetry) under the $SU(3)$ gauge transformations, i.e. local rotations among the color indices

$$\Omega(x) = \exp\left\{ i \sum_{a=1}^{8} \frac{\lambda^a}{2}\theta^a(x) \right\}, \tag{B.4}$$

where θ^a are the parameters of the transformation (since it is local they depend on x) and $\lambda^a/2$ are the generators. Therefore, in order to define $\mathcal{L}^{QCD}$, like for any Yang-Mills Lagrangian, one starts from the Dirac Lagrangian for the quark fields and requires its invariance under the transformation

$$\begin{aligned} q(x) &\rightarrow q'(x) = \Omega(x)q(x)\,, \\ \overline{q}(x) &\rightarrow \overline{q}'(x) = \overline{q}(x)\Omega^\dagger(x)\,. \end{aligned} \tag{B.5}$$

To achieve gauge invariance it is necessary to replace the partial derivative ∂_μ with the covariant derivative D_μ, which is defined by the property

$$D_\mu(x)q(x) \rightarrow [D_\mu(x)q(x)]' \equiv D_\mu(x)'q(x)' = \Omega(x)D_\mu(x)q(x)\,. \tag{B.6}$$

Thus, we define

$$D_\mu(x) = \partial_\mu - ig_s A_\mu(x) \tag{B.7}$$

where g_s is the gauge coupling related to α_s by $g_s^2 = 4\pi\alpha_s$.

In order to satisfy Eq. (B.6) we require that the gauge field $A_\mu(x)$ transforms as

$$A_\mu(x) \rightarrow A'_\mu(x) = \Omega(x)A_\mu(x)\Omega^\dagger(x) - \frac{i}{g_s}(\partial_\mu\Omega(x))\Omega^\dagger(x) \tag{B.8}$$

If we rewrite the field $A_\mu(x)$ in terms of the eight gluon scalar fields $A^a_\mu(x)$ the transformation becomes

$$A^a_\mu(x) \rightarrow A^{a\prime}_\mu(x) = A^a_\mu(x) + \frac{1}{g_s}\partial_\mu\theta^a(x) + f^{abc}A^b_\mu(x)\theta^c(x) \tag{B.9}$$

where we omitted the explicit sum over the repeated color indices, and f^{abc} are the structure constants defined in Appendix A by Eq. (A.5).

Now we have the elements to define the QCD Lagrangian for fermionic fields as[1]

$$\mathcal{L}_F = \sum_f \overline{q}_f\left(i\not{D} - m_f\right)q_f \tag{B.10}$$

where m_f is the quark mass and the summation is performed over the possible flavors of the quarks, $f = \{u,\ d,\ c,\ s,\ t,\ b\}$. We use the covariant derivative also to write the gluon kinetic term which is constructed starting from the gluon field strength tensor $G_{\mu\nu}$, defined as

$$G_{\mu\nu} = \frac{i}{g_s}\left[D_\mu, D_\nu\right] = \partial_\mu A_\nu - \partial_n u A_\mu - ig_s\left[A_\mu,\ A_\nu\right]\,. \tag{B.11}$$

$G_{\mu\nu}$, like A_μ, is a traceless hermitian 3x3 matrix that can be expanded in the basis of generators of $SU(3)$, that is

$$\sum_a \frac{\lambda^a}{2}G^a_{\mu\nu}\,. \tag{B.12}$$

[1]From now on we will often omit the space-time dependence of fields and tensors.

where $G^a_{\mu\nu}$ are scalars on the color space.

Using Eqs. (B.3) and (B.12) in Eq. (B.11) we find that

$$G^a_{\mu\nu} = \partial_\mu A^a_\nu - \partial_\nu A^a_\mu + g_s f^{abc} A^b_\mu A^c_\nu \,. \tag{B.13}$$

From the transformation property (B.8) of A_μ it follows that

$$G_{\mu\nu} \to G'_{\mu\nu} = \Omega G_{\mu\nu} \Omega^\dagger \,, \tag{B.14}$$

that is $G_{\mu\nu}$ transforms as an element of the adjoint representation of $SU(3)$. The gluon Lagrangian $\mathcal{L}_G$ for QCD is then written as

$$\mathcal{L}_G = -\frac{1}{2} Tr \left[G^{\mu\nu} G_{\mu\nu} \right] = -\frac{1}{4} G^{\mu\nu}_a G^a_{\mu\nu} \,, \tag{B.15}$$

this is indeed a gauge invariant term due to the unitarity of the transformation Ω and to the cyclic property of the trace. With respect to the photon field strength tensor, there is an additional term in Eq. (B.13) that depends on the structure constants. It causes the appearance of extra terms in $\mathcal{L}_G$ that represent the self-interactions of three or four gauge fields. Auto-interaction of the gauge bosons is the substantial difference between Abelian and non-Abelian gauge theories.

The complete QCD Lagrangian is written as

$$\mathcal{L}_{QCD} = \mathcal{L}_F + \mathcal{L}_G \,, \tag{B.16}$$

where $\mathcal{L}_F$ and $\mathcal{L}_G$ are defined respectively in Eqs. (B.10) and (B.15). However, we point out that Eq. (B.16) is only the classical definition of $\mathcal{L}_{QCD}$, the covariant quantization of a non-Abelian gauge theory is rather convoluted and other terms have to be included, e.g. the gauge fixing term and the ghost fields Lagrangian.

The classical, or "continuum", QCD action is written as

$$S_{QCD} = \int d^4x \mathcal{L}_{QCD} = \int d^4x \left[\sum_f \overline{q}_f \left(i \not{D} - m_f \right) q_f - \frac{1}{4} G^{\mu\nu}_a G^a_{\mu\nu} \right] \,. \tag{B.17}$$

B.2 The generating functional

The path-integral approach is an alternative but equivalent method to the Second Quantization, which allows us to study interacting and relativistic quantum field theories at non-perturbative scales through the numerical evaluation of functional integrals. For simplicity now we present the path-integral method for a theory in which there is only one scalar field $\phi(x)$, it will be straightforward to extend the definitions to a generic theory.

In order to obtain the physical quantities of a theory, like the S matrix or the mass spectrum, it is necessary to compute the n-points Green functions, which are the vacuum expectation values of the T-products of an arbitrary number of fields,

$$G_n(x_1, ..., x_n) = \langle 0| T\left[\phi(x_1)...\phi(x_n)\right]|0\rangle \,, \tag{B.18}$$

where $|0\rangle$ is the ground state (or vacuum state) of the interacting theory. In the formalism of functional integrals, the n-points Green functions can be expressed as

$$\langle 0| T\left[\phi(x_1)...\phi(x_n)\right]|0\rangle = \frac{\int \mathcal{D}\left[\phi\right] \phi(x_1)...\phi(x_n) e^{iS[\phi]}}{\int \mathcal{D}\left[\phi\right] e^{iS[\phi]}} \,. \tag{B.19}$$

Now we define the generating functional as

$$Z\left[J\right] = \int \mathcal{D}\left[\phi\right] \exp\left\{iS\left[\phi\right] + i\int d^4x J(x)\phi(x)\right\} \,, \tag{B.20}$$

It is possible to evaluate the n-points Green functions through the space-time derivatives of the generating functional

$$\langle 0| T\left[\phi(x_1)...\phi(x_n)\right]|0\rangle = \frac{1}{Z\left[J=0\right]}(-i)^n \left.\frac{\delta^n Z\left[J\right]}{\delta J(x_1)...\delta J(x_n)}\right|_{J=0} \,. \tag{B.21}$$

We proceeded with formal definitions, but there are two issues that have to be dealt with in order to be able to actual compute all these quantities, or even just to be sure that they are well-defined, the issues are:

- The measure $\mathcal{D}\left[\phi\right]$ indicates an integration over all the possible configurations of the field ϕ. Clearly they are infinite, and so we have to perform a ∞-dimension integral.
- Each path is weighted by a complex exponential factor, which potentially can be a very rapidly oscillating function.

These problems make it necessary to manipulate the path integral and the generating functional in a way that we obtain well-defined quantities that can be actually computed.

B.2.1 Wick rotation

The Wick rotation allows transforming the oscillating term into an exponentially decreasing term, which extremely improve the convergence of the path-integral, by rotating the Minkowskian space into the Euclidean one. With this procedure, we are able to find a solution to a problem in Minkowskian space from a solution to a related problem in Euclidean space. This procedure consists in performing the analytical continuation of the Minkowskian time to complex space

$$x^0_M \to x^0 e^{-i\theta} \,, \tag{B.22}$$

where a complex phase is given to the time. In particular, if we choose $\theta = \pi/2$ we see that the Minkowskian metric turns to the classical Euclidean metric in four dimension

$$x_M^2 = (x_M^0)^2 - \boldsymbol{x}^2 \to (ix^0)^2 - \boldsymbol{x}^2 = (x_E)^2\,, \tag{B.23}$$

where we have defined $(x_E)^2 = (x^0)^2 + \boldsymbol{x}^2$.

In the clockwise rotation of the time axis towards the imaginary axis, the path-integral cannot pass through the singularities, i.e. the poles of the Green function. Otherwise, one have to take the residues of the function at the poles into careful account. Practically, to find how the partition function transforms under a Wick rotation, it is sufficient to make the following substitutions:

$$\begin{aligned} x_M^0 &\to ix_E^4\,, \\ dx_M^0 &\to idx_E^4\,, \\ \partial_M^0 &\to i\partial_E^4\,. \end{aligned} \tag{B.24}$$

Now we can rewrite the generating functional in Euclidean space-time

$$Z_E[J] = \int \mathcal{D}\,[\phi] \exp\left\{-S_E[\phi] - \int d^4x J(x)\phi(x)\right\}\,, \tag{B.25}$$

so that

$$\langle\phi(x_1)...\phi(x_n)\rangle = \frac{\int \mathcal{D}[\phi]\phi(x_1)...\phi_(x_n)e^{S_E[\phi]}}{\int \mathcal{D}[\phi]e^{S_E[\phi]}}\,. \tag{B.26}$$

By $\langle...\rangle$ we indicate the analytical continuation of the T-product in Euclidean space-time, that is

$$\langle\phi(x_1)...\phi(x_n)\rangle = \langle 0|T_E\left[\phi(x_1)...\phi(x_n)\right]|0\rangle\,. \tag{B.27}$$

We point out that the Euclidean expectation value of the product of n fields is not equal to the n-points Green function of the original theory, but they are related through an analytical continuation, and so we can apply an inverse Wick rotation to obtain the desired solution.

Since the Euclidean action S_E is positive definite, and there is no more the imaginary unit "i", in the Euclidean path-integral we have now a convergence factor which decrease very rapidly. Despite the fact that the range of the possible configurations is infinite, however, the distribution is very highly peaked around the configurations that minimize the action. They are called the “importance sampled” configurations. More generally, the factor e^S can be considered as a probability weight for generating configurations in the path-integral. It is analogous to the Boltzmann factor in the partition function for statistical mechanics systems, and so we will call $Z[J = 0]$ the partition function of the quantum theory. Due to this fact, it is possible to implement many typical techniques of statistical mechanics on the numerical analyses of lattice simulation, as we will see in this chapter further on.

B.2.2 Discretization of the path integral and boundary conditions

So far we have not actually defined the measure of integration appearing in Eq. (B.20), we have only said that the generating functional is an integral over all the possible configurations of the fields, that is an integration over a continuum infinity of degrees of freedom. Even in the simplest case of a scalar theory, we have to perform an integral over the variable $\phi(x)$ for every point x of the space-time. To solve this problem, the idea is to consider the infinite dimensional integral as the limit of a finite one.

First we define a regularized theory through the substitution of the continuum space-time with a finite number of point, that is we introduce a *lattice*. A very simple choice for the lattice is a four dimensional hypercube with *lattice spacing* a and volume $V = L^3 \times T$, where $L = aN_L$ and $T = aN_T$. That is we consider the substitution

$$x^\mu \to x_n^\mu = an^\mu\,, \quad x_n^\mu \in V\,, \tag{B.28}$$

often we will indicate the lattice points x_n^μ in units of a, i.e. only with the integer valued vector n^μ.

For the theory defined on the lattice, the measure of the path-integral is the product of a finite number of measures for the classical field variables in each lattice site, so we replace

$$\mathcal{D}\left[\phi\right] \to \prod_{n\in V} \delta\phi(n)\,. \tag{B.29}$$

The original generating functional can be defined as the limit of the discretized one, that is

$$Z[J] \;=\; \lim_{\substack{a\to 0\\ V\to\infty}} Z^{(a,V)}[J]\,, \tag{B.30}$$

where

$$Z^{(a,V)}[J] = \int \prod_{n\in V} \delta\phi(n) \exp\left\{-a^4 \sum_n \left(\mathcal{L}\left[\phi(n), \nabla_\mu[\phi(n)]\right] + J(n)\phi(n)\right)\right\}\,. \tag{B.31}$$

With $\nabla_\mu[\phi(n)]$ we indicate a generic discretized version of the derivative $\partial_\mu\phi(x)$. For example, the so-called *naive discretization* consists on the substitution of the ordinary derivative with the symmetrized difference:

$$\partial_\mu\phi(x) \to \nabla_\mu[\phi(n)] = \frac{\phi(n+\hat\mu) - \phi(n-\hat\mu)}{2a}\,, \tag{B.32}$$

where $\hat\mu$ is the unit vector connecting two next lattice sites in the μ-direction. If we use the Taylor series expansion of $\phi(x)$ we can easily see that $\nabla_\mu[\phi]$ differs from the continuum derivative $\partial_\mu\phi$ by terms of order $O(a^2)$. The naive discretization is only the simplest choice, it is possible to implement more complicated discretization in order to obtain the so-called *improved actions*, which differ from the continuum action by terms which go to zero with higher powers of the lattice spacing, for example of order $O(a^4)$.

A very important feature of the lattice discretization is that it naturally provides an infrared and an ultraviolet regulator. More precisely, the infrared regulator comes from the finite volume of the lattice, while the ultraviolet one comes from the lattice spacing a.

Introducing a lattice, the Poincarè invariance is reduced to a discrete group, since on a hypercubic lattice only rotations by 90° are allowed and translations have to be by at least one lattice unit. For every function defined on the lattice $f(n)$, the toroidal boundary conditions impose

$$f(n + \hat{\mu}N_\mu) = e^{i2\pi\theta_\mu} f(n)\,, \tag{B.33}$$

where N_μ is the number of lattice sites in the μ direction, periodic boundary conditions correspond to $\theta_\mu = 0$ and anti-periodic ones correspond to $\theta_\mu = 1/2$.

In order to obey the boundary conditions (B.33) the allowed momenta values are

$$p_\mu = \frac{2\pi}{aN_\mu}(k_\mu + \theta_\mu)\,, \quad k_\mu = -\frac{N_\mu}{2} + 1,\ \dots\ , \frac{N_\mu}{2}\,. \tag{B.34}$$

The boundary conditions of Eq. (B.1boundary), with $\theta \neq 0, 1/2$, are called *twisted boundary conditions*. They are very useful for lattice simulations since they allow shifting the quantized momentum $\boldsymbol{p} = \frac{2\pi}{aN}\boldsymbol{n}$ by a continuum amount. We point out that, on present lattice simulations, we have typically $\frac{2\pi}{aN} \sim 0.4\ GeV$. By choosing small values of θ it is possible to assign arbitrary momentum to a specific fermion. Clearly, it is possible to assign different boundary conditions to different fields. More details about twisted boundary conditions can be found in [35].

We have shown that the boundary conditions associated to the finite volume are responsible for the discretization of the momenta which provides the infrared regulator. Instead, the finite lattice spacing a introduce an ultraviolet cut-off, since it restricts all four components of momenta to the first Brillouin zone $[\pi/a, \pi/a]$. What we have now is a regularized theory in which, for a fixed value of the lattice spacing a, the Green functions are well-defined quantities. However, the regularized theory depends on the cut-off $1/a$, while in the real physical theory there is no lattice spacing. Thus, in order to obtain physical results, it is necessary to send the ultraviolet cut-off $1/a$ to infinity (i.e. the lattice spacing must go to zero). A naive limit $a \to 0$ would give the original divergences back, thus the *continuum limit* has to be performed very carefully, in the context of a renormalization procedure. We will address this crucial topic in section B.4.

B.2.3 Path-integral formulation of QCD

Before to apply the discretization procedure to QCD, we want to define the relevant quantities for the path-integral formulation of QCD and obtain some useful results for the generating functional. We consider now $S = S^{QCD}$ of Eq. (B.17), by performing the Wick rotations as explained in section B.2.1 we get the substitution

$$e^{iS^{QCD}} \to e^{-S_E^{QCD}}\,, \tag{B.35}$$

with

$$S_E^{QCD}[\boldsymbol{q},\overline{\boldsymbol{q}},A] = \int d^4x_E \left[\sum_f \overline{q}_f \left(\gamma_E^\mu D^\mu + m_f\right) q_f + \frac{1}{4} G_a^{\mu\nu} G_a^{\mu\nu} \right] . \tag{B.36}$$

γ_E^μ are the Euclidean Gamma matrices defined in Appendix A. From now on we will omit the subscript "E" taking for granted that we are working in Euclidean space-time.

To write the generating functional, we have to introduce a source for each field that appears in the action. So we have

$$\begin{aligned} Z_{QCD}[\boldsymbol{\eta},\overline{\boldsymbol{\eta}},J] = \int \mathcal{D}[A] \left(\prod_f \int \mathcal{D}[q_f]\mathcal{D}[\overline{q}_f] \right) \times \\ \times \exp\left\{ -S^{QCD}[\boldsymbol{q},\overline{\boldsymbol{q}},A] - \int d^4x \left[\sum_f \overline{\eta}_f(x) q_f(x) + \overline{q}_f(x)\eta_f(x) + J(x)A(x) \right] \right\} . \end{aligned} \tag{B.37}$$

Fermions must satisfy the Pauli exclusion principle, to do so the n-point Green functions have to be antisymmetric under the exchange of two fermionic fields:

$$\langle q(x_1)\overline{q}(x_2)\rangle = -\langle \overline{q}(x_2) q(x_1)\rangle . \tag{B.38}$$

To obtain this property in the formalism of the generating functional, even the source η and $\overline{\eta}$ have to anti-commute. So the quark fields and their sources cannot be normal variables in the path integrals, they are complex anti-commuting variables, such variables are called *Grassmann variables*. In Appendix A are collected the relevant results for the Grassmann algebra, which are used in the following.

The fermionic part of the generating functional of Eq. (B.37) is

$$Z_F^{QCD}[\boldsymbol{\eta},\overline{\boldsymbol{\eta}},A] = \prod_f \int \mathcal{D}[q_f]\mathcal{D}[\overline{q}_f] \exp\left\{ - \int d^4x (\overline{q}_f K_f[A] q_f + \overline{\eta}_f q_f + \overline{q}_f \eta_f) \right\} \tag{B.39}$$

where $K_f[A] = \not{D}[A] + m_f$ is the *Dirac operator*.

To solve this integral we first complete the square at the exponent, that is we rewrite as:

$$-\int d^4x \left[\left(\overline{q}_f + \overline{\eta}_f K_f^{-1}\right) K_f \left(q_f + K_f^{-1}\eta_f\right) - \overline{\eta}_f K_f^{-1} \eta_f \right] . \tag{B.40}$$

Now we perform a transformation of variables which leaves the measure invariant:

$$q_f \to q'_f = q_f + K_f^{-1}\eta_f , \qquad \overline{q}_f \to \overline{q}'_f = \overline{q}_f + \overline{\eta}_f K_f^{-1} , \tag{B.41}$$

obtaining

$$
\begin{aligned}
Z_F^{QCD}[\boldsymbol{\eta}, \overline{\boldsymbol{\eta}}, A] &= e^{-\int d^4x \sum_f \overline{\eta}_f K_f^{-1} \eta_f} \prod_f \int \mathcal{D}[q'_f]\mathcal{D}[\overline{q}'_f] e^{-\int d^4x \overline{q}'_f K_f q'_f} \\
&= e^{-\int d^4x \sum_f \overline{\eta}_f K_f^{-1} \eta_f} \prod_f \det\left[K_f\right] .
\end{aligned} \tag{B.42}
$$

In the previous formula, we have used the results collected in Appendix A for the integration of Grassmann variables to solve exactly the integral over the quark field configurations.

To give an example of an application of the previous formula we can compute the 2-point quark Green functions through Eq. (B.42), using Eq. (B.21) we have

$$
S_f(x, y, A) = \langle q_f(y)\overline{q}_f(x)\rangle_F = \frac{1}{Z[0,0,A]} \frac{\delta^2 Z_F^{QCD}[\eta_f, \overline{\eta}_f, A]}{\delta\overline{\eta}_f(y)\eta_f(x)}\bigg|_{\eta_f=\overline{\eta}_f=0} = K_f^{-1}[A] . \tag{B.43}
$$

This result is a simple case of the *Wick's theorem.* The 2-point Green function $S_f(x, y, A)$ propagates a quark q_f from the space-time point x to the point y and for this reason is called *Dirac propagator.* It is dependent on A, so it is not a simple function as in the free case, but it is a complicated object whose solution requires the inversion of the Dirac operator $K_f^{-1}[A]$.

The determinant of an operator can be written as the product of its eigenvalues, thus we can use the relation

$$
\log\det[K] = \log\left(\prod_i k_i\right) = \sum_i \log k_i = \mathrm{Tr}\log K . \tag{B.44}
$$

from which it follows that

$$
\det[K] = \exp\left\{\mathrm{Tr}\log K\right\} . \tag{B.45}
$$

Using this result, we can write the partition function of QCD in a form more useful for numerical simulations:

$$
Z^{QCD}[0] = \int \mathcal{D}[A] e^{-S_{eff}[A]} , \tag{B.46}
$$

where

$$
S_{eff}[A] = -\int d^4x \frac{1}{4} G^a_{\mu\nu} G^a_{\mu\nu} + \mathrm{Tr}\log\left(\not{D}[A] + m_f\right) . \tag{B.47}
$$

The trace in the exponent is responsible for the creation of the fermion loops. Indeed, by explicitly computing the determinant of the Dirac operator $K_f[A]$, one can find that it is equal to the exponential of the sum of Feynman diagrams containing virtual quarks loops and an arbitrary number of insertions of the gauge fields. Thus, the functional determinant contains the so-called *sea quark corrections.* For this reason, we can say that the functional determinant represent the fermionic vacuum, in where pairs of virtual quarks and antiquarks (sea quarks) are created and annihilated. These contributions are strongly non-local[2]. Hence, from the computational point of view, the determination of the expectation values using the action (B.47) would require an enormous number of operations, making this method possible to be used only for small lattices.

In order to avoid this problem, the *quenched approximation* was often used in the past. It consists in eliminating the second term of Eq. (B.47) by setting the determinant of the fermionic matrix equal to one, so that one can study the gauge fields in absence of the quark contributions[3]. The quenched approximation can be considered as the limit in which the mass of the sea quarks is so heavy that they cannot be generated from the vacuum as particle–antiparticle pairs. A simulation that include the determinant and therefore allows for the complete dynamical structure of the fermionic vacuum is called a simulation with *dynamical quarks*.

Combining Eq. (B.46) with Eq. (B.26) we obtain that the expectation value of a physical observable $\mathcal{O}$ is given by

$$\langle \mathcal{O} \rangle = \frac{1}{Z[0]} \int \mathcal{D}[A] \mathcal{O}[A] \, e^{-S_{eff}[A]} \,, \tag{B.48}$$

where we have now omitted the superscript "QCD". $\mathcal{O}$ is a generic operator expressed in terms of products of quark and gluon fields.

A very important example are quark bilinear operators, which have the form

$$\mathcal{O}_\Gamma(x) = \overline{q}_f \Gamma q_{f'} \,, \tag{B.49}$$

where Γ is a generic combination of the Dirac matrices. Typically, these operators are used in 2-point correlation functions, like

$$C_{ij}(x) = \langle \mathcal{O}_{\Gamma_i}(x) \overline{\mathcal{O}}_{\Gamma_j}(0) \rangle \,, \tag{B.50}$$

to compute the meson mass spectrum and some matrix elements, as we will see further on.

In order to compute the correlator (B.50), we have to reorder the Grassmann variables and to apply the Wick's theorem so that we have

$$C_{ij}(x) = -\langle \mathrm{Tr} \left[\Gamma_i S_{f'}(0, x; A) \Gamma_j S_f(x, 0; A) \right] \rangle \,, \tag{B.51}$$

where the trace is performed over the Dirac and color indices. We notice that the two bilinear operators must involve the same two flavor f and f' in order to give a non-vanishing result. We will often omit the dependence of the quark propagator from the gauge configurations.

Later on we will see how these correlators can be actually computed in the simulations and how to use them to extract physical observable, now instead we address the lattice transcription of the fields and the action of QCD.

[2]That is, a *link variable* (which we define further on when we address the discretization of S^{QCD}) can interact also with far other ones, not only with the nearest ones.

[3]Actually, its contribution was partially accounted for in the gauge action by a suitable redefinition of the gauge couplings.

B.3 Lattice regularization of QCD

In this section we deal with the transcription of the gauge and fermions degrees of freedom on the lattice and with the construction of a discretized action. This procedure is characterized by a certain degree of arbitrariness, indeed the only requirement of the discretized action is to preserve the gauge symmetry and that it has to recover the continuum action in Eq. (B.17) in the continuum limit $a \to 0$. Obviously, it is convenient to consider discretized action which share as many symmetries as possible with the continuum action, but not always. For example, we will see that every discretized action who benefit of the chiral symmetry (in the limit of massless quarks) involves the introduction of fictitious particles called *doublers*. The solution is then adding a so-called *Wilson term*, which disappears in the continuum limit but for $a \neq 0$ it breaks explicitly the chiral symmetry even in the massless limit. Finally, we consider the implications and the possible advantages of adding a *twisted mass* term.

B.3.1 Discretization of free fermions

The discretization of free fermions is straightforward. The quark fields are represented by anti-commuting Grassmann variables defined at each site of the lattice, belonging to the fundamental representation of $SU(3)$. Since the fermion action is linear in q and $\overline{q}$, the Grassmann rules for integration can be used to integrate over them so that the path-integral reduces to the one over the gauge fields. The continuum action S_F^0 for a free fermion is given by the expression

$$S_F^0[q, \overline{q}] = \int d^4x \overline{q}(x)(\not{\partial} + m)q(x)\,. \tag{B.52}$$

By replacing the continuum derivative with its naive discretization defined in Eq. (B.32) we obtain the lattice version of the free fermionic action as

$$S_F^0[q, \overline{q}] = a^4 \sum_{n\in\Lambda} \overline{q}(n) \left(\sum_{\mu=1}^{4} \gamma_\mu \frac{q(n+\hat{\mu}) - q(n-\hat{\mu})}{2a} + mq(n) \right)\,. \tag{B.53}$$

B.3.2 Link variables

The gauge fields in the continuum are introduced by requiring the invariance of the action under local $SU(3)$ color rotation of the fermion fields, as we showed in Section B.1. We can implement on the lattice the same local transformation by choosing an element $\Omega(n)$ of $SU(3)$ for each site n and transforming the quark fields according to

$$\begin{aligned} q(n) \to q'(n) &= \Omega(n)q(n)\,, && \text{(B.54)} \\ \overline{q}(n) \to \overline{q}'(n) &= \overline{q}(n)\Omega^\dagger(n)\,. && \text{(B.55)} \end{aligned}$$

The mass term of (B.53) is clearly invariant under the transformation (B.54), but this is not true for the discretized derivative term , since it involves the product of quark fields evaluated in different sites of the lattice.

In order to build a gauge invariant action, we need to introduce a field $U_\mu(n)$ which under color rotation transforms as

$$U_\mu(n) \to U'_\mu(n) = \Omega(n)U_\mu(n)\Omega^\dagger(n+\hat{\mu})\,. \tag{B.56}$$

In the continuum, the gauge fields $A_\mu(x)$ are defined as elements of the algebra of $SU(3)$, while on the lattice the fields $U_\mu(n)$ has to be an element of the gauge group $SU(3)$.

These matrix-valued variables are oriented and attached to the links of the lattice, and so they are commonly referred to as *link variables*. The link variables connect two nearest lattice points. Indeed, $U_\mu(n)$ lives on the link which connect the point n to the point $n+\hat{\mu}$. The $\hat{\mu}$ direction of the link variables can also be negative: $U_{-\mu}(n)$ connect n to $n-\hat{\mu}$ and is related to the positively oriented link variable $U_\mu(n\hat{\mu})$ through the relation

$$U_{-\mu}(n) = U^\dagger_\mu(n\hat{\mu})\,. \tag{B.57}$$

In the continuum, a fermion moving from site x to y, along some curve C_{xy}, in presence of a gauge field $A_\mu(x)$ picks up a phase factor according to

$$q(y) = \mathcal{P}e^{ig\int dz_\mu A_\mu(z)}q(x) = G(x,y)q(x)\,. \tag{B.58}$$

The operator $G(x,y)$ is a path-ordered exponential which shares the same transformation properties of $U_\mu(n)$, it is called *gauge transporter* operator. The idea is to interpret the link variable $U_\mu(n)$ as a lattice version of the gauge transporter connecting the points n and $n+\hat{\mu}$, i.e. we wish to establish $U_\mu(n) = G(n, n+\hat{\mu}) + O(a)$. Thus, we introduce $A_\mu(n)$ as the lattice version of the gauge field, and we write

$$U_\mu(n) = e^{igaA_\mu(n)} = \mathbb{I} + igaA_\mu(n) + O(a^2)\,. \tag{B.59}$$

Therefore, we approximate the integral along the path $C_{n,n+\hat{\mu}}$ with the length a of the path times the value of the field $A_\mu(n)$ at the starting point. This is an approximation of the gauge transporter at order $O(a)$ and at this order the path-ordering is not necessary.

When we perform a gauge transformation $\Omega(n)$, the link and quark variables transform according to (B.56) and (B.54) respectively. Using these two transformation properties we are able to construct two kinds of gauge invariant objects:

- A *string*, which is a product of the link variables along a path of links connecting two lattice sites, capped by a quark and an anti-quark:

$$\overline{q}(n)U_\mu(n)U_\nu(n+\hat{\mu})...U_\rho(m-\hat{\rho})q(m)\,. \tag{B.60}$$

  This object is clearly the lattice version of the continuum gauge transporter $G(x,y)$.

- A *Wilson loop*, which is the trace over the color indices of the product of link variables along

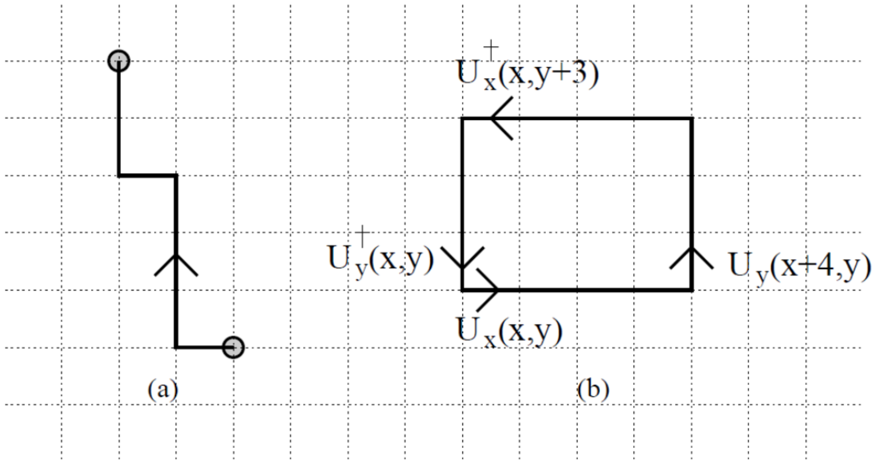

Figure B.1: The two gauge invariants objects on the lattice. a) An ordered string. b) A 3×4 closed Wilson loop. (a= 1)

a closed path of links. The simplest example is the *plaquette*, which is the 1×1 loop

$$W^{1\times1}_{\mu\nu} = \mathrm{Tr}\left\{U_\mu(n)U_\nu(n+\hat{\mu})U^\dagger_\mu(n+\hat{\nu})U^\dagger_\nu(n)\right\} . \tag{B.61}$$

For $SU(N \geq 3)$, the trace of any Wilson loop in the fundamental representation is in general complex, with the two possible path-orderings giving complex conjugate values.

In Fig. (B.1) we show a bidimensional example of these two objects, clearly they can have arbitrary sizes and shapes. In the next sections, we will see how these two types of gauge invariant terms can be used to build a gauge invariant action. The only limitation to follow is that the discretized action must approach the continuum action when the limit $a \to 0$ is performed.

B.3.3 Gauge action

The closed loops can be used to write a discretized gauge action. Starting from the definition of the plaquette (B.61), and by using the definition of the link variables (B.59), we have

$$\begin{aligned} W^{1\times1}_{\mu\nu} &= \mathrm{Tr}\left\{U_\mu(n)U_\nu(n+\hat{\mu})U^\dagger_\mu(n+\hat{\nu})U^\dagger_\nu(n)\right\} \\ &= e^{igaA_\mu(n)}e^{igaA_\nu(n+\mu)}e^{-igaA_\mu(n+\nu)}e^{-igaA_\nu(n)} . \end{aligned} \tag{B.62}$$

The link variables are non-commuting $SU(3)$ matrices and so now we use the Baker-Campbell-Ausdorff formula for non-commuting matrices

$$e^A e^B = e^{A+B+\frac{1}{2}[A,B]+\dots} . \tag{B.63}$$

We also expand around the point n in which the plaquette starts,

$$A_\mu(n+\nu) = A_\mu(n) + a\partial_\nu A_\mu(n) + O(a^2) . \tag{B.64}$$

By combining Eqs. (B.63) and (B.64) we obtain

$$\begin{aligned} W^{1\times1}_{\mu\nu} &= \exp\left\{ia^2 g\left(\partial_\mu A_\nu - \partial_\nu A_\mu + ig[A_\mu, A_n u] + ...\right)\right\} \\ &= \mathbb{I} + ia^2 g G_{\mu\nu} - \frac{a^4 g^2}{2}(G_\mu \nu)^2 + O(a^6)\,. \end{aligned} \tag{B.65}$$

From the previous formula, we point out that the plaquette is indeed connected to the gluon field strength tensor $G_{\mu\nu}$ and that the Wilson loop is indeed a complex object.

The real and the imaginary parts of the loop give

$$\mathrm{Re}\left[\mathbb{I} - W^{1\times1}_{\mu\nu}\right] = \frac{a^4 g^2}{2}(G_{\mu\nu})^2 + ... \tag{B.66}$$

$$\mathrm{Im}\left[W^{1\times1}_{\mu\nu}\right] = a^2 g G_{\mu\nu} + ...\,. \tag{B.67}$$

Now we have the results necessary to present the *Wilson gauge action*:

$$S^W_G[U] = \beta \sum_n \sum_{\nu<\mu} \frac{1}{N_C} \mathrm{Re}\left[\mathrm{Tr}\left(\mathbb{I} - W^{1\times1}_{\mu\nu}\right)\right]\,. \tag{B.68}$$

The sum is performed over all the lattice points at which the plaquettes are located, being counted with only one orientation (at each site there are 6 distinct positively oriented plaquettes, $\mu < \nu$). It is possible to properly choose the constant β in order to obtain the continuum gauge action starting with the Wilson action (B.68) and performing the limit $a \to 0$, $V \to \infty$. Indeed, by using the result in (B.66), and setting $\beta = \frac{2N_C}{g^2}$ we have

$$\begin{aligned} S^W_G[U] &= \beta \frac{g^2}{2N_C} a^4 \sum_n \sum_{\nu<\mu} \mathrm{Tr}\left[G^2_{\mu\nu}\right] \\ &= \beta \frac{g^2}{4N_C} a^4 \sum_n \sum_{\nu,\mu} \mathrm{Tr}\left[G^2_{\mu\nu}\right] \to \frac{1}{2}\int d^4x \mathrm{Tr}\left[G_{\mu\nu}G^{\mu\nu}\right]\,. \end{aligned} \tag{B.69}$$

Traditionally, the lattice calculations are presented in terms of the lattice coupling β, rather than the coupling constant g. It is important to underline that, in making the Taylor expansion, all terms containing derivatives at odd orders cancel out. As a consequence of this fact, the first correction to the Wilson gauge action is of $O(a^2)$.

In choosing a suitable action, it is fundamental that it approaches the right continuum limit and highly desirable that its discretization errors are as small as possible. We have already pointed out that there are infinity different way to discretize the action on the lattice, as long as the continuum action is obtained in the continuum limit. In particular, the gauge action can be expressed in terms of others gauge invariant objects, which are made by generic closed paths of links. A relevant example is the *Iwasaki action* [55], made by the loops represented in Fig.(B.2),

$$S^I_G = \frac{1}{g^2}\left[c_0 \sum \mathrm{Tr}(\text{plaquette loops}) + c_1 \sum \mathrm{Tr}(\text{rectangle loops})\right.$$

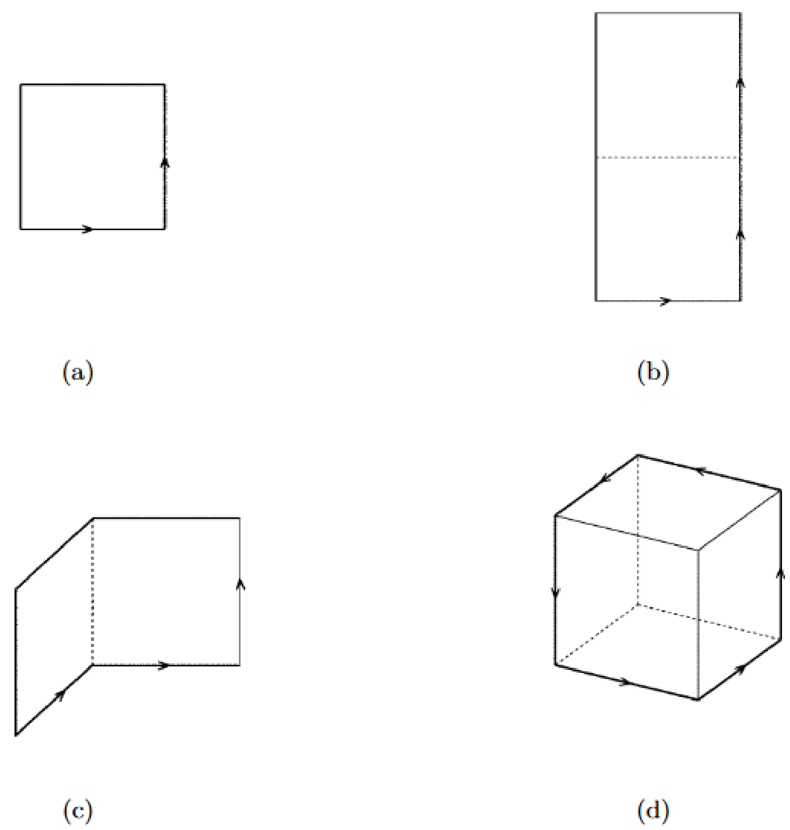

Figure B.2: Four types of Wilson loops in the action: (a) simple plaquette loop; (b) rectangle loop; (c) chair-type loop; (d) three-dimensional loop.

$$+c_2 \sum \mathrm{Tr}(\text{chair-type loops}) + c_3 \sum \mathrm{Tr}(\text{three-dimensional loops})\Bigg] \,. \tag{B.70}$$

By requiring that in the continuum limit the action B.70 approaches the continuum gauge action, we obtain the condition

$$c_0 + 8c_1 + 16c_2 + 8c_3 = 1\,. \tag{B.71}$$

The improved Iwasaki action is obtained by choosing properly the coefficients in order to reduce the cut-off effects. Namely, the choice is $c_1 = 0.331$ and $c_2 = c_3 = 0$ and thus the Iwasaki action explicitly reads

$$S_G^I = \frac{\beta}{3}\left[\sum_{n,\nu>\mu}(1-8c_1)W_{\mu\nu}^{1\times 1} + c_1 \sum_{n,\mu\neq\nu} W_{\mu\nu}^{1\times 2}\right], \tag{B.72}$$

where $W_{\mu\nu}^{1\times 1}$ is the usual plaquette term and $W_{\mu\nu}^{1\times 2}$ represents the rectangle loops. Another possible choice for the gluon action is the tree-level Symanzik improved action proposed by Weisz [56], which differs from the Iwasaki action for the values of the Symanzik coefficients c_i. In this case $c_1 = 1/12$,

$c_2 = c_3 = 0$.

B.3.4 Quark action

Naive action

In Sec. B.3.1 we have found the lattice version of the free fermion action. When we consider the presence of an external gauge field U it comes natural to write the *naive fermion action* as

$$S_F^N[q,\overline{q},U] = a^4 \sum_n \overline{q}(n) \left(D^N[U] + m\right) q(n)\,, \tag{B.73}$$

with

$$D^N[U] = \frac{1}{2}\sum_\mu \gamma_\mu(\nabla_\mu + \nabla_\mu^*)\,. \tag{B.74}$$

∇_μ and ∇_μ^* are the forward and backward discretized versions of the covariant derivatives. They are defined as

$$\nabla_\mu q(n) = \frac{U_\mu(n)q(n+\hat{\mu}) - q(n)}{a}\,, \qquad \nabla_\mu^* q(n) = \frac{q(n) - U_{-\mu}(n)q(n-\hat{\mu})}{a}\,. \tag{B.75}$$

As for the continuum action, the introduction of the gauge links is necessary to maintain the gauge invariance of the action.

One can verify that the action (B.73) reduces correctly to the Dirac action in the continuum limit. For the mass term this is trivial, and for the derivative part $D^N[U]$ this is achieved by considering the Taylor expansion of $U_\mu(n)$ and $q(n+\hat{\mu})$ in powers of the lattice spacing a. Keeping only the leading term in a the two strings become

$$\begin{aligned}
\overline{q}(n)\gamma_\mu U_\mu(n)q(n+\hat{\mu}) &= \overline{q}(n)\gamma_\mu(1+iagA_\mu(n))(q(n)+a\partial_\mu q(n)) + ... \\
&= \overline{q}(n)\gamma_\mu[q(n) + a(\partial_m u + igA_\mu)q(n)] + ...\,, && \text{(B.76)}\\
\overline{q}(n)\gamma_\mu U_{-\mu}(n)q(n-\hat{\mu}) &= \overline{q}(n)\gamma_\mu(1-iagA_\mu(n))(q(n)-a\partial_\mu q(n)) + ... \\
&= \overline{q}(n)\gamma_\mu[q(n) - a(\partial_m u + igA_\mu)q(n)] + ...\,. && \text{(B.77)}
\end{aligned}$$

With these results and with the definition of the lattice covariant derivatives, we find

$$\begin{aligned}
a^4\sum_n \overline{q}(n)D^N[U]q(n) &= a^4\sum_n \overline{q}(n)\left[\gamma_\mu \frac{U_\mu(n)q(n+\hat{\mu}) - U_{-\mu}(n)q(n-\hat{\mu})}{2a}\right] \\
&\xrightarrow[\substack{a\to 0\\ V\to\infty}]{} \int d^4x \overline{q}(x)\gamma_\mu[\partial_\mu + igA_\mu(x)]q(x) = \int d^4x \overline{q}(x)\not{D} q(x)\,. && \text{(B.78)}
\end{aligned}$$

Even in this case, the discretization errors are of order $O(a^2)$.

A more compact and useful way to write the naive action is the following:

$$S_F^N[q,\overline{q},U] = a^4 \sum_{n,m} \overline{q}(n) K^N_{nm}[U] q(m)\,, \tag{B.79}$$

where the naive Dirac matrix $K^N[U]$ is

$$K^N_{nm}[U] = \frac{1}{2a}\sum_\mu \left[\gamma_\mu U_\mu(n)\delta_{n+\hat{\mu},m} - \gamma_\mu U_{-\mu}(n)\delta_{n-\hat{\mu},m}\right] + m\,\delta_{n,m}\,. \tag{B.80}$$

However, the naive discretization gives rise to a serious problem called the *fermion doubling problem.*

The doubling problem

To illustrate this problem, it is sufficient to consider the case of free fermions, so we set all $U_\mu(n) = \mathbb{I}$. We are going to show that the naive discretization of the Dirac action in the massless limit $m \to 0$ gives rise to $2^d = 16$ fermion species instead of one. To do so we consider the propagator, obtained computing the Fourier Transform of the lattice Dirac operator, we have

$$\begin{aligned}\tilde{K}^N(p \mid q) &= \frac{1}{\mid \Lambda \mid}\sum_{n,m\in\Lambda} e^{-ip\cdot na} K^N_{nm} e^{iq\cdot ma} = \\ &= \frac{1}{\mid \Lambda \mid}\sum_{n\in\Lambda} e^{-i(p-q)\cdot na}\left(\sum_\mu \frac{1}{2a}\gamma_\mu[e^{iq_\mu a} - e^{-iq_\mu a}] + m\mathbb{I}\right) = \delta(p-q)\tilde{K}^N(p)\,.\end{aligned} \tag{B.81}$$

Thus the free propagator in Fourier space is

$$S(p) = (\tilde{K}^N(p))^{-1} = \left(\frac{i}{a}\sum_\mu \gamma_\mu \sin(ap_\mu) + m\mathbb{I}\right)^{-1} = \frac{m\mathbb{I} - ia^{-1}\Sigma_\mu\gamma_\mu\sin(p_\mu a)}{m^2 + a^{-2}\Sigma_\mu \sin(p_\mu a)^2}\,. \tag{B.82}$$

In the continuum and in the chiral limit $m \to 0$, the momentum space propagator has a pole in $p_\mu = 0$. However, in the discretized propagator we find a pole both for $p = 0$ and for all the possible combinations of $p_\mu = 0$ and $p_\mu = \pi/a$. The momentum space of the lattice theory is a d-dimensional Brillouin zone $\mathbb{B} = (-\pi/a, \pi/a]^d$ with periodic boundary conditions, thus the naive lattice Dirac propagator, in the chiral limit, has 16 poles (the zeros of Eq. (B.82)) at

$$p = (0,0,0,0),\ \left(\frac{\pi}{a},0,0,0\right),\ \left(0,\frac{\pi}{a},0,0\right),\ldots,\ \left(\frac{\pi}{a},\frac{\pi}{a},\frac{\pi}{a},\frac{\pi}{a}\right)\,. \tag{B.83}$$

Except for the physical pole $p_\mu = (0,0,0,0)$, the others are 15 unwanted poles, the so-called doublers.

The inclusion of gauge fields in the action does not solve the doubling problem. It is in fact a manifestation of a deep fundamental problem of lattice regularized fermionic theories which respect the chiral symmetry and the axial anomaly [57]. Indeed, the naive action is invariant under the following *vector global transformation*

$$q \to e^{i\alpha} q, \quad \overline{q} \to \overline{q} e^{-i\alpha}\,, \tag{B.84}$$

and also, in the chiral limit, under the *axial global transformation*

$$q \to e^{i\alpha\gamma_5} q, \quad \overline{q} \to \overline{q} e^{i\alpha\gamma_5}\,. \tag{B.85}$$

The chiral symmetry follows from the anticommuting property

$$\left\{\gamma_5,\, K^N\mid_{m=0}\right\} = 0\,, \tag{B.86}$$

valid in the chiral limit.

The problem is that in the regularized theory anomalies cannot occur, while the physical theory (the one in the continuum) is characterized by chiral anomaly. Indeed, by studying the properties of these extra poles under chiral transformations, in the limit of vanishing quark mass one can find that the 16 fermion species breaks up into two sets of 8 with chiral charge ± 1, and render the theory anomaly-free. This fact is an inevitable consequence of a *no-go theorem* established by Nielsen-Ninomiya [58] which states that it is not possible to define a local, translationally invariant hermitian lattice action that preserves chiral symmetry and does not have doublers. While it would be desirable to preserve chiral symmetry even at finite a, in order to exploit Ward Identities (WI) that provide relations between matrix elements, one cannot solve the fermion doubling problem without breaking chiral symmetry for vanishing fermion masses. This suggests that one may get rid of the doubling problem at the price of breaking chiral symmetry explicitly on the lattice.

A possible way to solve the problem is to implement a lattice version of chiral symmetry which may be preserved on the lattice at finite a, without introducing doublers. This is the so-called Ginsparg-Wilson formulation [59].

Circumventing the Nielsen-Ninomiya theorem, the anomaly originates from the non-invariance of the fermion integration measure under the Ginsparg-Wilson chiral transformation. Ginsparg and Wilson proposed to replace the anti-commuting expression (B.86) with

$$\{\gamma_5, K\mid_{m=0}\} = aK\gamma_5 K\,. \tag{B.87}$$

In this way it is possible to define a modified chiral rotation which leaves the chiral lattice action invariant, this rotation is defined by

$$q \to \exp\left\{i\alpha\gamma_5\left(\mathbb{I} - \frac{a}{2}K\right)\right\} q\,, \quad \overline{q} \to \overline{q}\exp\left\{i\alpha\left(\mathbb{I} - \frac{a}{2}K\right)\gamma_5\right\}\,. \tag{B.88}$$

For $a \to 0$ this transformation reduces to the ordinary chiral one and the axial symmetry is then restored in the continuum limit such that it reproduces the right anomaly. Circumventing the Nielsen-Ninomiya theorem, the anomaly originates from the non-invariance of the fermion integration measure under the Ginsparg-Wilson chiral transformation.

Instead, we follow a different proposal originally made by Wilson [52], who introduced an explicit chiral symmetry breaking term in the action by hand. This term reproduces correctly the axial anomaly in the continuum limit [60].

Wilson action

The lattice action is not unique and one has the freedom to add an arbitrary number of operators to the action, provided that they vanish in the continuum limit $a \to 0$. The Wilson solution to the doublers problem consists in including an additional term proportional to the discretized Laplace operator, the so-called Wilson term:

$$-\frac{ar}{2}\nabla_\mu \nabla^*_\mu \,, \tag{B.89}$$

where r is called the *Wilson Parameter*. According to Eq. (B.75) the discretized Laplace operator is explicitly written as

$$\nabla_\mu \nabla^*_\mu q(n) = \frac{U_\mu(n)q(n+\hat{\mu}) + U_{-\mu}(n)q(n-\hat{\mu}) - 2q(n)}{2a} \,. \tag{B.90}$$

By adding the Wilson term to the naive action we obtain the Wilson action, given by

$$S^W_F[\overline{q}, q, U] = a^4 \sum_n \overline{q}(n) \left(D^W[U] + m \right) q(n) \,, \tag{B.91}$$

where

$$D^W[U] = \frac{1}{2}\gamma_\mu(\nabla_\mu + \nabla^*_\mu) - \frac{ar}{2}\nabla_\mu \nabla^*_\mu \,. \tag{B.92}$$

We can expand all the covariant derivatives finding the following explicit form

$$S^W_F[\overline{q}, q, U] = a^4 \sum_{n,m} \overline{q}(n) K^W_{nm}[U] q(m) \,, \tag{B.93}$$

where the Wilson Dirac matrix $K^W_{nm}[U]$ is defined as

$$\begin{aligned} K^W_{nm}[U] &= \left(m + \frac{4r}{a} \right) \sigma_{nm} \\ &+ \sum_\mu \frac{1}{2a} \left[(\gamma_\mu - r) U_\mu(n) \sigma_{n+\hat{\mu},m} - (\gamma_\mu + r) U_{-\mu}(n) \delta_{n-\hat{\mu},m} \right] . \end{aligned} \tag{B.94}$$

The additional terms, proportional to r, make the Dirac matrix such that in the chiral limit the anti-commuting property with the γ_5 is not satisfied,

$$\left\{ \gamma_5, \, K^W \, |_{m=0} \right\} \neq 0 \,. \tag{B.95}$$

As a consequence, the Wilson fermion action is no more invariant under the axial transformation in Eq. (B.85) and the explicit breaking of chiral symmetry is a hard breaking of $O(a)$. It is easy to prove

[54] that the Wilson action has the following discrete symmetries on the lattice: charge conjugation, parity, Euclidean reflections, time reflection and γ_5–hermiticity, that is $\left(K^W\right)^\dagger = \gamma_5 K^W \gamma_5$.

Now we show how the Wilson action solves the doubling problem. To do so, we compute the Fourier transform of the action (B.93) with all $U_\mu(n) = \mathbb{I}$ and obtain

$$S^{-1}(p) = \tilde{K}^W(p) = m + \frac{i}{a}\sum_\mu \gamma_\mu \sin(ap_\mu) + \frac{r}{a}\sum_\mu (1 - \cos(ap_\mu))\,. \tag{B.96}$$

We can see that only the 15 doublers get an additional mass term $\frac{2rn}{a}$, even in the chiral limit, where n is the number of momentum components with $p_\mu = \pi/a$. Thus, when $a \to 0$ the doublers become very heavy and decouple from the theory. In conclusion, the lattice Wilson QCD action is given by

$$S^W[\overline{q}, q, U] = S_G^W[U] + S_F^W[\overline{q}, q, U]\,, \tag{B.97}$$

with $S_G^W[U]$ and $S_F^W[\overline{q}, q, U]$ given in Eqs. (B.68) and (B.93) respectively. Usually in the simulations, the *hopping parameter representation* of the Wilson lattice action is used. It consists of rescaling the fermionic fields as

$$q \to \sqrt{\kappa} q\,, \quad \overline{q} \to \sqrt{\kappa}\overline{q}\,, \tag{B.98}$$

where κ is called *hopping parameter* and it is defined by

$$\kappa = \frac{1}{2am_0 + 8r}\,. \tag{B.99}$$

In this parametrization, the Dirac operator now reads

$$aK^W_{nm}[U] = \delta_{n,m} + \kappa \sum_\mu [(\gamma_\mu - r)U_\mu(n)\delta_{n+\hat{\mu},m} - (\gamma_\mu + r)U_{-\mu}(n)\delta_{n-\hat{\mu},m}]\,. \tag{B.100}$$

However, despite it solves the doublers' problem, the explicit breaking of chiral symmetry in the Wilson action, at finite lattice spacing, has also unintended serious consequences. All relations based on the axial Ward Identity now have corrections at order $O(ra)$ beyond tree level and involve mixing with wrong chirality operators that usually would be absent. Moreover, the quark mass term goes now under additive renormalization, that is the renormalized quark mass is of the form $m_R = Z_m(m_0 - m_{cr})$, where the *critical mass* is linearly divergent, i.e. $m_{cr} \propto 1/a$. Thus, the quark mass gets both additive and multiplicative renormalization.

Finally, we want to point out that the leading cutoff effects with Wilson fermions start at order $O(a)$, due to the Wilson term, rather than $O(a^2)$. In the following section, we are going to see the *twisted mass* formulation, which can be used to gain an $O(a)$ improvement with respect to ordinary Wilson formulation.

B.3.5 Twisted mass QCD

In this section, we introduce the *twisted mass QCD* (tmQCD) [61, 38]. In this formulation the theory involves a doublet of two light mass-degenerate quark flavors, u and d, and is characterized by an additional mass term with a non-trivial isospin structure, which is called the *twisted mass term* and is given by

$$i\mu_q\gamma_5\tau_3\,, \tag{B.101}$$

where τ_3 is the third Pauli matrix acting in flavor space and μ_q is called the *twisted mass*.

The twisted mass term breaks both parity and flavor symmetry, but can be very useful for two reasons. The first is that it provides a cure for the problem of the so-called *exceptional configurations*, which are certain fluctuations of the gauge fields U that lead to small eigenvalues of the Dirac operator $K[U]$. In these configurations the numerical inversion of the Dirac operator, necessary to compute the propagators, can be very problematic, and the twisted mass term provides an infrared regulator to those small eigenvalues. This was in fact one of the original motivations for introducing a twisted mass description.

In addition, the second useful property of this formulation is that it allows, by tuning only one parameter, to obtain an automatic $O(a)$–improvement of the physical correlation functions, without introducing therefore the several coefficients required for other improvement programs [62, 63].

Continuum twisted mass QCD for degenerate quarks

We first consider the continuum limit of the twisted mass QCD for $N_f = 2$ light degenerate flavors, we denote by χ and $\overline{\chi}$ the quark field flavor doublets, with

$$\chi = \begin{pmatrix} \chi_u \\ \chi_d \end{pmatrix}$$

The set of fermion fields $\{\chi, \overline{\chi}\}$ is called *twisted basis*. In this basis, the tmQCD action is given by

$$S_F^{tm}[\chi,\overline{\chi},A] = \int d^4x\overline{\chi}(x)\left(D + m_q + i\mu_q\gamma_5\tau^3\right)\chi(x)\,. \tag{B.102}$$

With m_q we have indicated the *untwisted mass* of the quark and is obtained in terms of the quark bare mass and the critical mass by the relation $m_q = m - m_{cr}$, i.e. the untwisted mass vanishes when m assume the critical value m_{cr}. The tmQCD action (B.102) is just a rewriting of the standard QCD action in a different basis. We can see that by applying the quark field transformation

$$\chi(x) \to q(x) = e^{i\omega\gamma_5\frac{\tau_3}{2}}\chi(x), \quad \overline{\chi}(x) \to \overline{q}(x) = \overline{\chi}(x)e^{i\omega\gamma_5\frac{\tau_3}{2}}\,, \tag{B.103}$$

which changes the expression of the action only in the mass terms, through

$$m_q' = m_q\cos\omega + \mu_q\sin\omega \quad \mu_q' = -m_q\sin\omega + \mu_q\cos\omega\,. \tag{B.104}$$

Now we can see that the standard QCD action is obtained if $\mu_q' = 0$, and so if the *twisted angle* ω satisfies the relation

$$\tan\omega = \frac{\mu_q}{m_q}\,. \tag{B.105}$$

The *physical basis* $\{q, \overline{q}\}$ is the one in which the continuum QCD action takes the standard form. The two basis are related by the rotation (B.103) with ω satisfying Eq. (B.105).

We point out that the chiral rotation (B.103) leaves invariant the combination

$$M = \sqrt{m_q^2 + \mu_q^2}\,, \tag{B.106}$$

and so it is convenient to use polar mass coordinates

$$\begin{cases} m_q = M\cos\omega \\ \mu_q = M\sin\omega \end{cases}, \tag{B.107}$$

where M is called *polar mass*.

When $\omega = \pi/2$ we have $m_q = 0$ and $\mu_q = M$. This case is referred as *full* or *maximal twist* and we want to show that this choice implies an automatic $O(a)$-improvement, but first we need to check how the twist reflects in expectation values. The standard and the twisted mass QCD are related by a change of variables in the path integral. The transformation (B.103) is non-anomalous and so the integration measure remains invariant, that is we can write $\mathcal{D}[\overline{q}, q] = \mathcal{D}[\overline{\chi}, \chi]$. This means we can state that

$$\langle \mathcal{O}[q, \overline{q}, A]\rangle_{(M,0)} = \langle \mathcal{O}[\chi, \overline{\chi}, A]\rangle_{(m_q,\mu_q)}\,, \tag{B.108}$$

where the l.h.s refers to the ordinary QCD while the r.h.s to the twisted mass QCD.

Thus, standard QCD correlation functions can be expressed as linear combinations of correlators in tmQCD. This equivalence remains valid at finite lattice spacing for Wilson fermions up to discretization errors, if the theory is correctly renormalized in a mass independent scheme [38]. So the expectation values in the twisted mass formulation assume the form

$$\langle \mathcal{O}^{tm}\rangle_{tm} = \frac{1}{Z_{tm}} \int \mathcal{D}[\overline{\chi}, \chi, A] e^{-S_F^{tm}[\overline{\chi},\chi,A] - S_G[A]} \mathcal{O}^{tm}[\overline{\chi}, \chi, A]\,, \tag{B.109}$$

and we have to relate the operators $\mathcal{O}[q, \overline{q}, A]$ in the physical basis with their counterparts $\mathcal{O}[\chi, \overline{\chi}, A]$ in the twisted basis. Moreover, standard QCD and tmQCD actions share all the symmetries since the symmetry transformations in the twisted basis are simply obtained by using Eq. (B.103) on the standard symmetry transformations. For example, we can re-express the Ward Identities in the twisted basis, finding respectively the partially conserved axial current (PCAC) and partially conserved vector current (PCVC) equations:

$$\partial_\mu A_\mu^a \;=\; 2m_q P^a + i\mu_q \delta^{3a} S^0\,, \tag{B.110}$$

$$\partial_\mu V_\mu^a = -2\mu_q \epsilon^{3ab} P^b \,, \tag{B.111}$$

where we have considered the axial and vector currents and the scalar and pseudoscalar densities defined respectively as

$$\begin{aligned} A_\mu^a &= \overline{\chi}\gamma_\mu\gamma_5 \frac{\tau^a}{2}\chi, \quad V_\mu^a = \overline{\chi}\gamma_\mu \frac{\tau^a}{2}\chi \\ P^a &= \overline{\chi}\gamma_5 \frac{\tau^a}{2}\chi, \quad S^0 = \overline{\chi}\chi \,. \end{aligned} \tag{B.112}$$

Continuum twisted mass QCD for non-degenerate quarks

Now we want to generalize the strategy presented above for the study of theories characterized by a doublet of non-degenerate quarks [43]. One possibility, known as *flavor off-diagonal splitting*, is to modify the action in the following way

$$S_F^{tm} = \int d^4x \overline{\chi}(x) \left(\not{D} + m_q + i\mu_q\gamma_5\tau^3 + \epsilon_q\tau^1 \right) \chi \,, \tag{B.113}$$

with $\mu_q, \epsilon_q > 0$. This approach preserves all the good properties of the twisted mass QCD at maximal twist. The physical basis is obtained by performing two transformations: an isovector rotation with $\omega_2 = \pi/2$ followed by an axial rotation, that is

$$\begin{aligned} \chi' &= e^{i\omega_2\tau^2/2}\chi \,|_{\omega_2=\frac{\pi}{2}} = \frac{1}{\sqrt{2}}(1 + i\tau^2)\chi \,, \\ \overline{\chi}' &= \overline{\chi} e^{-i\omega_2\tau^2/2} \,|_{\omega_2=\frac{\pi}{2}} = \overline{\chi}\frac{1}{\sqrt{2}}(1 + i\tau^2) \,, \end{aligned} \tag{B.114}$$

followed by

$$\begin{aligned} q &= e^{-i\omega_1\gamma_5\tau^1/2}\chi' \,, \\ \overline{q} &= \overline{q} e^{-i\omega_1\gamma_5\tau^1/2} \,. \end{aligned} \tag{B.115}$$

If we set ω_1 according to Eq. (B.105) we find the action of the physical basis

$$S_F = \int d^4x \overline{q} \left(\not{D} + M + \epsilon_q\tau^3 \right) q \,. \tag{B.116}$$

A different way to consider non-degenerate quarks is to consider the untwisted and the twisted masses present in the action as diagonal matrices. In this case, we have that the mass terms remain flavor diagonal, but the disadvantage of this method is that one has to take in account a large number of parameters that need to be fixed. In this way we notice that it is sufficient only a rotation to obtain the physical basis, the action so found will present the polar mass as a matrix just like the twisted and the untwisted mass.

Lattice twisted mass QCD

For Wilson quarks, the lattice tmQCD action is given by

$$S_F^{tm}[\overline{\chi}, \chi, U] = a^4 \sum_n \overline{\chi} \left(D^W[U] + m + i\mu_q \gamma_5 \tau^3 \right) \chi(n) \,, \tag{B.117}$$

where $D^W[U]$ is the Dirac operator given in Eq. (B.92), m and μ_q are respectively the bare untwisted and twisted quark masses. As we have already pointed out, the Wilson term in $D^W[U]$ breaks explicitly the axial symmetry. This implies that the twisted mass term cannot be rotated away by a chiral transformation, and the exact equivalence between the Wilson action with vanishing and non-vanishing twisted mass is lost. This means that Wilson and Wilson twisted mass are different lattice regularizations of QCD, the exact equivalence being recovered only in the continuum limit. This lattice feature is of great utility since we have the freedom to choose the Wilson term and the mass term to point in different relative "directions" in the Dirac and flavor space. This freedom is the key to constrain the form of the cutoff effects induced by the Wilson term, as we will discuss now.

Maximal twist

With the introduction of the twisted mass term, we now have two parameters, m_q and μ_q, which define the physics we want to describe. The relative size of the two mass parameters is given by the twist angle ω. For each value of the angle we have a different theory that, however, is equivalent in the continuum limit to the original one.

Among all the possible values of ω, the most interesting one is the case of

$$\omega = \frac{\pi}{2} \,, \tag{B.118}$$

called maximal twist. In this case, we have that $m_q = 0$, thus $m = m_{cr}$, and only the twisted mass term μ_q survives in the continuum action (B.102). The special role of $\omega = \pi/2$ can already be seen in the free case. In fact, the quark propagator in momentum space, given by inverting the Wilson twisted mass Dirac operator, gives rise to a dispersion relation in which $O(a)$ corrections come with a factor of $\cos\omega$ [54]. This allows to turn off the $O(a)$ term by choosing maximal twist, i.e. $\omega = \pi/2$. This happens because at maximal twist the Wilson term and the mass term are orthogonal in isospin space, thus a mixed term, which is of order $O(a)$, cannot emerge [61]. The $O(a)$–improvement can also be established for the full interactive tmQCD. This problem can be solved by performing the Symanzik improvement program.

In order to have maximal twist in the renormalized theory, we need a vanishing renormalized quark mass parameter m_R. Setting $m = m_{cr}$ implies for the renormalized quark mass parameter, $m_R = 0$, as needed for maximal twist. In order to have the bare standard mass parameter m tuned to its critical value, $m = m_{cr}$, we can impose a vanishing PCAC quark mass, where the PCAC quark mass is defined, according to the Ward identities in Eq. (B.110), as

$$m_{PCAC} = \frac{\langle \partial_0 A_0^a(x) P^a(0) \rangle}{2\langle P^a(x) P^a(0) \rangle} \,. \tag{B.119}$$

The automatic $O(a)$-improvement of the physical correlators can be demonstrated in many different ways, just comparing the symmetries of the continuum action and of the lattice action. The detailed proofs can be seen in [61, 43].

Finally, we write the explicit expression for the twisted Wilson Dirac action at maximal twist in the physical basis:

$$S_F^{Wtm}[\overline{q}, q, U] \mid_{\omega=\frac{\pi}{2}} = a^4 \sum_n \overline{q}(n) \left(\gamma\tilde{\nabla} + i\gamma_5\tau^3 r W_{cr} + \mu_q \right) q(n) \,, \tag{B.120}$$

where we have defined

$$\gamma\tilde{\nabla} = \frac{1}{2}\sum_\mu \gamma_\mu(\nabla_\mu + \nabla^*_\mu) \,, \qquad W_{cr} = \frac{a}{2}\sum_\mu \nabla_\mu\nabla^*_\mu - m_{cr} \,. \tag{B.121}$$

The automatic $O(a)$ improvement and the technical advantages in the removal of exceptional configurations make tmQCD a very popular lattice formulation.

Obviously, there are disadvantages related to the breaking of the isospin flavor symmetry, causing for example a splitting between the neutral and charged pion masses caused by cutoff effects. This is a discretization effect of $O(a^2)$ for improved actions, which vanishes in the continuum limit. Moreover, in the spectral analysis of hadronic two–point correlation functions, all excited states with the same lattice quantum numbers may contribute. Even though the states violating continuum symmetries are multiplied by coefficients proportional to a^2, these states have to be taken into account when working at fixed lattice spacing. A very complex case is the neutral pion, since it has the same quantum numbers of the vacuum, and this may require a multistate analysis just to identify and subtract states which are pure lattice artifacts. For a recent study about these problems and how to overcome them, one can see for example [64].

B.4 Renormalization

When one tries to use a quantum field theory to make a physical prediction, one typically find divergent quantities. In order to obtain finite values for these quantities, one has to regularize the theory, and there are many ways to do it. Usually, it is preferable to choose a regularization which preserve as many symmetries as possible of the original action. There are a lot of different regularizations to choose from. Until now, we have studied lattice QCD as a regularization of QCD, defining it in terms of bare quantities.

In the regularized theory, at fixed cut-off, it is possible to compute all quantities of interest using the bare parameters and to obtain finite results, however the results we obtain in this way are unphysically dependent on the cut-off. Indeed, after we have regularized a theory, we have to remove the cut-off, in lattice regularization this consists in performing the continuum limit $a \to 0$. Obviously, this limit must be performed very carefully, because a naive limit would give back the divergences we had before the regularization. The only way to remove the cutoff properly is through the introduction of the Renormalization Constants (RC) that are constructed to absorb the divergences in the continuum limit.

On the lattice, renormalization can be performed using both perturbative and non-perturbative methods. A very used perturbative scheme is the modified Minimal Subtraction, $\overline{\text{MS}}$, scheme, which makes use of dimensional regularization at a given renormalization scale which is usually set to $\mu = 2\,GeV$. It is possible to implement the $\overline{\text{MS}}$ scheme on the lattice, but lattice perturbation theory is more complicated as respect to the continuum, moreover its convergence is typically poor and one prefers the use of non-perturbative schemes.

We will consider the RI-MOM (Regularization Independent at subtracted MOMentum) renormalization scheme, whose renormalization constants can be "converted" to those of the $\overline{\text{MS}}$ through relations like

$$Z_i^{\overline{\text{MS}}}(\mu) = R_i(\mu) Z_i^{RI}(\mu) \tag{B.122}$$

where the calculation of the matching coefficient $R_i(\mu)$ requires continuum perturbation theory only. For scheme independent quantities, this connection is not even required.

B.4.1 RI-MOM scheme

In the RI-MOM scheme one imposes renormalization conditions non-perturbatively, directly on Green functions, computed in the chiral limit in a fixed gauge, with given off-shell external states, with large virtualities [65]. This idea is typically used also in perturbation theory, the renormalization conditions of a certain operator are fixed by imposing that suitable Green functions coincide with their tree level values. The Green functions are computed in the chiral limit, since in this way we have that the RI-MOM scheme is a mass-independent scheme and the operator renormalization constants depend only on the subtraction scale μ and on the coupling constant.

This method works properly if one can fix the virtuality of the external states μ within the conditions

$$\Lambda_{QCD} \ll \mu \ll \frac{1}{a}\,. \tag{B.123}$$

Indeed, in this window we can use continuum perturbation theory to connect different schemes, since μ is much larger than the QCD scale. Due to the fact that the renormalization scale μ is small compared to the inverse of the lattice spacing, we are able to neglect the discretization effects.

Now we are going to study the renormalization of bilinear quark operators

$$\mathcal{O}_\Gamma = \overline{q}_f \Gamma q_{f'}\,, \tag{B.124}$$

where Γ is any combinations of the Dirac matrices. So we start from the bare (unrenormalized) expectation value

$$\mathcal{O}_\Gamma(x, a, g(a)) \equiv \langle \mathcal{O}_\Gamma(x) \rangle_a = \langle \overline{q}_f(x) \Gamma q_{f'}(x) \rangle_a\,. \tag{B.125}$$

Now we introduce the renormalization constant Z_Γ in order to define the renormalized operator

$\mathcal{O}_{R_\Gamma}$ through the relation

$$\mathcal{O}_{R_\Gamma(x,\mu,g(\mu))} = Z_\Gamma(\mu a, g(a)) O_\Gamma(x, a, g(a))\,. \tag{B.126}$$

Z_Γ is defined by the requirement that $\mathcal{O}_{R_\Gamma}$ keeps finite even in the limit $a \to 0$, and the renormalization scale μ is chosen such that it satisfies the condition (B.123).

To found the RC Z_Γ in the RI-MOM scheme, we impose the conditions on the Green function

$$G_\Gamma(x,y) = \langle q_f(x) \mathcal{O}_\Gamma(0) \overline{q}_{f'}(y) \rangle_a\,, \tag{B.127}$$

which is built from the operator $O_\Gamma(0)$ with the insertion of two external quark fields. Now we project the Green function on the off-shell quark states of momentum p through

$$G_\Gamma(ap) = \frac{1}{V} \sum_{x,y} e^{-ip(x-y)} \langle q_f(x) \mathcal{O}_\Gamma(0) \overline{q}_{f'}(y) \rangle_a\,. \tag{B.128}$$

Then we define the amputated Green function $\Lambda_\Gamma(ap)$ as

$$\Lambda_\Gamma(ap) = S_f^{-1}(ap) G_\Gamma(ap) S_{f'}^{-1}(ap)\,, \tag{B.129}$$

where $S_f(ap)$ is the Landau gauge quark propagator in momentum space

$$S_f(ap) = \frac{1}{V} \sum_x e^{-ipx} \langle q_f(x) \overline{q}_f(0) \rangle_a\,. \tag{B.130}$$

Since the amputated Green function Λ_Γ is a matrix in Dirac and color space it is convenient to saturate the indices taking the trace, with a normalization factor 1/12 (4 Dirac indices and 3 color indices), so we define

$$\Gamma_\Gamma(ap) = \frac{1}{12} \mathrm{Tr}[P_\Gamma \Lambda_\Gamma(ap)]\,. \tag{B.131}$$

P_Γ is a suitable projector which respects the property

$$\frac{1}{12} \mathrm{Tr}[P_\Gamma \Gamma] = 1\,, \tag{B.132}$$

that is, the projector is defined by requiring that the projected Green function at tree level is equal to 1. For example for $\Gamma = \{\mathbb{I}, \gamma_5, \gamma_\mu, \gamma_\mu\gamma_5\}$ we have $P_\Gamma = \{\mathbb{I}, \gamma_5, \frac{1}{4}\gamma_\mu, -\frac{1}{4}\gamma_\mu\gamma_5\}$.
Finally, we can express the RI-MOM conditions requiring that the projected amputated Green functions in momentum space computed at a scale $p^2 = \mu^2$ and in the chiral limit, between off-shell quark states, coincide with their tree level value. That is, we impose

$$\Gamma_\Gamma^R(ap, \mu, g(\mu))\,|_{p^2=\mu^2} = \frac{Z_\Gamma(\mu a, g(a))}{Z_q(\mu a, g(a))} \Gamma_\Gamma(ap, a, g(a)) \Big|_{p^2=\mu^2} = 1\,. \tag{B.133}$$

In the previous formula we have introduced the RC of the quark fields $\sqrt{Z_q}$, which in the RI-MOM scheme is defined as

$$Z_q(\mu a, g(a)) = -\frac{i}{12}\mathrm{Tr}\left[\frac{\partial S_f^{-1}(ap)}{\partial \not{p}}\right]\Bigg|_{p^2=\mu^2}. \tag{B.134}$$

Another scheme typically used is the RI'-MOM scheme, whose only difference is the definition of Z_q, instead of Eq. (B.134) we have

$$Z_q(\mu a, g(a)) = -\frac{i}{12}\mathrm{Tr}\left[\frac{\not{p} S_f^{-1}(ap)}{p^2}\right]\Bigg|_{p^2=\mu^2}. \tag{B.135}$$

Usually it is preferred the RI'-MOM scheme, because it does not require any derivative calculation in Z_q.

So the RI'-MOM renormalization conditions are given from the two Eqs. (B.133) and (B.135), then the determination of the RCs of bilinear quark operators requires the computation of two Green functions: the quark propagator $S_q(ap)$ and the amputated $\Lambda_\Gamma(ap)$. We remark that this is a mass-independent scheme, since it is defined in the chiral limit, and that for this reason, in order to compute the RCs, the ensembles generated to compute physical observables can not be used. Instead, there are dedicated lattice simulations which use a sequence of progressively smaller dynamical quark mass values in order to extrapolate to the chiral limit [66, 67].

B.5 Numerical simulations

In section B.2.3, we have seen that, using the integration rules for Grassmann variables, it is always possible to integrate over the fermion fields, and that the expectation value of a physical observable $\mathcal{O}$ is given by a path-integral over the gauge configurations only, according to

$$\langle \mathcal{O} \rangle = \frac{\int \mathcal{D}[U]\mathcal{O}[U]\, e^{-S_{eff}[U]}}{\int \mathcal{D}[U] e^{-S_{eff}[U]}}\,, \tag{B.136}$$

where

$$S_{eff}[A] = S_G[U] + \sum_f \mathrm{Tr}\log K_f[U]\,. \tag{B.137}$$

The number of integration involved in the expectation value however is accessible from the actual computation power only for very small lattice.

The relevant observation that makes lattice QCD simulation workable is that each gauge field configuration is weighted by the factor $e^{-S_{eff}[U]}$. This means that only a small fraction of them gives a significant contribution, being the distribution highly peaked on those that are close to minimize the action. Thus, in order to evaluate expectation values in any simulation only a representative sample of gauge configurations is used, which is generated with a method called *importance sampling*.

Being more specific, the strategy consists in replacing the path-integral by an average made on the representative set of gauge configurations which are generated according to a probability distribution given by the Boltzmann factor $e^{-S_{eff}}$. Practically, we want to generate an importance sample field configurations according to the probability distribution

$$P(U) = \frac{e^{-S_{ee}[U]}}{Z} \,. \tag{B.138}$$

To generate the importance sample, one uses *Markov chain Monte Carlo algorithm* like the *Metropolis* algorithm [54].

Once one has generated an appropriate set of N configurations $\{U_i\}$, we can approximate the expectation value of Eq. (B.136) with the average

$$\langle \mathcal{O} \rangle \sim \hat{\mathcal{O}} = \frac{1}{N} \sum_{i=1}^{N} \mathcal{O}(U_i) \,, \tag{B.139}$$

where the equivalence is true in the limit $N \to \infty$.

We have already pointed out that the computational cost of including sea quarks is very high, and so for a very long time lattice simulations were performed in the quenched approximation. However, the effects of this simplification are not negligible, indeed the estimates of the quenched errors are in the range $10-15\%$. Present day techniques allows dynamical simulations which include in the sea quark the light flavors u, d, taken as mass degenerate, and also the heavier flavors s and c, making use of the *hybrid Monte Carlo* algorithm [68].

B.5.1 Autocorrelation

We have said that in order to generate the importance sample, a Markov chain is used. This means that each configuration U_{i+1} is calculated from the previous one U_i through an appropriate transition probability. Thus, consecutive configurations are correlated, and we have to use configurations which are well spaced out in order to consider them statistically independent.

To study the correlation between the value of an observable computed on two successive configurations, $\mathcal{O}_{i+t} = \mathcal{O}[U_{i+t}]$ and $\mathcal{O}_i = \mathcal{O}[U_i]$, we use the autocorrelation function

$$C_{\mathcal{O}}(\mathcal{O}_i, \mathcal{O}_{i+t}) = \langle \mathcal{O}_i \mathcal{O}_{i+t} \rangle - \langle \mathcal{O}_i \rangle \langle \mathcal{O}_{i+t} \rangle \,. \tag{B.140}$$

For a Markov chain in equilibrium, the autocorrelation function depends only on the computational time separation t[4] and so we can write

$$C_{\mathcal{O}}(t) = C_{\mathcal{O}}(\mathcal{O}_i, \mathcal{O}_{i+t}) \,. \tag{B.141}$$

For large t, the leading contribution to the normalized correlation function $\Gamma_{\mathcal{O}}$ is typically a

[4]In this case t represents the number of steps of Markov chain between one "measurement" of the observable and another.

decreasing exponential

$$\Gamma_{\mathcal{O}}(t) = \frac{C_{\mathcal{O}}(t)}{C_{\mathcal{O}}(0)} \sim e^{-\frac{t}{\tau_{\mathcal{O}}}}\,, \tag{B.142}$$

where we have defined $\tau_{\mathcal{O}}$ the *exponential autocorrelation time* for $\mathcal{O}$. This parameter gives us an information on how much subsequent measurements are correlated. If the computer time between subsequent measurements is t we can expect a systematic error of order $O(\exp(-t/\tau_{\mathcal{O}}))$ due to autocorrelation.

For a set of correlated configurations, it can be shown [54] that the uncertainty associated to the corresponding average $\hat{\mathcal{O}}$ is given by

$$\sigma_{\mathcal{O}} = \sqrt{\frac{1}{N} 2\tau_{int}\hat{\sigma}^2_{\mathcal{O}}}\,, \tag{B.143}$$

where

$$\hat{\sigma}^2_{\mathcal{O}} = \frac{1}{N-1}\sum_{i=1}^{N}(\mathcal{O}_i - \hat{\mathcal{O}})^2\,, \tag{B.144}$$

and τ_{int} is the *integrated correlation time* given by

$$\tau_{int} = \frac{1}{2} + \sum_{t=1}^{N}\Gamma_{\mathcal{O}}(t)\,. \tag{B.145}$$

Usually the autocorrelation time requires a computational cost which is too expensive, and so one relies on others statistical techniques which allows a more accessible analysis. One example is the *data blocking methods*, which consists in dividing the set of data into smaller sub-blocks of size K. Then one computes the averages on the sub-block and considers them as new variables $\mathcal{O}'_i$. Assuming that the original variables were independent, the variance of these blocked $\mathcal{O}'_i$ should decrease as $1/K$. So it is necessary to repeat this procedure for different values of K and when the $1/K$ behavior is observed one may consider these block variables as statistically independent. Once the block variables can be considered independent, it is possible to determine the expectation values of the observable and their errors. However, this usually happens when K is large, and so the number of usable data becomes very small. Moreover, the total number of data is often too small to get a reliable estimate of the variance of the computed expectation values. To deal with these problems, we show now two very practical techniques, known as the *Jacknife* and *Bootstrap* resampling methods. Both assume that the data are not correlated, and so they are usually combined with data blocking methods. The main usefulness of these techniques is that they allow an unbiased estimate of the statistical error for non-trivial estimators.

B.5.2 Resampling Methods

Resampling methods are a set of statistical techniques that involve repeatedly sampling from a given data set in order to estimate population parameters, quantify the uncertainty in a statistic, and perform hypothesis tests. They are particularly useful in situations where the distribution of the population or the underlying statistical assumptions are unknown or difficult to estimate. In this section, we are going to present two of the most commonly used ones, which are the jackknife and the bootstrap resampling techniques. Before going into the details of the two methods, we first explain better which is the practical need for resampling methods when dealing with lattice simulations.

We start by considering a set of N independent and identically distributed random variables $x_1, \ldots, x_N$, for example a sample of N appropriate configurations, which are uncorrelated. Suppose now that we are interested in estimating, from this sample, the exact average

$$\langle x \rangle = \int dx\, x\, P(x)\,,$$

with $P(x)$ being the probability distribution of x from which the sample is drawn, and to estimate the uncertainty on our estimate as well. An *unbiased* estimate of the exact mean is then given by the *sample* mean

$$\overline{x} = \sum_{i=1}^{N} x_i\,, \tag{B.146}$$

while an unbiased estimate of the variance of the sample mean is given by

$$(\delta\overline{x})^2 = \frac{\sigma^2_{samp}}{N-1}\,, \tag{B.147}$$

with $\sigma^2_{samp} = \overline{x^2} - \overline{x}^2$ being the variance of the sample[5]. The meaning of *unbiased estimate* can be understood in the following way: imagine performing many repetitions of our experiment, or simulation; then the average of $\overline{x}$ and $(\delta\overline{x})^2$ over the different samples will tend to the exact mean and to the exact variance of the sample mean. In other words, the bias can be defined as the difference between the exact average of an estimator and the real value of the quantity we want to estimate. In the end, what matters is that unbiased estimates will become more and more accurate as the number of data points is increased, while a biased estimate do not continue to improve with increasing N once the corresponding error is smaller than the bias. Hence, we should work with unbiased estimators.

So far everything works fine, Eqs. (B.146)-(B.147) provide an unbiased estimate of the exact average for x and of the corresponding uncertainty for that estimate, by only employing data from the drawn sample. However, suppose now that we are not interested in computing the average of x itself, but to compute a certain function of that average, that is $f(\langle x \rangle)$. If $f(x)$ is a non-linear function, then $\overline{f(x)}$, that is the average over the sample of the quantity $f(x_i)$, would be a poor estimator for $f(\langle x \rangle)$, since it would actually represent an estimate for $\langle f(x) \rangle$. Using $\overline{f(x)}$ as an estimator for $f(\langle x \rangle)$ would produce a bias equal to

$$\begin{aligned}
\langle \overline{f(x)} \rangle - f(\langle x \rangle) &= \int P(x)\,(f(x) - f(\langle x \rangle))\,dx \\
&= f'(\langle x \rangle) \int P(x)\,(x - x\rangle)\,dx + \frac{1}{2} f''(\langle x \rangle) \int P(x)\,(x - x\rangle)^2\,dx + \ldots
\end{aligned}$$

[5]Usually N is large, and the difference between N and $N-1$ is negligible.

$$
\begin{aligned}
&= \frac{1}{2} f''(\langle x \rangle) \left[\langle x^2 \rangle - \langle x \rangle^2 \right] + \ldots \\
&= \frac{1}{2} f''(\langle x \rangle) \sigma^2 + \ldots \,, \qquad \text{(B.148)}
\end{aligned}
$$

with σ^2 being the variance of the x distributions and with the neglected terms involving higher moments of the $(x - \langle x \rangle)$ distribution together with higher derivatives of $f(\langle x \rangle)$[6]. This difference would persist even if averaging the result over infinite repetitions of the simulation, or if sending N to infinity. A better, *less* biased estimator, is instead $f(\overline{x})$, for which

$$
\begin{aligned}
\langle f(\overline{x}) \rangle - f(\langle x \rangle) &= \int P(x) \left(f(\overline{x}) - f(\langle x \rangle) \right) dx \\
&= \frac{1}{2} f''(\langle x \rangle) \left[\langle \overline{x}^2 \rangle - \langle \overline{x} \rangle^2 \right] + \ldots \\
&= \frac{1}{2N} f''(\langle x \rangle) \sigma^2 + \ldots \,, \qquad \text{(B.149)}
\end{aligned}
$$

where we used that the variance of the sample mean $\sigma^2_{\overline{x}}$ is related to the variance σ^2 of the x distribution as

$$
\sigma^2_{\overline{x}} = \left[\langle \overline{x}^2 \rangle - \langle \overline{x} \rangle^2 \right] = \frac{\sigma^2}{N} \,. \qquad \text{(B.150)}
$$

Eq. (B.149) shows that the bias in using $f(\overline{x})$ as an estimator for $f(\langle x \rangle)$ is of order $1/N$, which for large N is much smaller than the statistical error associated to the estimator, that instead is of order $1/\sqrt{N}$, and so the bias can be safely neglected.

We showed that a satisfactory estimate for $f(\langle x \rangle)$ is given by $f(\overline{x})$. However, the problem now is how to estimate the uncertainty in this estimate. Resampling methods, as the jackknife and the bootstrap, which we now discuss, offer a very simple and practical solution to this issue.

Jackknife

The jackknife resampling method involves systematically omitting one observation at a time from the original sample to create a set of "leave-one-out" samples. Each of these samples is then used to calculate the statistic of interest. The average of these statistics is then used to estimate the bias of the statistic, while the variance is estimated by calculating the sum of the squared differences between each of the "leave-one-out" statistics and the full sample statistic. Let's see how the method works in practice.

We start defining the *jackknife* averages x_i^J as the average over all the x values with the exception of x_i, that is

$$
x_i^J \equiv \frac{1}{N-1} \sum_{j \neq i} x_j \,. \qquad \text{(B.151)}
$$

[6]As expected, if f is a linear function all the derivatives beyond the first one are zero and so only in that case $\langle f(x) \rangle$ constitutes an unbiased estimate of $f(\langle x \rangle)$.

Now we similarly define f_i^J as

$$f_i^J \equiv f(x_i^J)\,. \tag{B.152}$$

We now state that the jackknife estimate of $f(\langle x\rangle)$ is the average of the f_i^J, that is

$$f(\langle x\rangle) \simeq \overline{f^J} \equiv \frac{1}{N}\sum_i^N f_i^J\,, \tag{B.153}$$

and the uncertainty on this estimate is given by

$$\sigma_{f(\overline{x})} = \sqrt{N-1}\sigma_{f^J}\,, \tag{B.154}$$

where

$$\sigma_{f^J}^2 \equiv \overline{(f^J)^2} - \left(\overline{f^J}\right)^2\,. \tag{B.155}$$

It can be shown that $\overline{f^J}$, as an estimator for $f(\langle x\rangle)$, gives rise to a bias which is of order of $1/N$, and so that goes to zero as $N \to \infty$. In particular, we have

$$\langle\overline{f^J}\rangle - f(\langle x\rangle) = \frac{1}{2(N-1)}f''(\langle x\rangle)\sigma^2 + \dots\,, \tag{B.156}$$

with the dots representing terms suppressed by higher powers of N. This is essentially the same bias as for $f(\overline{x})$ and so we can employ this result to eliminate the leading, $O(1/N)$, contribution to the bias and estimate $f(\langle x\rangle)$ as

$$f(\langle x\rangle) \simeq Nf(\overline{x}) - (N-1)\overline{f^J}\,, \tag{B.157}$$

with the resulting bias being of order $1/N^2$. However, since the statistical error is of order $1/\sqrt{N}$, and N is typically large, this $1/N$ correction turns out to be negligible.

The most important advantage of using the jackknife method is that it allows an estimate of the uncertainty for the $f(\langle x\rangle)$ estimator without the need of explicitly performing some complicated error propagation, which could be very tedious when we are considering non-trivial estimators.

Bootstrap

The bootstrap, like the jackknife, is a resampling of the N data points x_i. While before we considered N new data sets, each of them containing all the original data points except for one, bootstrap uses N_{boot} data sets, each containing N points obtained by random (Monte Carlo) sampling of the original set of N points. Notice that each drawing is made from the entire data set, so a simulated data set is likely to miss some points and have duplicates or triplicates of others. In other words, the probability that a data point is picked is $1/N$ irrespective of whether it has been picked before, and for this reason this process is also called picking from a set “with replacement”. Thus, a given data point x_i will, on average, appear once in each Monte Carlo-generated data set, but may appear not at all, or twice, and so on. We shall use the term "bootstrap" data sets to denote the Monte Carlo-generated data sets.

Similarly, as what we did before for the jackknife method, we define x_α^B, for $\alpha = 1, \dots, N_{\text{boot}}$, as the average of the x variable over a given bootstrap data set, that is

$$x_\alpha^B = \frac{1}{N}\sum_{i=1}^{N} n_i^\alpha x_i \,, \tag{B.158}$$

where n_i^α is the number of times that x_i appears in the α-th bootstrap data set.

We now use the x_α^B to define the corresponding f_α^B quantities as

$$f_\alpha^B = f(x_\alpha^B)\,. \tag{B.159}$$

The final bootstrap estimate for $f(\langle x\rangle)$ is then the average of these, namely

$$\overline{f^B} = \frac{1}{N_{\text{boot}}}\sum_{\alpha=1}^{N_{\text{boot}}} f_\alpha^B \,, \tag{B.160}$$

while the corresponding uncertainty can be estimated as

$$\sigma_{f(\overline{x})} = \sqrt{\frac{N}{N-1}}\sigma_{f^B} \,, \tag{B.161}$$

with

$$\sigma_{f^B}^2 = \overline{\left(f^B\right)^2} - \left(\overline{f^B}\right)^2 \,. \tag{B.162}$$

Similarly to what happens for the jackknife method, the bias in the $\overline{f^B}$ estimator is of order $1/N$, which can be improved, eliminating the $O(1/N)$ contribution to the bias, by defining

$$f(\langle x\rangle) \simeq 2f(\overline{x}) - \overline{f^B} \,, \tag{B.163}$$

for which the bias starts at order $1/N^2$. As we said before, this improvement is typically negligible with respect to the $O(1/\sqrt{N})$ statistical error on the estimate.

B.5.3 Systematic errors

Until now, we have seen some methods to deal with statistical errors, but there are other sources of uncertainty given by the several approximations which have been made. Obviously systematic errors arise since we have formulated the theory on the lattice, consequently measured quantities depends not only on the input parameters (quark masses and coupling constants) but also on both the lattice spacing a and the lattice size L.

But these are not the only sources of systematic errors, which now we briefly present.

- QUENCHING: We have already discussed how it is expensive to take in account the full fermionic determinant in the path-integral, so the final uncertainty it will be influenced by the number of dynamical quark flavors N_f implemented in the simulation.

- SETTING PARAMETERS: In order to extract physical values from data simulations (and this operation require several interpolations and extrapolations) the first step is to establish the value of several parameters, like the quark masses, the lattice spacing, and the renormalization constants. All these values have their own uncertainties which affect any physical value which is then extracted.

- DISCRETIZATION: Obviously there are terms of order $O(a)$ (or of higher order in a for improved actions) which disappear only in the continuum limit $a \to 0$. This limit is reached by performing several simulations at different values of a and then by extrapolating $a \to 0$. However, the extrapolation itself implies systematic errors.

- FINITE VOLUME: In the simulations the real infinite system is represented by a finite lattice, with boundary conditions, and this gives rise to finite volume corrections. In the simplest case, these errors are due to the contributions of the so-called *mirror states*, originated by the boundary conditions. It can be shown that these corrections decay exponentially as e^{-ML} where M is the mass of the state. The pion is the lightest physical state which has to be taken in account in lattice QCD simulations, and so to make these contributions small it is necessary to require $M_\pi L \gg 1$.

- LIGHT EXTRAPOLATION: For the real masses of the light quarks u and d the numerical computation of the quark propagator becomes very expensive. Moreover, the condition $M_\pi L \gg 1$ becomes more difficult to satisfy. For these reasons, lattice simulations used to be performed with larger values of $m_{u,d}$ than the physical ones, and then extrapolates the results to the physical limit. As every extrapolation, this procedure implies other systematic errors which have to be estimated. However, thanks to the increasing computational power, nowadays lattice simulations are often performed at physical quark mass values.

- EXCITED STATES: As we will see in the next sections, in order to extrapolate the physical observables of interest from the correlation functions one has to isolate the fundamental state, and neglect other excited states, which however contribute to the correlation functions. Thus, the contribution of the excited states becomes systematic error, we will show that these errors are of order $O(e^{-\Delta E\, t})$, where ΔE is the difference in energy between the fundamental state and the first excited state. In order to make these errors small, it is necessary the requirement of a lattice time extent T big enough to allow values of t for which we have $\Delta E\, t \gg 1$.

B.6 Lattice correlators

In this section, we deal with the extraction of the physical quantities of interest from correlation functions, which are the objects that are actually computed in lattice simulations.

Figure B.3: Quantum numbers of the most commonly used meson interpolators. The classification with respect to C is for the flavor neutral interpolators only.

B.6.1 Two-point correlation function

The simplest quantities involving fermions that one can compute on the lattice are the masses of hadrons e and some simple matrix elements between an hadronic state and the vacuum. This is a very significant test for the correctness of lattice QCD, since the hadronic spectrum is determined from the low energy dynamics of QCD and so it can not be computed within a perturbative approach. The extraction of the hadron masses requires the analysis of two-point Green functions, which we study in this section.

The first thing one has to do is to identify the composite operators $\mathcal{O}$, known as *hadron interpolators*, such that the corresponding Hilbert space operators $\hat{\mathcal{O}}$ and $\hat{\mathcal{O}}^\dagger$ annihilate and create from the vacuum the states we want to analyze. For this reason, $\hat{\mathcal{O}}$ and $\hat{\mathcal{O}}^\dagger$ are called *sink* and *source interpolators*. On the lattice the hadron interpolator is a functional of the lattice fields with the quantum numbers of the state we are interested in. The aim of this thesis concerns only mesons, and so we now focus our attention on meson interpolators.

In the case of a meson with quantum numbers J^{PC} it is usually used a local operator of the form

$$\mathcal{O}_\Gamma(x) = \overline{q}_f(x)\Gamma q_{f'}(x)\,, \tag{B.164}$$

where the index f and f' denote the flavors of the valence quarks and Γ is a generic combination of Dirac matrices, which has to reproduce the other quantum numbers J^{PC}; on the lattice $x = an$. In Fig.B.3 are shown some typical examples.

Meson masses and the matrix elements associated to the transitions between the one particle states of the theory and the vacuum can be extracted from the study of the two-point Green functions

$$G(x) = \langle 0|T\{\hat{\mathcal{O}}_\Gamma(x)\hat{\mathcal{O}}^\dagger_\Gamma(0)\}|0\rangle\,. \tag{B.165}$$

Usually we are interested in states with definite spatial momentum $\boldsymbol{q}$ and thus we perform a Fourier transformation on the spatial position $\boldsymbol{x}$, obtaining

$$C(t,\boldsymbol{q}) = \sum_{\boldsymbol{x}} G(x)e^{-i\boldsymbol{q}\cdot\boldsymbol{x}} = \sum_{\boldsymbol{x}}\langle 0|T\{\hat{\mathcal{O}}_\Gamma(x)\hat{\mathcal{O}}^\dagger_\Gamma(0)\}|0\rangle e^{-i\boldsymbol{q}\cdot\boldsymbol{x}}\,. \tag{B.166}$$

Now it is necessary to insert a complete set of energy eigenstates $|E_m\rangle$ which are covariantly normalized according to

$$\langle E_m|E_n\rangle = L^3 2E_n\delta_{n,m} \tag{B.167}$$

and satisfy the completeness relation

$$\mathbb{I} = |0\rangle\langle 0| + \sum_n \frac{1}{L^3 2E_n} |E_n\rangle\langle E_n| \,. \tag{B.168}$$

Moreover, due to the spatial and temporal translational invariance, we can use the Minkowski space-time translation operator $e^{-i\hat{p}x} = e^{-i(Et-\boldsymbol{p}\cdot\boldsymbol{x})}$ to write

$$\hat{\mathcal{O}}_\Gamma(x) = e^{i\hat{p}x}\hat{\mathcal{O}}_\Gamma(0)e^{-i\hat{p}x} \,. \tag{B.169}$$

Now we assume that $t > 0$ and that the meson interpolator $\mathcal{O}_\Gamma$ does not have the quantum numbers of the vacuum, thus we can ignore the $|0\rangle\langle 0|$ term within the intermediate sum, and we find

$$\begin{aligned} C(t,\boldsymbol{q}) &= \sum_n \sum_{\boldsymbol{x}} \frac{1}{2L^3 E_n} \langle 0|\hat{\mathcal{O}}_\Gamma(0)|E_n\rangle \; \langle E_n|\hat{\mathcal{O}}^\dagger_\Gamma(0)|0\rangle \, e^{-iE_n t} e^{i(\boldsymbol{p}_n-\boldsymbol{q})\cdot\boldsymbol{x}} \\ &= \sum_n \frac{1}{2E_n} \mid \langle 0|\hat{\mathcal{O}}_\Gamma(0)|E_n\rangle \mid^2 e^{-iE_n t}\, \delta_{\boldsymbol{p}_n \boldsymbol{q}} \\ &= \sum_{n:\boldsymbol{p}_n=q} \frac{1}{2E_n} \mid \langle 0|\hat{\mathcal{O}}_\Gamma(0)|E_n\rangle \mid^2 e^{-iE_n t} \,, \end{aligned} \tag{B.170}$$

where now all the states $|E_n\rangle$ in the sum have spatial momentum $\boldsymbol{p}_n = \boldsymbol{q}$.

It is sufficient to project only one of the two interpolators of a correlation function to definite momentum, while the other can remain placed in a single point of the lattice and usually is placed at the origin. Indeed, by writing the real space operator as a sum of its Fourier components and using the fact that states with different momenta are orthogonal between each other, one sees that only the correct momentum term survives[7].

The lattice simulations are performed in Euclidean space-time, and so we have to perform a Wick rotation in order to obtain the Euclidean correlation function, in which the oscillating term is transformed into an exponentially decreasing one. So, by applying the transformation $t \to -it$ we obtain

$$C(t,\boldsymbol{q}) \;=\; \sum_{n:\boldsymbol{p}_n=q} \frac{1}{2E_n(\boldsymbol{q})} \mathcal{Z}_\Gamma e^{-E_n t} \,, \tag{B.171}$$

where we have defined the matrix element as

$$\sqrt{\mathcal{Z}^n_\Gamma} = \langle 0|\hat{\mathcal{O}}_\Gamma(0)|E_n\rangle \,, \tag{B.172}$$

which quantifies the overlap beetween the interpolator $\hat{\mathcal{O}}_\Gamma$ and state $|E_n\rangle$.

In the limit of large t the leading term of $C(t,\boldsymbol{q})$ is the contribution given by the *fundamental state*, that is the lightest state excited from the vacuum by the interpolator $\hat{\mathcal{O}}_\Gamma$, with energy E_0.

[7]Note, however, that this is strictly correct only for the exact expectation values, whereas it is only approximate for a sum over a finite number of configurations.

All the other states, with $E_n > E_0$ are called *excited states*. So, for large t, we have

$$\begin{aligned} C(t,\boldsymbol{q}) &= \frac{\mathcal{Z}_\Gamma}{2E_0} e^{-E_0 t} \left(1 + \sum_{n\neq 0} O(e^{-(E_n - E_0)t}) \right) \\ &\sim \frac{\mathcal{Z}_\Gamma}{2E_0} e^{-E_0 t} \,, \end{aligned} \tag{B.173}$$

where $\sqrt{\mathcal{Z}_\Gamma} = \langle 0|\hat{\mathcal{O}}_\Gamma(0)|E_0\rangle$ and $E_0 = \sqrt{M_0^2 + \boldsymbol{q}^2}$, with M_0 denoting the mass of the lightest stable particle with the same quantum numbers of the interpolator $\hat{\mathcal{O}}$.

To extract the mass of the lightest state, one considers the case $\boldsymbol{q} = 0$ and uses the condition

$$C(t) \xrightarrow[t\gg 0]{} \frac{\mathcal{Z}_\Gamma}{2M_0} e^{-M_0 t} \,, \tag{B.174}$$

to define the *effective mass* as

$$m_{eff}(t) = \log \frac{C(t)}{C(t+1)} \,. \tag{B.175}$$

The effective mass becomes constant only at large t, where it exhibits a plateau $m_{eff} = M_0$.

In real simulations we have to take in account the reflected wave coming from the boundaries of the lattice and traveling in the opposite direction with respect to the signal, due to which the correlation function becomes

$$C(t) \simeq \frac{\mathcal{Z}_\Gamma}{2m_{eff}} \left[e^{-m_{eff} t} + e^{-m_{eff}(T-t)} \right] = \frac{\mathcal{Z}_\Gamma}{2m_{eff}} e^{-m_{eff} \frac{T}{2}} \cosh[m_{eff}(t - T/2)] \,. \tag{B.176}$$

Now we have

$$\frac{C(t)}{C(t+1)} = \frac{\cosh[m_{eff}(t - T/2)]}{\cosh[m_{eff}(t + 1 - T/2)]} \,. \tag{B.177}$$

Though it is more complicated than before, it is possible to plot $m_{eff}(t)$ solving Eq. (B.177) for every t. Then one identifies the plateau, and performs a constant fit on it in order to extract the value M_0.

It is very important to choose carefully an appropriate interval $[t_{min}, t_{max}]$ for the fit. Indeed, the interval must be far enough from 0 and T so that the contributions from the excited states can be safely neglected. Nevertheless, the interval can not become too small since the ratio of signal and noise becomes weaker as time increase and in the region of t around $T/2$ there are strong fluctuations. For these reasons, a poor choice of t_{min} and t_{max} can introduce large systematic errors in the evaluation of the spectrum.

Once the mass M_0 has been estimated it is possible to use the correlation function to extract the matrix element $\mathcal{Z}_\Gamma$, from which the meson decay constants f_P can be obtained, which enclose all the non-perturbative strong dynamics entering the leptonic decays of pseudoscalar mesons (in absence of QED corrections). Indeed, it is sufficient to choose for the pseudoscalar meson P, with valence flavors f and f', the hadron interpolator

$$\mathcal{O} = \overline{q}_f \gamma_0 \gamma_5 q_{f'}\,, \tag{B.178}$$

so we have

$$\mathcal{Z} = \langle 0|\overline{q}_f \gamma_0 \gamma_5 q_{f'}|P(\boldsymbol{q}=0)\rangle = iM_P f_P\,. \tag{B.179}$$

We conclude this section about two-point correlation functions, remarking that in order to compute $C(t)$ for mesons which are not flavor singlet, it is necessary to calculate on the lattice only the quark propagators starting from the origin at fixed gauge configuration. Indeed, Eq. (B.164) can be rewritten on the lattice as

$$\begin{aligned} C(x) &= \frac{1}{Z}\int \prod_l dU_l \prod_{f,n} dq_f d\overline{q_f}\,\mathcal{O}_\Gamma(x)\mathcal{O}_\Gamma^\dagger(0)e^{-S_G+S_F} \\ &= \frac{1}{Z}\int \prod_l dU_l \Big\{ -\mathrm{Tr}[S_{f'}(x,0)\Gamma S_f(0,x)\Gamma] + \\ &\quad +\delta_{f,f'}\mathrm{Tr}[S_f(x,x)\Gamma]\mathrm{Tr}[S_f(0,0)\Gamma]\Big\}\, e^{-S_{eff}[U]}\,. \end{aligned} \tag{B.180}$$

For $f \neq f'$ only the first trace contributes, and we can employ the useful property

$$S = \gamma_5 S^\dagger \gamma_5 \tag{B.181}$$

to express the correlator only in terms of propagators which start from the origin.

B.6.2 Three-point correlation function

The correlators we study in this thesis, for the extraction of the form factors, belongs to the class of the three-point correlation functions, so now we are going to show some of their characteristics. Generally, three-point Green functions can be used to obtain the matrix element of an operator $\mathcal{O}$ between two hadronic states A and B.

Let $\mathcal{O}_A$ and $\mathcal{O}_B$ be the hadronic interpolators for the states A and B, respectively. Then we consider the following three-point correlator, in spatial momentum space:

$$C(t_x, t_y) = \sum_{\boldsymbol{x},\boldsymbol{y}} \langle 0|T\left[\mathcal{O}_A(y)\mathcal{O}(x)\mathcal{O}_B\right]|0\rangle\, e^{-i\boldsymbol{p}\cdot\boldsymbol{x}-i\boldsymbol{q}\cdot\boldsymbol{y}}\,. \tag{B.182}$$

Now we assume $t_y > t_x > 0$ and insert two sums on a complete basis of energy eigenstates, obtaining

$$C(t_x, t_y) = \sum_{i,j} \langle 0|\mathcal{O}_A|A_i\rangle\, \langle A_i|\mathcal{O}(0)|B_i\rangle\, \langle B_i|\mathcal{O}_B|0\rangle\, \frac{e^{-E_{A_i}(t_y-t_x)-E_{B_j}t_x}}{4E_{A_i}E_{B_i}}\,. \tag{B.183}$$

with

$$E_{A_i} = \sqrt{M_{A_i}^2 + \boldsymbol{q}^2}\,, \qquad E_{B_j} = \sqrt{M_{B_j}^2 + |\boldsymbol{q}+\boldsymbol{p}|^2}\,, \tag{B.184}$$

where M_{A_i} and M_{B_j} are the masses of the states $|A_i\rangle$ and $|B_j\rangle$[8]. As before every term in the sum is exponentially suppressed as time increases, if we denote with $|A\rangle$ and $|B\rangle$ the lightest hadronic states with the appropriate quantum numbers, we can write

$$C(t_x, t_y) \xrightarrow[t \gg 0]{} \frac{\sqrt{\mathcal{Z}_A \mathcal{Z}_B}}{4 E_A E_B} \langle A|\mathcal{O}|B\rangle\, e^{-E_A(t_y - t_x) - E_B t_x}\,. \tag{B.185}$$

Once the two points functions have been studied, and the parameters $\mathcal{Z}_A$, $\mathcal{Z}_B$, E_A and E_B have been obtained, the previous expression can be used to obtain the desired matrix element $\langle A|\mathcal{O}|B\rangle$.

To compute on the lattice the three-point Green functions it is not sufficient the calculation of the propagators which start from the origin, as we now show. As a realistic example let's assume that A is a pseudoscalar meson, and $\mathcal{O}$ is a flavor changing operator which transforms $|B\rangle$ in $|A\rangle$, thus

$$\mathcal{O}_A = \bar{q}_1 \gamma_5 q_2\,, \quad \mathcal{O} = \bar{q}_2 \Gamma q_3\,, \quad \mathcal{O}_B = \bar{q}_3 \Gamma_B q_1\,. \tag{B.186}$$

By using these operators, instead of Eq. (B.180) we have

$$C(t_x, t_y) = -\frac{1}{Z}\int \prod_l d[U_l] e^{-S_G[U]} \sum_{\boldsymbol{x},\boldsymbol{y}} e^{-i(\boldsymbol{q}\cdot\boldsymbol{x} + \boldsymbol{p}\cdot\boldsymbol{y})} \mathrm{Tr}[S_{q_1}(0,y)\gamma_5 S_{q_2}(y,x)\Gamma S_{q_3}(x,0)\Gamma_B]\,. \tag{B.187}$$

Usually one rewrites the previous expression in terms of the *generalized propagator*, which is defined as

$$S^{gen}_{q_1,q_2}(x, 0, t_y, \boldsymbol{p}) = \sum_{\boldsymbol{y}} S_{q_1}(x,y)\gamma_5 S_{q_2}(y,0) e^{-i\boldsymbol{p}\cdot\boldsymbol{y}}\,. \tag{B.188}$$

Just like the ordinary propagator, the generalized propagator is a matrix in Dirac and color space. Using Eq. (B.188) we write

$$C(t_x, t_y) = -\frac{1}{Z}\int \prod_l d[U_l] e^{-S_G[U]} \sum_{\boldsymbol{x}} e^{-i\boldsymbol{q}\cdot\boldsymbol{x}} \mathrm{Tr}[S^{gen}_{q_1,q_2}(0,x)\Gamma S_{q_3}(x,0)\Gamma_B]\,. \tag{B.189}$$

The generalized propagator satisfies the equation

$$S_{gen}(0,x) = \gamma_5 S^{\dagger}_{gen}(x,0)\gamma_5\,, \tag{B.190}$$

which is analogous to Eq. (B.181) for the ordinary propagator. Due to this property, it is possible to compute the three-point correlators with the calculation of only the ordinary and generalized

[8]They are not necessarily single particle states, M is the invariant mass of a generic state.

propagators which start from the origin.

Appendix C

Decay rates formulae for $\ell \neq \ell'$

In this appendix we collect the expressions of the several functions entering the differential decay rate we computed in section 3.1, with different charged leptons in the final state, i.e. for $\ell \neq \ell'$.

We start by defining the following quantity:

$$\Delta_{\log}(x_k, x_q) = \log\big(\, 1 + 2A(x_k, x_q)\,\big)\,, \tag{C.1}$$

with

$$A(x_k, x_q) =$$
$$\frac{x_q^2\sqrt{x_k^4 - 2x_k^2(x_q^2+1) + (x_q^2-1)^2} - r_\ell\sqrt{-2(x_k^2+1)x_q^2 + (x_k^2-1)^2 + x_q^4}}{-x_q^2\sqrt{x_k^4 - 2x_k^2(x_q^2+1) + (x_q^2-1)^2} + r_\ell\sqrt{-2(x_k^2+1)x_q^2 + (x_k^2-1)^2 + x_q^4} + r_\ell(x_k^2-1) + x_q^2(-x_k^2 + x_q^2 + r_\ell - 1)}\,, \tag{C.2}$$

where x_k and x_q are defined in Eq. (2.1) and r_ℓ is defined in Eq. (3.7).

The point-like contribution to the decay rate of Eq. (3.11) is given by

$$\begin{aligned}\Gamma''_{\rm pt}(x_k, x_q) \;&=\; \frac{f_K^2\, r_\ell\, x_q}{24\pi^3\, m_K^3\, x_k}\sqrt{1 - \frac{4r_{\ell'}}{x_k^2}}\,\left(\frac{2r_{\ell'}}{x_k^2} + 1\right) \times \\ &\left(\frac{2}{x_q^2-1}\Big(-x_k^2x_q^2 + x_k^2 + x_q^4 - 2x_q^2 r_\ell - 2(r_\ell-1)r_\ell + 1\Big)\,\Delta_{\log}(x_k,x_q) + \sqrt{(x_k^2 - x_q^2+1)^2 - 4x_k^2}\,(x_q^2 - r_\ell)\right. \\ &\left.\times\Big(\frac{x_k^2\,x_q^2 - x_k^2\,r_\ell - 2x_q^4 + 4x_q^2\,r_\ell - 2}{(x_q^2-1)^2\,x_q^2} + \frac{2\,(r_\ell-1)\,(x_k^2+2r_\ell)}{(x_q^2-1)^2\,r_\ell - x_k^2\,(r_\ell-1)\,(x_q^2-r_\ell)}\Big)\right), \end{aligned} \tag{C.3}$$

where $r_{\ell'}$ is also defined in Eq. (3.7).

The interference contribution to the decay rate of Eq. (3.11) can be expressed in the form

$$\begin{aligned}\Gamma''_{\rm int}(x_k,x_q) &= \Big[g_V(x_k,x_q)\,F_V(x_k,x_q)+g_A(x_k,x_q)\,F_A(x_k,x_q)\\ &\quad + g_1(x_k,x_q)\,H_1(x_k,x_q)+g_2(x_k,x_q)\,H_2(x_k,x_q)\Big]\,, \end{aligned}\tag{C.4}$$

where the kernels are

$$\begin{aligned}
g_V(x_k,x_q) &= \frac{f_K r_\ell\, x_q}{12\pi^3 m_K x_k}\sqrt{1-\frac{4r_{\ell'}}{x_k^2}}\left(\frac{2r_{\ell'}}{x_k^2}+1\right)\Bigg\{\Big(x_k^2(x_q^2-2r_\ell+1)-(x_q^2-1)^2\Big)\Delta_{\log}(x_k,x_q)\\
&\quad+\frac{(x_k^2+x_q^2-1)(x_q^2-r_\ell)\sqrt{(x_k^2-x_q^2+1)^2-4x_k^2}}{x_q^2}\Bigg\}\,,\\
g_A(x_k,x_q) &= \frac{f_K r_\ell\, x_q}{12\pi^3 m_K x_k (x_q^2-1)}\sqrt{1-\frac{4r_{\ell'}}{x_k^2}}\left(\frac{2r_{\ell'}}{x_k^2}+1\right)\Bigg\{(x_q^2-1)^2(-x_k^2-x_q^2-2r_\ell+1)\Delta_{\log}(x_k,x_q)\\
&\quad+\frac{(x_q^2-1)(x_q^2-r_\ell)(x_k^2+2x_q^2+r_\ell-1)\sqrt{-2(x_k^2+1)x_q^2+(x_k^2-1)^2+x_q^4}}{x_q^2}\Bigg\}\,,\\
g_1(x_k,x_q) &= \frac{f_K r_\ell\, x_k\, x_q}{24\pi^3 m_K}\sqrt{1-\frac{4r_{\ell'}}{x_k^2}}\left(\frac{2r_{\ell'}}{x_k^2}+1\right)\Bigg\{4(x_q^2+r_\ell-2)\Delta_{\log}(x_k,x_q)\\
&\quad-\frac{(x_q^2-r_\ell)\Big(r_\ell(-x_k^2+3x_q^2+1)+x_q^2(x_k^2+5x_q^2-9)\Big)\sqrt{-2(x_k^2+1)x_q^2+(x_k^2-1)^2+x_q^4}}{(x_q^2-1)\,x_q^4}\Bigg\}\,,\\
g_2(x_k,x_q) &= \frac{f_K r_\ell\, x_k\, x_q}{24\pi^3 m_K (x_q^2-1)^2}\sqrt{1-\frac{4r_{\ell'}}{x_k^2}}\left(\frac{2r_{\ell'}}{x_k^2}+1\right)\Bigg\{2(x_q^2-1)(x_q^2-r_\ell^2)\Delta_{\log}(x_k,x_q)\\
&\quad-\frac{(x_q^2-r_\ell)\Big(r_\ell(x_k^2-3x_q^2-1)+x_q^2(-x_k^2+x_q^2+3)\Big)\sqrt{(x_k^2-x_q^2+1)^2-4x_k^2}}{x_q^2}\Bigg\}\,.
\end{aligned}\tag{C.5}$$

Finally, the SD contribution to the decay rate of Eq. (3.11) can be expressed in the form

$$\begin{aligned}\Gamma''_{\rm SD}(x_k,x_q) &= g_{VV}(x_k,x_q)F_V^2(x_k,x_q)+g_{AA}(x_k,x_q)F_A^2(x_k,x_q)+g_{11}(x_k,x_q)H_1^2(x_k,x_q)\\ &\quad+g_{22}(x_k,x_q)H_2^2(x_k,x_q)+g_{A1}(x_k,x_q)F_A(x_k,x_q)H_1(x_k,x_q)\\ &\quad+g_{12}(x_k,x_q)H_1(x_k,x_q)H_2(x_k,x_q)\,,\end{aligned}\tag{C.6}$$

where

$$g_{VV}(x_k,x_q) = \frac{1}{24\pi^3 x_k\, x_q}\sqrt{1-\frac{4r_{\ell'}}{x_k^2}}\left(\frac{2r_{\ell'}}{x_k^2}+1\right)\Big((x_k^2-x_q^2+1)^2-4x_k^2\Big)^{3/2}(x_q^2-r_\ell)^2\,,$$

$$
\begin{aligned}
g_{AA}(x_k, x_q) &= \frac{1}{144\pi^3 x_k\, x_q^3}\sqrt{1-\frac{4r_{\ell'}}{x_k^2}}\left(\frac{2r_{\ell'}}{x_k^2}+1\right)\left(x_k^4+x_k^2(4x_q^2-2)+(x_q^2-1)^2\right)(x_q^2-r_\ell)^2(2x_q^2+r_\ell) \\
&\qquad \times\sqrt{(x_k^2-x_q^2+1)^2-4x_k^2}\;, \\
g_{11}(x_k, x_q) &= \frac{x_k}{144\pi^3 x_q^5}\sqrt{1-\frac{4r_{\ell'}}{x_k^2}}\left(\frac{2r_{\ell'}}{x_k^2}+1\right)(x_q^2-r_\ell)^2\sqrt{(x_k^2-x_q^2+1)^2-4x_k^2} \\
&\quad \times\left(2x_q^4(5x_k^2+r_\ell-1)+x_q^2\left(2(x_k^2-2)r_\ell+(x_k^2-1)^2\right)+2(x_k^2-1)^2 r_\ell+x_q^6\right)\;, \\
g_{22}(x_k, x_q) &= \frac{r_\ell\, x_k}{96\pi^3 (x_q^2-1)^2 x_q}\sqrt{1-\frac{4r_{\ell'}}{x_k^2}}\left(\frac{2r_{\ell'}}{x_k^2}+1\right)\left((x_k^2-x_q^2+1)^2-4x_k^2\right)^{3/2}(x_q^2-r_\ell)^2\,, \\
g_{A1}(x_k, x_q) &= -\frac{x_k}{24\pi^3 x_q^3}\sqrt{1-\frac{4r_{\ell'}}{x_k^2}}\left(\frac{2r_{\ell'}}{x_k^2}+1\right)(x_k^2+x_q^2-1)(x_q^2-r_\ell)^2(2x_q^2+r_\ell)\sqrt{(x_k^2-x_q^2+1)^2-4x_k^2}\,, \\
g_{12}(x_k, x_q) &= -\frac{r_\ell\, x_k}{48\pi^3 (x_q^2-1)\, x_q^3}\sqrt{1-\frac{4r_{\ell'}}{x_k^2}}\left(\frac{2r_{\ell'}}{x_k^2}+1\right)\left((x_k^2-x_q^2+1)^2-4x_k^2\right)^{3/2}(x_q^2-r_\ell)^2\,. \qquad \text{(C.7)}
\end{aligned}
$$

Bibliography

[1] G. Gagliardi, F. Sanfilippo, S. Simula, V. Lubicz, F. Mazzetti, G. Martinelli, C. T. Sachrajda, and N. Tantalo. "Virtual photon emission in leptonic decays of charged pseudoscalar mesons". In: *Phys. Rev. D* 105 (2022), p. 114507. DOI: `10.1103/PhysRevD.105.114507`. arXiv: `2202.03833 [hep-lat]`.

[2] N. Carrasco et al. "Up, down, strange and charm quark masses with $N_f = 2+1+1$ twisted mass lattice QCD". In: *Nucl. Phys. B* 887 (2014), pp. 19–68. DOI: `10.1016/j.nuclphysb.2014.07.025`. arXiv: `1403.4504 [hep-lat]`.

[3] V. Lubicz, G. Martinelli, C. T. Sachrajda, F. Sanfilippo, S. Simula, and N. Tantalo. "Finite-Volume QED Corrections to Decay Amplitudes in Lattice QCD". In: *Phys. Rev. D* 95 (2017), p. 034504. DOI: `10.1103/PhysRevD.95.034504`. arXiv: `1611.08497 [hep-lat]`.

[4] D. Giusti, V. Lubicz, C. Tarantino, G. Martinelli, C. T. Sachrajda, F. Sanfilippo, S. Simula, and N. Tantalo. "First Lattice Calculation of the QED Corrections to Leptonic Decay Rates". In: *Phys. Rev. Lett.* 120 (2018), p. 072001. DOI: `10.1103/PhysRevLett.120.072001`. URL: `https://link.aps.org/doi/10.1103/PhysRevLett.120.072001`.

[5] M. Di Carlo, G. Martinelli, D. Giusti, V. Lubicz, C. T. Sachrajda, F. Sanfilippo, S. Simula, and N. Tantalo. "Light-meson leptonic decay rates in lattice QCD + QED". In: *Phys. Rev. D* 100 (2019), p. 034514. DOI: `10.1103/PhysRevD.100.034514`. URL: `https://link.aps.org/doi/10.1103/PhysRevD.100.034514`.

[6] A. Desiderio et al. "First lattice calculation of radiative leptonic decay rates of pseudoscalar mesons". In: *Phys. Rev. D* 103 (2021), p. 014502. DOI: `10.1103/PhysRevD.103.014502`. arXiv: `2006.05358 [hep-lat]`.

[7] R. Frezzotti, M. Garofalo, V. Lubicz, G. Martinelli, C. T. Sachrajda, F. Sanfilippo, S. Simula, and N. Tantalo. "Comparison of lattice QCD+QED predictions for radiative leptonic decays of light mesons with experimental data". In: *Phys. Rev. D* 103 (2021), p. 053005. DOI: `10.1103/PhysRevD.103.053005`. URL: `https://link.aps.org/doi/10.1103/PhysRevD.103.053005`.

[8] R. L. Workman et al. “Review of Particle Physics”. In: *PTEP* 2022 (2022), p. 083C01. DOI: 10.1093/ptep/ptac097.

[9] A. A. Poblaguev et al. “Experimental study of the radiative decays $K^+ \to \mu^+\nu_\mu e^+e^-$ and $K^+ \to e^+\nu_e e^+e^-$”. In: *Phys. Rev. Lett.* 89 (2002), p. 061803. DOI: 10.1103/PhysRevLett.89.061803. arXiv: hep-ex/0204006.

[10] H. Ma et al. “First observation of the decay $K^+ \to e^+\nu_e\mu^+\mu^-$”. In: *Phys. Rev. D* 73 (2006), p. 037101. DOI: 10.1103/PhysRevD.73.037101. URL: https://link.aps.org/doi/10.1103/PhysRevD.73.037101.

[11] R. Aaij et al. “Search for the rare decay $B^+ \to \mu^+\mu^-\mu^+\nu_\mu$”. In: *The European Physical Journal C* 79 (2019), p. 675. DOI: 10.1140/epjc/s10052-019-7112-x. URL: https://doi.org/10.1140/epjc/s10052-019-7112-x.

[12] R. Aaij et al. “Test of lepton universality in beauty-quark decays”. In: *Nature Physics* 18 (2022), pp. 277–282. DOI: 10.1038/s41567-021-01478-8. URL: https://doi.org/10.1038/s41567-021-01478-8.

[13] Andreas Crivellin and Martin Hoferichter. “Hints of lepton flavor universality violations”. In: *Science* 374.6571 (2021), pp. 1051–1052. DOI: 10.1126/science.abk2450. eprint: https://www.science.org/doi/pdf/10.1126/science.abk2450. URL: https://www.science.org/doi/abs/10.1126/science.abk2450.

[14] Brian Batell, David McKeen, and Maxim Pospelov. “New Parity-Violating Muonic Forces and the Proton Charge Radius”. In: *Phys. Rev. Lett.* 107 (2011), p. 011803. DOI: 10.1103/PhysRevLett.107.011803. URL: https://link.aps.org/doi/10.1103/PhysRevLett.107.011803.

[15] Vernon Barger, Cheng-Wei Chiang, Wai-Yee Keung, and Danny Marfatia. “Constraint on Parity-Violating Muonic Forces”. In: *Phys. Rev. Lett.* 108 (2012), p. 081802. DOI: 10.1103/PhysRevLett.108.081802. URL: https://link.aps.org/doi/10.1103/PhysRevLett.108.081802.

[16] Steven Weinberg. “A New Light Boson?” In: *Phys. Rev. Lett.* 40 (1978), pp. 223–226. DOI: 10.1103/PhysRevLett.40.223. URL: https://link.aps.org/doi/10.1103/PhysRevLett.40.223.

[17] F. Wilczek. “Problem of Strong P and T Invariance in the Presence of Instantons”. In: *Phys. Rev. Lett.* 40 (1978), pp. 279–282. DOI: 10.1103/PhysRevLett.40.279. URL: https://link.aps.org/doi/10.1103/PhysRevLett.40.279.

[18] R. D. Peccei and Helen R. Quinn. “Constraints imposed by CP conservation in the presence of pseudoparticles”. In: *Phys. Rev. D* 16 (1977), pp. 1791–1797. DOI: 10.1103/PhysRevD.16.1791. URL: https://link.aps.org/doi/10.1103/PhysRevD.16.1791.

[19] John Preskill, Mark B. Wise, and Frank Wilczek. “Cosmology of the invisible axion”. In: *Physics Letters B* 120 (1983), pp. 127–132. ISSN: 0370-2693. DOI: https://doi.org/10.1016/0370-2693(83)90637-8. URL: https://www.sciencedirect.com/science/article/pii/0370269383906378.

[20] Johannes Albrecht, Emmanuel Stamou, Robert Ziegler, and Roman Zwicky. “Flavoured axions in the tail of $B_q \to \mu^+\mu^-$ and $B \to \gamma^*$ form factors”. In: *Journal of High Energy Physics* 2021.9 (2021), p. 139. DOI: 10.1007/JHEP09(2021)139. URL: https://doi.org/10.1007/JHEP09(2021)139.

[21] Francesco Dettori, Diego Guadagnoli, and Méril Reboud. “$B_s^0 \to \mu^+\mu^-\gamma$ from $B_s^0 \to \mu^+\mu^-$”. In: *Physics Letters B* 768 (2017), pp. 163–167. ISSN: 0370-2693. DOI: https://doi.org/10.1016/j.physletb.2017.02.048. URL: https://www.sciencedirect.com/science/article/pii/S0370269317301612.

[22] Xin-Yu Tuo, Xu Feng, Lu-Chang Jin, and Teng Wang. “Lattice QCD calculation of $K \to \ell\nu_\ell\ell'^+\ell'^-$ decay width”. In: *Phys. Rev. D* 105 (2022), p. 054518. DOI: 10.1103/PhysRevD.105.054518. arXiv: 2103.11331 [hep-lat].

[23] J. Bijnens, G. Ecker, and J. Gasser. “Radiative semileptonic kaon decays”. In: *Nuclear Physics B* 396.1 (1993), pp. 81–118. ISSN: 0550-3213. DOI: https://doi.org/10.1016/0550-3213(93)90259-R. URL: https://www.sciencedirect.com/science/article/pii/055032139390259R.

[24] Mikhail A. Ivanov and Dmitri Melikhov. “Theoretical analysis of the leptonic decays $B \to \ell\ell\ell'\bar{\nu}_{\ell'}$”. In: *Phys. Rev. D* 105 (2022), p. 014028. DOI: 10.1103/PhysRevD.105.014028. URL: https://link.aps.org/doi/10.1103/PhysRevD.105.014028.

[25] Mikhail A. Ivanov and Dmitri Melikhov. “Theoretical analysis of the leptonic decays $B \to \ell\ell\ell\bar{\nu}_\ell$: Identical leptons in the final state”. In: *Phys. Rev. D* 105 (2022), p. 094038. DOI: 10.1103/PhysRevD.105.094038. URL: https://link.aps.org/doi/10.1103/PhysRevD.105.094038.

[26] Chao Wang, Yu-Ming Wang, and Yan-Bing Wei. “QCD factorization for the four-body leptonic B-meson decays”. In: *JHEP* 02 (2022), p. 141. DOI: 10.1007/JHEP02(2022)141. arXiv: 2111.11811 [hep-ph].

[27] Martin Beneke, Philipp Böer, Panagiotis Rigatos, and Kimberley Keri Vos. "QCD factorization of the four-lepton decay $B^- \to \ell\bar{\nu}_\ell \ell^{(\prime)} \bar{\ell}^{(\prime)}$". In: *Eur. Phys. J. C* 81 (2021), p. 638. DOI: 10.1140/epjc/s10052-021-09388-y. arXiv: 2102.10060 [hep-ph].

[28] Aoife Bharucha, Bharti Kindra, and Namit Mahajan. "Probing the structure of the B meson with $B \to \ell\ell\ell'\nu$". In: (2021). arXiv: 2102.03193 [hep-ph].

[29] A. V. Danilina and N. V. Nikitin. "Four-Leptonic Decays of Charged and Neutral B Mesons within the Standard Model". In: *Phys. Atom. Nucl.* 81 (2018), pp. 347–359. DOI: 10.1134/S1063778818030092.

[30] A. Danilina, N. Nikitin, and K. Toms. "Decays of charged B mesons into three charged leptons and a neutrino". In: *Phys. Rev. D* 101 (2020), p. 096007. DOI: 10.1103/PhysRevD.101.096007. URL: https://link.aps.org/doi/10.1103/PhysRevD.101.096007.

[31] L. Maiani and M. Testa. "Final state interactions from euclidean correlation functions". In: *Physics Letters B* 245 (1990), pp. 585–590. ISSN: 0370-2693. DOI: https://doi.org/10.1016/0370-2693(90)90695-3. URL: https://www.sciencedirect.com/science/article/pii/0370269390906953.

[32] Laurent Lellouch and Martin Luscher. "Weak transition matrix elements from finite volume correlation functions". In: *Commun. Math. Phys.* 219 (2001), pp. 31–44. DOI: 10.1007/s002200100410. arXiv: hep-lat/0003023.

[33] C.H. Kim, C.T. Sachrajda, and Stephen R. Sharpe. "Finite-volume effects for two-hadron states in moving frames". In: *Nuclear Physics B* 727 (2005), pp. 218–243. ISSN: 0550-3213. DOI: https://doi.org/10.1016/j.nuclphysb.2005.08.029. URL: https://www.sciencedirect.com/science/article/pii/S0550321305007133.

[34] Raúl A. Briceño, Zohreh Davoudi, Maxwell T. Hansen, Matthias R. Schindler, and Alessandro Baroni. "Long-range electroweak amplitudes of single hadrons from Euclidean finite-volume correlation functions". In: *Phys. Rev. D* 101 (2020), p. 014509. DOI: 10.1103/PhysRevD.101.014509. URL: https://link.aps.org/doi/10.1103/PhysRevD.101.014509.

[35] G.M. de Divitiis, R. Petronzio, and N. Tantalo. "On the discretization of physical momenta in lattice QCD". In: *Physics Letters B* 595 (2004), pp. 408–413. ISSN: 0370-2693. DOI: https://doi.org/10.1016/j.physletb.2004.06.035. URL: https://www.sciencedirect.com/science/article/pii/S0370269304008937.

[36] S. M. Berman. "Radiative Corrections to Muon and Neutron Decay". In: *Phys. Rev.* 112 (1958), pp. 267–270. DOI: 10.1103/PhysRev.112.267. URL: https://link.aps.org/doi/10.1103/PhysRev.112.267.

[37] N. Carrasco, V. Lubicz, G. Martinelli, C. T. Sachrajda, N. Tantalo, C. Tarantino, and M. Testa. "QED Corrections to Hadronic Processes in Lattice QCD". In: *Phys. Rev. D* 91 (2015), p. 074506. DOI: `10.1103/PhysRevD.91.074506`. arXiv: `1502.00257 [hep-lat]`.

[38] Roberto Frezzotti, Pietro Antonio Grassi, Stefan Sint, and Peter Weisz. "Lattice QCD with a chirally twisted mass term". In: *JHEP* 08 (2001), p. 058. DOI: `10.1088/1126-6708/2001/08/058`. arXiv: `hep-lat/0101001`.

[39] Roberto Frezzotti and Gian Carlo Rossi. "Chirally improving Wilson fermions 1. O(a) improvement". In: *Journal of High Energy Physics* 2004.08 (2004), p. 007. DOI: `10.1088/1126-6708/2004/08/007`. URL: `https://dx.doi.org/10.1088/1126-6708/2004/08/007`.

[40] G. M. de Divitiis, R. Frezzotti, V. Lubicz, G. Martinelli, R. Petronzio, G. C. Rossi, F. Sanfilippo, S. Simula, and N. Tantalo. "Leading isospin breaking effects on the lattice". In: *Phys. Rev. D* 87 (2013), p. 114505. DOI: `10.1103/PhysRevD.87.114505`. URL: `https://link.aps.org/doi/10.1103/PhysRevD.87.114505`.

[41] Jonathan M. Flynn, Andreas Jüttner, ChristopherT. Sachrajda, Peter A. Boyle, James M. Zanotti, and UKQCD collaboration. "Hadronic form factors in lattice QCD at small and vanishing momentum transfer". In: *Journal of High Energy Physics* 2007 (2007), p. 016. DOI: `10.1088/1126-6708/2007/05/016`. URL: `https://dx.doi.org/10.1088/1126-6708/2007/05/016`.

[42] C. T. Sachrajda and G. Villadoro. "Twisted boundary conditions in lattice simulations". In: *Phys. Lett. B* 609 (2005), pp. 73–85. DOI: `10.1016/j.physletb.2005.01.033`. arXiv: `hep-lat/0411033`.

[43] R. Frezzotti and G. C. Rossi. "Twisted mass lattice QCD with mass nondegenerate quarks". In: *Nucl. Phys. B Proc. Suppl.* 128 (2004). Ed. by A. C. Kalloniatis, D. B. Leinweber, and A. G. Williams, pp. 193–202. DOI: `10.1016/S0920-5632(03)02477-0`. arXiv: `hep-lat/0311008`.

[44] Johan Bijnens and Gerhard Ecker. "Mesonic Low-Energy Constants". In: *Annual Review of Nuclear and Particle Science* 64 (2014), pp. 149–174. DOI: `10.1146/annurev-nucl-102313-025528`. eprint: `https://doi.org/10.1146/annurev-nucl-102313-025528`. URL: `https://doi.org/10.1146/annurev-nucl-102313-025528`.

[45] S. Krishna and H. S. Mani. "Study of the Decays $K \to \mu\nu e^+e^-$ and $K \to e\nu\mu^+\mu^-$". In: *Phys. Rev. D* 5 (1972), pp. 678–681. DOI: `10.1103/PhysRevD.5.678`. URL: `https://link.aps.org/doi/10.1103/PhysRevD.5.678`.

[46] Vladyslav Shtabovenko, Rolf Mertig, and Frederik Orellana. “FeynCalc 9.3: New features and improvements”. In: *Computer Physics Communications* 256 (2020), p. 107478. ISSN: 0010-4655. DOI: `https://doi.org/10.1016/j.cpc.2020.107478`. URL: `https://www.sciencedirect.com/science/article/pii/S001046552030223X`.

[47] G Peter Lepage. “A new algorithm for adaptive multidimensional integration”. In: *Journal of Computational Physics* 27 (1978), pp. 192–203. ISSN: 0021-9991. DOI: `https://doi.org/10.1016/0021-9991(78)90004-9`. URL: `https://www.sciencedirect.com/science/article/pii/0021999178900049`.

[48] Michael E. Peskin and Daniel V. Schroeder. *An Introduction to quantum field theory*. Reading, USA: Addison-Wesley, 1995. ISBN: 978-0-201-50397-5.

[49] H. Georgi. *Lie algebras in particle physics. From isospin to unified theories*. Vol. 54. 1982.

[50] Guido Altarelli. “A QCD primer”. In: *AIP Conf. Proc.* 631 (2002). Ed. by H. T. Elze, E. Ferreira, T. Kodama, J. Letessier, Johann Rafelski, and R. L. Thews, p. 70. DOI: `10.1063/1.1513677`. arXiv: `hep-ph/0204179`.

[51] Jeff Greensite. *An introduction to the confinement problem*. Vol. 821. 2011. DOI: `10.1007/978-3-642-14382-3`.

[52] Kenneth G. Wilson. “Confinement of quarks”. In: *Phys. Rev. D* 10 (1974), pp. 2445–2459. DOI: `10.1103/PhysRevD.10.2445`. URL: `https://link.aps.org/doi/10.1103/PhysRevD.10.2445`.

[53] Rajan Gupta. “Introduction to lattice QCD: Course”. In: *Les Houches Summer School in Theoretical Physics, Session 68: Probing the Standard Model of Particle Interactions*. 1997, pp. 83–219. arXiv: `hep-lat/9807028`.

[54] Christof Gattringer and Christian B. Lang. *Quantum chromodynamics on the lattice*. Vol. 788. Berlin: Springer, 2010. ISBN: 978-3-642-01849-7, 978-3-642-01850-3. DOI: `10.1007/978-3-642-01850-3`.

[55] Y. Iwasaki. “Renormalization Group Analysis of Lattice Theories and Improved Lattice Action: Two-Dimensional Nonlinear O(N) Sigma Model”. In: *Nucl. Phys. B* 258 (1985), pp. 141–156. DOI: `10.1016/0550-3213(85)90606-6`.

[56] P. Weisz and R. Wohlert. “Continuum limit improved lattice action for pure Yang-Mills theory (II)”. In: *Nuclear Physics B* 236 (1984), pp. 397–422. ISSN: 0550-3213. DOI: `https://doi.org/10.1016/0550-3213(84)90543-1`. URL: `https://www.sciencedirect.com/science/article/pii/0550321384905431`.

[57] J. F. Donoghue, E. Golowich, and Barry R. Holstein. *Dynamics of the standard model*. Vol. 2. CUP, 2014. DOI: 10.1017/CBO9780511524370.

[58] Holger Bech Nielsen and M. Ninomiya. “No Go Theorem for Regularizing Chiral Fermions”. In: *Phys. Lett. B* 105 (1981), pp. 219–223. DOI: 10.1016/0370-2693(81)91026-1.

[59] Paul H. Ginsparg and Kenneth G. Wilson. “A Remnant of Chiral Symmetry on the Lattice”. In: *Phys. Rev. D* 25 (1982), p. 2649. DOI: 10.1103/PhysRevD.25.2649.

[60] Luuk H. Karsten and Jan Smith. “Lattice fermions: Species doubling, chiral invariance and the triangle anomaly”. In: *Nuclear Physics B* 183 (1981), pp. 103–140. ISSN: 0550-3213. DOI: https://doi.org/10.1016/0550-3213(81)90549-6. URL: https://www.sciencedirect.com/science/article/pii/0550321381905496.

[61] Andrea Shindler. “Twisted mass lattice QCD”. In: *Phys. Rept.* 461 (2008), pp. 37–110. DOI: 10.1016/j.physrep.2008.03.001. arXiv: 0707.4093 [hep-lat].

[62] K. Symanzik. “Continuum Limit and Improved Action in Lattice Theories. 2. O(N) Nonlinear Sigma Model in Perturbation Theory”. In: *Nucl. Phys. B* 226 (1983), pp. 205–227. DOI: 10.1016/0550-3213(83)90469-8.

[63] Martin Luscher, Stefan Sint, Rainer Sommer, and Peter Weisz. “Chiral symmetry and O(a) improvement in lattice QCD”. In: *Nucl. Phys. B* 478 (1996), pp. 365–400. DOI: 10.1016/0550-3213(96)00378-1. arXiv: hep-lat/9605038.

[64] Remi Baron et al. “Computing K and D meson masses with $N_f = 2{+}1{+}1$ twisted mass lattice QCD”. In: *Comput. Phys. Commun.* 182 (2011), pp. 299–316. DOI: 10.1016/j.cpc.2010.10.004. arXiv: 1005.2042 [hep-lat].

[65] G. Martinelli, C. Pittori, Christopher T. Sachrajda, M. Testa, and A. Vladikas. “A General method for nonperturbative renormalization of lattice operators”. In: *Nucl. Phys. B* 445 (1995), pp. 81–108. DOI: 10.1016/0550-3213(95)00126-D. arXiv: hep-lat/9411010.

[66] David Palao et al. “Renormalization constants of quark bilinears in lattice QCD with four dynamical Wilson quarks”. In: *PoS* Lattice 2011 (2012), p. 233. DOI: 10.22323/1.139.0233.

[67] M. Constantinou et al. “Non-perturbative renormalization of quark bilinear operators with $N_f = 2$ (tmQCD) Wilson fermions and the tree-level improved gauge action”. In: *JHEP* 08 (2010), p. 068. DOI: 10.1007/JHEP08(2010)068. arXiv: 1004.1115 [hep-lat].

[68] Karl Jansen and Carsten Urbach. “tmLQCD: A program suite to simulate Wilson twisted mass lattice QCD”. In: *Computer Physics Communications* 180 (2009), pp. 2717–2738. DOI: 10.1016/j.cpc.2009.05.016. arXiv: 0905.3331 [hep-lat].